Risk Assessment of Gold Nanoparticles in a Stable Arabidopsis Exposition System

Dissertation

der Mathematisch-Naturwissenschaftlichen Fakultät

der Eberhard Karls Universität Tübingen

zur Erlangung des Grades eines

Doktors der Naturwissenschaften

(Dr. rer. nat.)

vorgelegt von

M. Sc. Eleonora Ferrari

aus Verona, Italien

Tübingen

2022

Gedruckt mit Genehmigung der Mathematisch-Naturwissenschaftlichen Fakultät der Eberhard Karls Universität Tübingen.

Tag der mündlichen Qualifikation:	20.07.2022
Dekan:	Prof. Dr. Thilo Stehle
1. Berichterstatterin:	PD Dr. Birgit Kemmerling
2. Berichterstatter:	Prof. Dr. Thorsten Nürnberger

Table of contents

Table of contents ..... **I**

List of abbreviations ..... **IV**

List of figures ..... **VII**

List of tables ..... **IX**

1 Introduction **1**

1.1 Nanotechnology 1

1.1.1 Nanomaterials 3

1.2 The environmental significance of NPs 4

1.2.1 Physicochemical evolution of NPs in environmental and biological media 7

1.2.2 Impact of surface stabilizers on the stability of colloidal NPs 9

1.3 Gold nanoparticles 11

1.3.1 Synthesis of AuNPs 12

1.3.2 AuNPs aggregation 13

1.3.3 Physicochemical characterization of AuNPs 13

1.3.3.1 UV-Vis spectroscopy 13

1.3.3.2 Dynamic light scattering 14

1.3.3.3 Zeta potential 15

1.4 Plant-AuNPs interaction 15

1.4.1 Phytotoxicity 16

1.4.2 Effects on plant defence responses 16

1.4.3 Uptake and transport in plants 17

1.5 Aim of the thesis 19

2 Materials and Method **20**

2.1 Materials 20

2.1.1 Chemicals 20

2.1.2 Nanoparticles 20

2.1.3 Media 20

2.1.4 Plant genotype 20

2.2 Methods 21
2.2.1 Gold nanoparticles synthesis 21
2.2.1.1 AuNP-SC 21
2.2.1.2 AuNP-SCTA 21
2.2.1.3 AuNP-PVP 21
2.2.2 Gold nanoparticle characterization 21
2.2.2.1 AuNP concentration 21
2.2.2.2 Size determination by electron microscopy 21
2.2.2.3 UV-Vis spectroscopy 22
2.2.2.4 Size and Zeta potential measurements 22
2.2.3 Gold nanoparticle sterilization 22
2.2.4 Plant growth methods 22
2.2.4.1 Seed sterilization 22
2.2.4.2 Plant growth conditions 22
2.2.4.3 NP exposure in agar-solidified medium 23
2.2.4.4 NP exposure in hydroponic culture 23
2.2.4.5 NP exposure in soil 23
2.2.5 RNA-analysis 24
2.2.5.1 RNA extraction from plant roots 24
2.2.5.2 Transcriptome sequencing analysis 24
2.2.6 Protein-analysis 24
2.2.6.1 Total protein extraction 24
2.2.6.2 NanoLC-MS/MS analysis 25
2.2.6.3 MS data processing 25
2.2.7 Functional assays 26
2.2.7.1 Recording the phenotypes of plants 26
2.2.7.2 Oxidative burst 26
2.2.7.3 FOX assay 26
2.2.7.4 Statistical analysis 27
2.2.8 Transmission electron microscopy (TEM) 27
3 Results 29
3.1 Identification of physicochemical properties of AuNPs 29

3.1.1 Synthesis and surface engineering of high quality, monodispersed AuNPs .. 30
3.1.2 Over time characterization of AuNPs dispersed in plant growth media 32
3.2 Physiological effects of AuNPs coatings on *A. thaliana* growth 35
3.2.1 Capping agents: SCTA vs PVP 35
3.2.1.1 AuNP-SCTA sterilization 37
3.3 Physiological effects of AuNP-SCTA on *A. thaliana* growth 38
3.4 Immune responses upon AuNP-SCTA treatment 39
3.5 Transcriptomic analysis of the effect of AuNP-SCTA in A. thaliana 41
3.6 Proteomic analysis of the effect of AuNP-SCTA in A. thaliana 43
3.7 AuNP-SCTA uptake and detection in *A. thaliana* roots 44
4 Discussion 48
4.1 Plant nanotoxicology: major challenges 48
4.2 Physicochemical evaluation of AuNPs 49
4.2.1 Surface stabilizing agents determine behaviour of AuNPs in plant media 49
4.2.2 Toxicity of surface stabilizing agents 50
4.2.3 Sterilization by filtration preserves the physical properties of AuNP-SCTA .. 51
4.3 Plant responses to AuNPs 52
4.3.1 AuNP-SCTA affect Arabidopsis root growth in a dose-dependent manner .. 52
4.3.2 AuNP-SCTA decrease stress responses in Arabidopsis seedlings 53
4.4 Alterations in transcriptome and proteome after AuNP exposure 54
4.5 AuNPs uptake in plants 56
4.6 Conclusion 58
5 Summary 61
6 Zusammenfassung 62
7 References 63
8 Appendix 78
8.1 Supplemental data 78
8.2 Acknowledgment 92

List of abbreviations

%	Percent sign
°C	Degree Celsius
0D	Zero-dimensional
1D	One-dimensional
2D	Two-dimensional
3D	Three-dimensional
AgNP	Silver nanoparticle
ANM	Anthropogenic nanomaterial
ANP	Anthropogenic nanoparticle
Au	Gold
AuNP	Gold nanoparticle
CeO_2	Cerium dioxide
CME	Cellulose mixed ester
d	Day
D	Translational diffusion coefficient
Da	Dalton
DEG	Differentially expressed gene
DEP	Differentially expressed protein
DGR1	DUF642 L-GalL-responsive gene 1
DGR2	DUF642 L-GalL-responsive gene 2
DLS	Dynamic light scattering
DLVO	Derjaguin-Landau-Verwey-Overbeek
ENM	Engineered nanomaterial
ENP	Engineered nanoparticle
EPM	Electrophoretic mobility
FOX	Ferrous oxidation xylenol orange
GO	Gene ontology
GSTF6	Glutathione S-transferase F6
h	Hour
$HAuCl_4$	Tetrachloroauric acid
ICP-MS	Inductively coupled plasma mass spectrometry

K_B	Boltzmann constant
LC-MS/MS	Liquid chromatography-mass spectrometry/mass spectrometry
LDV	Laser doppler velocimetry
LOOH	Lipid hydroperoxide
LSPR	Localized surface plasmon resonance
M	Molar
MAMP	Microbe-associated molecular pattern
min	Minute
MNP	Metal nanoparticle
MS	Murashige and Skoog
n	Sample size
NAS2	Nicotianamine synthase 2
NIR	Near infrared
NM	Nanomaterial
NNI	National Nanotechnology Initiative
NNM	Natural nanomaterial
NNP	Natural nanoparticle
NP	Nanoparticle
NPD	Nanotechnology Products Database
PAMP	Pathogen-associated molecular pattern
PCS	Photon correlation spectroscopy
PDI	Polydispersity index
PES	Polyethersulfone
ppm	Parts per million
PRR	Pattern-recognition receptor
PTI	pattern-triggered immunity
PVP	Polyvinylpyrrolidone
QELS	Quasi-elastic light scattering
r	Radius
R&D	Research and Development
R_H	Hydrodynamic radius
RLU	Relative light units
RNA-Seq	RNA-sequencing
ROS	Reactive oxygen species

s	Second
SC	Sodium citrate
SCTA	Sodium citrate and Tannic acid
SE	Standard error
SEM	Scanning electron microscopy
SPR	Surface plasmon resonance
STEM	Scanning transmission electron microscopy
T	Temperature
TA	Tannic acid
TEM	Transmission electron microscopy
UV	Ultra-violet
UV-Vis	Ultraviolet-visible
V	Volt
vis	Visible
x g	Times gravity
Z potential	Zeta potential
η	Solvent viscosity
θ	Scattering angle
λmax	Lambda max

List of figures

Figure 1-1: The Lycurgus Cup: an ancient and unaware use of nanotechnology (Adapted from Freestone et a., 2007). 2
Figure 1-2: Nanotechnology products currently used in different sectors and countries (Adapted from https://product.statnano.com/, accessed December 7, 2021). 3
Figure 1-3: Schematic representation of the major sources of natural and anthropogenic NMs on the Earth's surface and atmosphere (Hochella et al., 2019). 5
Figure 1-4: Main beneficial and detrimental effects of NMs on plants, animals and microbes (Hochella et al., 2019). 6
Figure 1-5: Physicochemical transformations of NPs. 7
Figure 1-6: Colloidal stability of metal NPs (Adapted from Barbero et al., 2017). 8
Figure 1-7: Schematic representation of electrostatic and steric stabilizations. 9
Figure 1-8: NP capping agents. 10
Figure 1-9: Surface Plasmon Resonance (SPR) of AuNPs (Adapted from Masson, 2020). 11
Figure 1-10: Dynamic light scattering (DLS) technology. 14
Figure 1-11: NPs uptake and accumulation in plants (Ali et al., 2021). 18
Figure 2-1: AuNP-Arabidopsis root exposure routes. 23
To assess the behaviour and fate of AuNP after their interaction with Arabidopsis roots, uptake experiments were performed in three different plant growth media, i.e., ½ MS (hydroponic system) (B), ½ MS-agar (A) and soil (C). 23
Figure 3-1: Physicochemical characterization of AuNPs stabilized with different surface engineering strategies. 31
Figure 3-2: Over time physicochemical characterization of AuNPs in plant working media. 34
Figure 3-3: Toxicity of surface stabilizing agents on A. thaliana seedling roots. 36
Figure 3-4: UV-Vis spectra of AuNP-SCTA before and after sterilization with different filter materials. 37
Figure 3-5: AuNP-SCTA affect Arabidopsis root growth in a dose-dependent manner 38
Figure 3-6: AuNP-SCTA exposition enhances growth of Arabidopsis seedlings. 39
Figure 3-7: AuNPs-SCTA decrease ROS production and lipid peroxidation levels. 41
Figure 3-8: DEGs after AuNP-SCTA treatment. 42
Figure 3-9: DEPs after AuNP-SCTA treatment. 43
Figure 3-10: *A. thaliana* growth media. 44

Figure 3-11: Physicochemical characterization of high-quality sub-10 nm, monodispersed AuNP-SCTA. 45
Figure 3-12: Over time physicochemical characterization of 4 nm AuNP-SCTA in plant working media. 46
Figure 3-13: 4 nm AuNP-SCTA are not taken up by Arabidopsis roots. 47
Figure 4-1: Venn diagram of DEGs after AuNP-SCTA exposure (this study) and KAuCl4 treatment (Tiwari et al., 2016). 56
Figure A-1: GO classification of DEGs after AuNP-SCTA treatment. 88
Figure A-2: Pathway classification of DEGs after AuNP-SCTA treatment. 89
Figure A-3: GO classification of DEPs after AuNP-SCTA treatment. 90
Figure A-4: Pathway classification of DEPs after AuNP-SCTA treatment. 91

List of tables

Table 2-1: Gold nanoparticles used in this work 20
Table 2-2: Cultivation media..... 20
Table A-1: Clean reads quality metrics and summary of genome mapping 78
Table A-2: Partial list of DEGs after short- (6h) AuNP-SCTA treatment with their expression information 78
Table A-3: Partial list of DEGs after long- (7d) AuNP-SCTA treatment with their expression information 84
Table A-4: Partial list of DEPs after short- (6h) AuNP-SCTA treatment with their expression information 84
Table A-5: Partial list of DEPs after long- (7d) AuNP-SCTA treatment with their expression information 86
Table A 6: Overlap between our DEGs and those published by Tiwari et al. (2016).....86

1 Introduction

The first evidence of the use of nanotechnology by ancient Indian artisans dates back to the 6th century BC (Kokarneswaran et al., 2020), long before the term itself was coined by the Japanese scientist Norio Taniguchi in 1974, and ever since there have been revolutionary developments in this field (Hulla et al., 2015). Nanotechnology encompasses all those areas of science and engineering conducted at the nanoscale, exploiting the unique advantageous properties of nanosized materials compared to their bulk counterparts (Miyazaki & Islam, 2007; Asha & Narain, 2020). The intensive use of nanotechnological products in the most disparate industries, ranging from electronics to medicine, significatively impacted almost all sectors of the global economy (Thiruvengadam et al., 2018; Zhidebekkyzy et al., 2019). On the other hand, the increasing production, use and disposal of nanomaterials (NMs) has translated into their enhanced and uncontrolled release into the environment (Giese et al., 2018). Currently, knowledge of the health and environmental risks associated with the disposal of manufactured nanosized materials is severely lacking, and critical questions about risk assessment arise (Krug, 2018). Therefore, nanosafety evaluations are necessary to investigate the detrimental but also beneficial effects of NMs on living organisms and their surrounding habitats (Boraschi et al., 2020).

1.1 Nanotechnology

While nanoscience is defined as the theoretical study of the properties of materials with at least one dimension in the nanoscale, nanotechnology is the field that encompasses all the approaches and technologies that exploit the unique chemical and physical characteristics of matter at the nanolevel (Mansoori & Soelaiman, 2005). The National Nanotechnology Initiative (NNI), a United States Government research and development (R&D) enterprise, defines nanotechnology as: “The understanding and control of matter at dimensions between approximately 1 and 100 nanometers, where unique phenomena enable novel applications” (Committee on Science, 2011). The Nobel Prize in Physics Richard Feynman in 1959, during the lecture titled: “There´s Plenty of Room at the Bottom”, considered for the first time the possibility to create nanosized products with the use of atoms as buildings particles (Feynman, 1959). Nowadays, this lecture is referred to as the origin of the nanotechnological paradigm. Although the field of nanotechnology was officially recognized in the 20th century, the unconscious use of NMs dates back to ancient history. The Lycurgus Cup, created by ancient Romans in the 4^{t}h century, is considered the greatest successes of the glass industry of antiquity and the most famous example of unaware use of nanoparticles (NPs) (Freestone et al., 2007) (Figure 1-1). The peculiar feature of this Cup, exhibited in the British Museum, is the colour change

depending on the direction of light in which it is viewed, i.e., green when backlit and red when frontlit. Since 1959, analytical studies carried out on the Cup have linked dichroism to the presence of minute amounts of gold (about 40 ppm) and silver (about 300 ppm) in the form of metal colloids (Chirnside & Proffitt, 1963; Brill, 1965). In particular, the localized surface plasmon resonance (SPR) of metal nanoparticles is the optical phenomenon responsible for the reddish transmission of gold nanoparticles (AuNPs) and the green reflection of silver nanoparticles (AgNPs) (Fong & Yung, 2013). Further analyses, i.e., analytical transmission electron microscopy (TEM) and X-rays identified the colloidal system as silver-gold alloy particles (silver-gold ratio approximately 7: 3) with a diameter between 50 and 100 nm and containing an additional 10% of copper (Barber & Freestone, 1990).

Figure 1-1: The Lycurgus Cup: an ancient and unaware use of nanotechnology (Adapted from Freestone et a., 2007).
4th-century AD Roman glass cup (British Museum, 1958,1202.1) made of dichroic glass, which exhibits a green hue in reflected light (A) and a reddish one in transmitted light (B). This unique optical characteristic depends on the presence of silver (AgNPs) and gold nanoparticles (AuNPs) in the glass, which selectively scatter and absorb blue and green light.

Nowadays, the unusual and unique physicochemical, optical and magnetic properties that many materials exhibit at the nanoscale are widely exploited by today's scientists and engineers in a variety of applications, such as electronics, medicine, cosmetics, food science and energy supply among many others (Schatz, 2007; S. Ali, 2020). In the last decade, nanotechnology has also been used in the new and promising field of environmental nanotechnology (Tyagi et al., 2018), which addresses the development of solutions to existing pollution problems and preventive measures to reduce the generation of new contaminants (Kharat et al., 2017). StatNano, the most comprehensive statistical bank dedicated to the collection, publication and analysis of bibliometric data in the area of nanotechnology, has created the Nanotechnology Products Database (NPD) (StatNano, 2016), which

provides statistical information on nanotechnology products currently in use worldwide. In particular, NPD focuses on the development of the NMs market, its trends and emerging prospects (Figure 1-2).

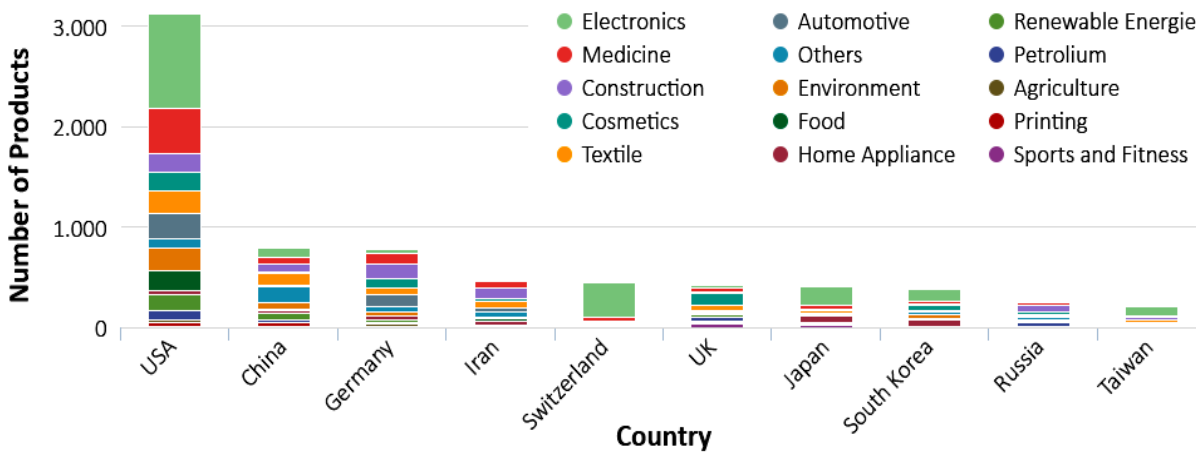

Figure 1-2: Nanotechnology products currently used in different sectors and countries (Adapted from https://product.statnano.com/, accessed December 7, 2021).
Total number of different nanotechnological items presently used by the top 10 consumer countries. Nanotechnology Products Database (NPD) collects and classifies data and statistical reports analysing the nanotechnology trend in different industries around the world.

Despite the significant commercial advantages deriving from the use of NMs, their presence in the environment can pose a biological hazard with potential health risks (Dobrovolskaia & McNeil, 2007). Therefore, a detailed understanding of the mechanisms of action of NMs and an adequate assessment of the risk associated with their exposure are key requirements for a safer future use of these products (Roberto & Christofoletti, 2019). For example, while recent advances in medical nanotechnology have revolutionized therapeutic and diagnostic approaches, to date little is known about NM-plant interactions and their possible implications for the environment and human health (Sanzari et al., 2019). Plants interact directly with soil, water and atmosphere, acting as potential exposure pathways of contaminants to higher species through the food chain (Stampoulis et al., 2009). For these reasons, novel nanotoxicology and nanosafety approaches are required to evaluate the impact of NMs on the environment and across living species (Boraschi et al., 2020).

1.1.1 Nanomaterials

NMs can be classified according to different criteria such as composition, shape, agglomeration state and surface chemistry (Rizwan et al., 2021). Furthermore, based on the number of their dimensions that falls within the nanoscale, they can be further classified as zero-dimensional (0D), one-dimensional (1D), two-dimensional (2D) or three-dimensional (3D) (Tiwari et al., 2012). 0D NMs have all three dimensions within the nanoscale and are called NPs (Wang et al., 2020). In turn, NPs are divided into different categories based on their main chemical and physical characteristics (material,

size, internal structure and surface properties) and can be synthesized through four main processes, namely the chemical, physical, mechanical and biological methods (Iravani et al., 2014; Anu Mary Ealia & Saravanakumar, 2017). The outstanding properties of NPs, compared to their bulk counterparts, depend on the high surface area to volume ratio and quantum effects at the nanoscale (Schwirn et al., 2014). As the radius (r) decreases, the surface area ($4\pi r^2$) of the particle increases exponentially in relation to its volume ($4/3\ \pi r^3$). Due to the increased area/volume ratio, the percentage of atoms on the surface and the surface forces of NPs become more dominant, causing an increase in their surface reactivity, reduced melting temperatures (Suttiponparnit et al., 2010; Antoniammal & Arivuoli, 2012; Gatoo et al., 2014) and improved mechanical properties such as bending, impact and tensile strength (Wu et al., 2020).

1.2 The environmental significance of NPs

In the last decade, the widespread use of NP-containing products has led to the direct exposure of both the terrestrial and aquatic environment to these nanosized materials, raising concerns regarding their safety and biocompatibility with living organisms (Singh & Kumar, 2014; Gupta & Xie, 2018; Liu et al., 2018; Bundschuh et al., 2018; Mittal et al., 2020). Anthropogenic nanoparticles (ANPs) can be released intentionally or unintentionally into the environment (Hochella et al., 2019; Lespes et al., 2020) through several routes, such as direct industrial and urban discharges of nanocomposites in water and soils, disposal and excretion of nanomedicine from human and veterinary products (Batley et al., 2013), wastewater treatment plants (Liu & Lal, 2015), mining and forest fires (Hochella et al., 2019). In addition, engineered NPs are deliberately released into the environment as nanopesticides and nanofertilizers in agricultural practices (Kah et al., 2018) and during soil and water remediation processes (Casals et al., 2014), increasing apprehension about their fate and impact once dispersed into surrounding habitats. On the other hand, natural nanoparticles (NNPs), produced in nature through geochemical or mechanical processes, have been ubiquitous in the environment for billions of years, but their role in the Earth's global biogeochemical cycle is not yet fully understood (Hochella et al., 2019). Many attempts have been made to explore the role of NNPs in the Earth system, including the use of exposure modelling, but the topic remains complex and their role in global biogeochemical cycles unclear (Sadik, 2012; Lespes et al., 2020). In order to obtain a complete assessment of the risk associated with the release of NPs into the environment, a detailed understanding of the mechanisms of action of NPs under natural conditions is required (Peijnenburg et al., 2015).

To date, between 1 and 10 teragrams (Tg, 1 Tg=10^{12} g) of anthropogenic nanomaterials (ANMs) have to be added to the thousands of Tg of nanocomposites naturally present on Earth (Hochella et al., 2019) (Figure 1-3). In the Earth´s critical zone, the heterogeneous near-surface environment including

soil, water, rocks and living organisms (Lin, 2010), mineral formation processes are the main sources of NNPs, with clays accounting for 10^7-10^8 Tg of naturally occurred inorganic NMs (Hochella et al., 2012). A smaller amount of natural nanomaterials (NNMs) (sulphides, metal oxides, carbonates and phosphates) is produced in the critical zone of the Earth through weathering processes. These compounds, although present in smaller quantities than clays, play a major role in biogeochemical cycles (Hochella et al., 2008). NNMs can also originate from volcanic gases (22 Tg) and wind-blown mineral dust aerosol (320 Tg), for a total of 342 Tg each year (Hochella et al., 2008). In nature, the greatest forces capable of moving these naturally produced NMs hundreds of kilometres (Km) away from the source of origin are winds and water currents (ground, ephemeral streams and open waters) (Hochella et al., 2008). The largest amount of unintentionally produced nanomaterials (incidental NMs) is released into the atmosphere, soil and water as a result of fossil fuel combustion, mining, industrial and agricultural practices (van der Zee et al., 2003). Although water covers 70% of the Earth's surface, there is still little knowledge about the distribution, behaviour and fate of NNMs in the oceans. On the other hand, the main source of incidental NMs in the oceans can undoubtedly be traced back to ship engine exhausts (Jaworek et al., 2014). Sulphates, with an average size of 60 nm, are the main constituents of these emissions (Coggon et al., 2012).

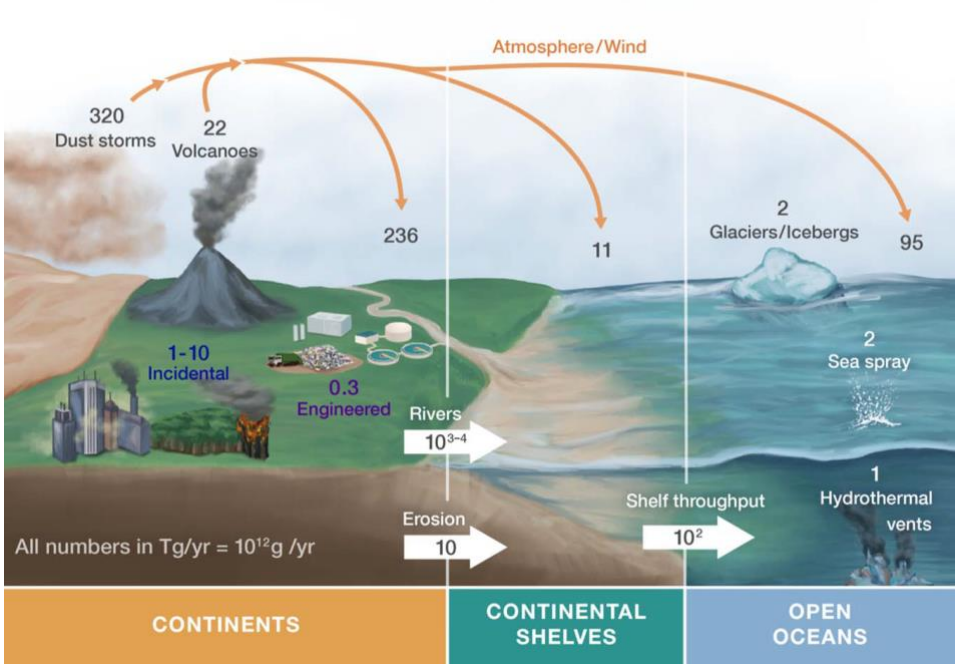

Figure 1-3: Schematic representation of the major sources of natural and anthropogenic NMs on the Earth's surface and atmosphere (Hochella et al., 2019).
NMs have been present in abundance on Earth since its origin, in constant balance with the life cycle of humans and other living organisms. Although NNMs have been ubiquitous in the environment for billions of years, the rate at which ANMs are released, whether intentionally or unintentionally, has increased exponentially in the last twenty years. Amount of natural (black and white numbers), incidental (blue) and engineered (purples) NMs, represented as Tg/year. NNMs fluxes from land to continental shelves and open oceans are represented by white arrows.

NMs interact with biological systems through multiple pathways, depending on the organism and the source of exposure. The effects resulting from these interactions, whether positive or negative, are in turn influenced by several factors such as dose, time and route of exposure and the physicochemical characteristics of the NM (Figure 1-4). For example, while the use of NPs in medicine has the potential to improve the diagnosis and treatment of life-threatening diseases by exploiting nanocomposites as imaging and drug delivery systems (Arms et al., 2018; Mitchell et al., 2021), ANMs, such as those produced during industrial coal combustion, raise serious health concerns with approximately 3.3 million premature deaths each year attributed to cardiovascular disease caused by the inhalation of particles with a diameter smaller than 2.5 µm (Lelieveld et al., 2015). Possible alterations in the properties and colloidal stability of NPs once released into an environment other than that of synthesis make studies under natural conditions difficult to interpret, thus nanosafety assessments under reproducible and controlled conditions help to interpret investigations in ecotoxicological assays (Kim et al., 2008; Barbero et al., 2017; Barbero et al., 2019).

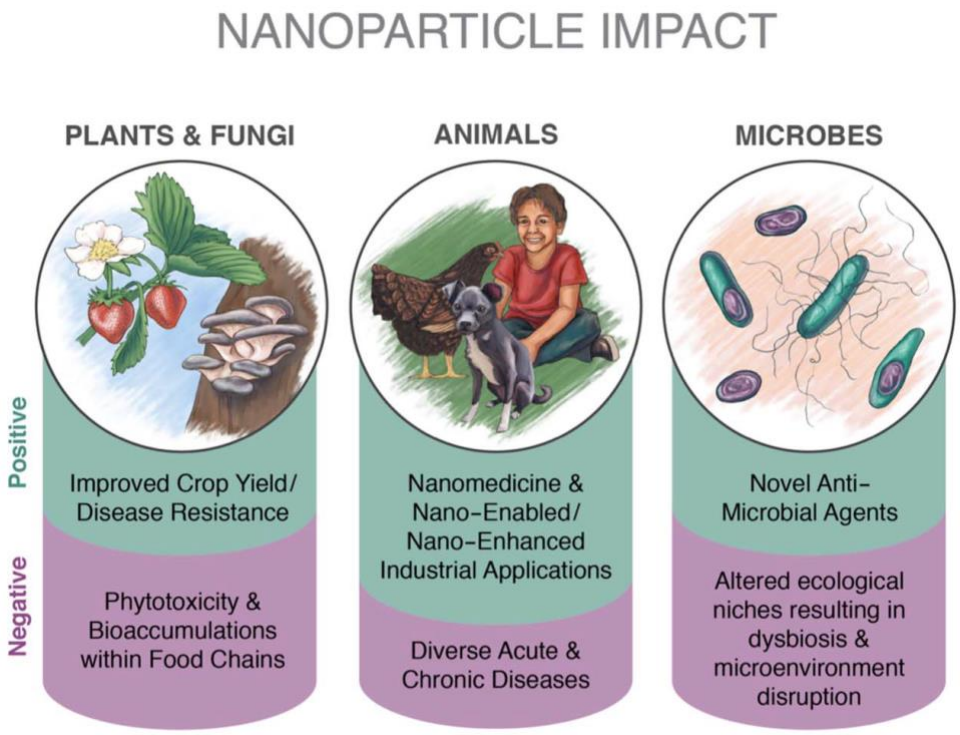

Figure 1-4: Main beneficial and detrimental effects of NMs on plants, animals and microbes (Hochella et al., 2019).
NMs are ubiquitous in the environment and have the potential to affect surrounding natural ecosystems. Although the ecotoxicological impact of such materials depends on the type, dose and route of exposure of the NM, the main beneficial and harmful effects can be classified according to the living organism considered.

1.2.1 Physicochemical evolution of NPs in environmental and biological media

The large surface area of NPs, along with the low coordination of atoms at their surface and the colloidal nature determine the characteristic high reactivity and behaviour of nanoscale materials (Auffan et al., 2011). This high reactivity leads NPs exposed to an environmental scenario different from the synthesis medium to sough for a more stable thermodynamic state via aggregation (homo- or hetero-aggregation), interaction with molecules present in the new surroundings, chemical transformations, adsorption to macro-organic matter and dissolution (Bastús et al., 2012) (Fig. 1-5). The fate, behaviour and biological impact of engineered nanoparticles (ENPs) are strictly dependent on the physicochemical transformations they undergo after their release into a new environment, which can lead to the formation of nano-objects with a new identity (Mueller & Nowack, 2008). Several studies have examined the physicochemical transformations of NPs after their release in culture media or aquatic and terrestrial habitats, correlating the nature of the particles and surrounding environments with the recorded modifications (Nowack et al., 2012; Batley et al., 2013; Peijnenburg et al., 2015).

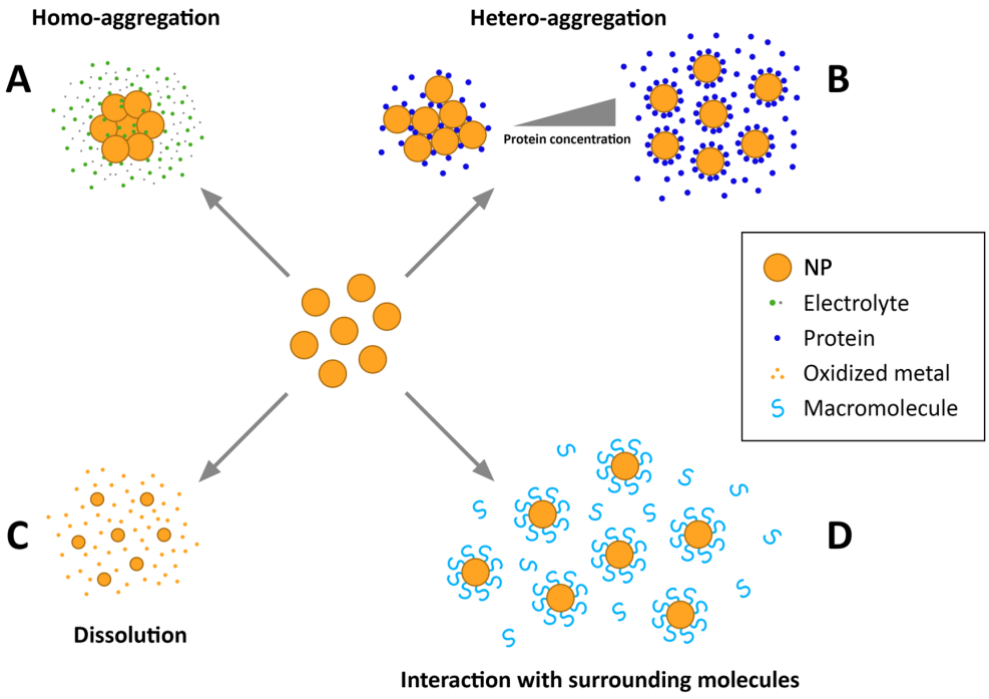

Figure 1-5: Physicochemical transformations of NPs.
Schematic representation of the main physicochemical transformations of NPs. Processes such as homo-aggregation (A), hetero-aggregation (B), dissolution (C) and interaction with macromolecules (D) depend both on the intrinsic properties of the particles and on the components of the environmental or biological medium to which they are exposed.

The main transformations (homo-aggregation, hetero-aggregation and dissolution) affecting unstable metal NPs dispersed in a biological medium can also coexist and their kinetics depend on the concentration of the agents responsible for each process. In particular, homo-aggregation occurs when the salt ions present in high-salinity exposure media screen weaker repulsive electrostatic interactions between NPs (Oncsik et al., 2015) (Fig. 1-6 A). Culture media are solutions containing a specific mix of nutrient substances to sustain the growth of the cultivated organisms and they are usually characterized by high ionic strength that can cause aggregation of NPs not properly stabilized such as pristine AuNPs (sodium citrate-stabilized AuNPs) (Macpherson et al., 2012). On the other hand, if an adequate concentration of proteins is available in the surrounding environment, they can provide electro-steric stabilization by adsorption onto NPs in a phenomenon called hetero-aggregation (Barbero et al., 2017). This process is strictly correlated with the concentration of proteins in the medium. In fact, NPs in high-salinity solutions have a strong tendency for homo-aggregation rather than hetero-aggregation and in order to avoid this the proteins must have a much higher concentration than the particles (Piella et al., 2017) (Fig. 1-6 B). Another mechanism that can reduce the colloidal stability of NPs, along with aggregation phenomena, is dissolution, a process in which NPs undergo a chemical transformation due to electrolyte ions oxidising the surface atoms (Fig. 1-6 C) (Misra et al., 2012). The conjugation of specific stabilizers on the NP surface has a strong influence on the interaction of the particles with the surrounding biological environment, consequently affecting their stability and reactivity (Blanco et al., 2015). All these parameters must be taken into account when testing NPs in in vitro or in vivo model systems.

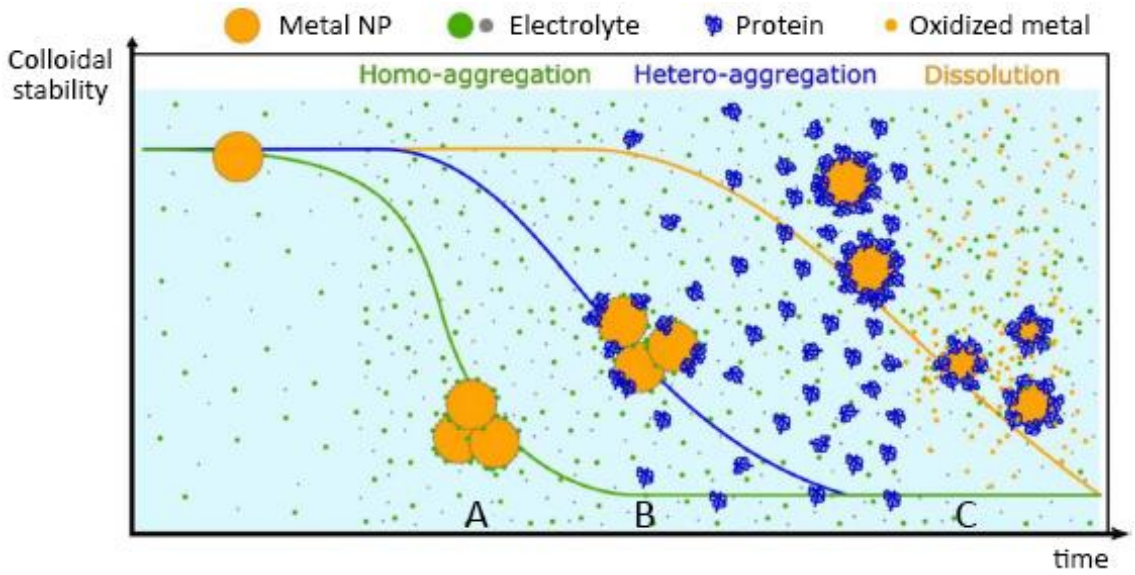

Figure 1-6: Colloidal stability of metal NPs (Adapted from Barbero et al., 2017).
The kinetics of the main physicochemical transformations affecting the stability of metal NPs depends on the concentration of electrolytes (A), proteins (B) and oxidizing agents (C) and their respective incubation times.

1.2.2 Impact of surface stabilizers on the stability of colloidal NPs

The stability of colloidal NPs plays a pivotal role in determining the fate and behaviour of nanosized materials and thus their biological impact and function in specific applications (Moore et al., 2015). To avoid aggregation, NPs in ionic solutions are usually coated with capping agents (Javed et al., 2020), which stabilize the interface between the NPs and their synthesis or release medium providing repulsive forces that prevail over the attractive ones (Bastús et al., 2012) . The nature of the stabilizing molecules affects the physicochemical characteristic of the NP surface, therefore it is possible to modulate the behaviour of the particles by specifically designing their surface according to the purpose for which they are used (Dreaden et al., 2012). On the other hand, it is important to highlight how the toxicity of stabilizers and their effects *in vitro* and *in vivo* models should be carefully tested in order to avoid potential adverse effects and artefacts due to the presence of such chemicals (Connor et al., 2005). Two main approaches are used to achieve colloidal stability, both based on repulsion forces, namely electrostatic repulsion and steric repulsion (Palihawadana et al., 2017) (Figure 1-7).

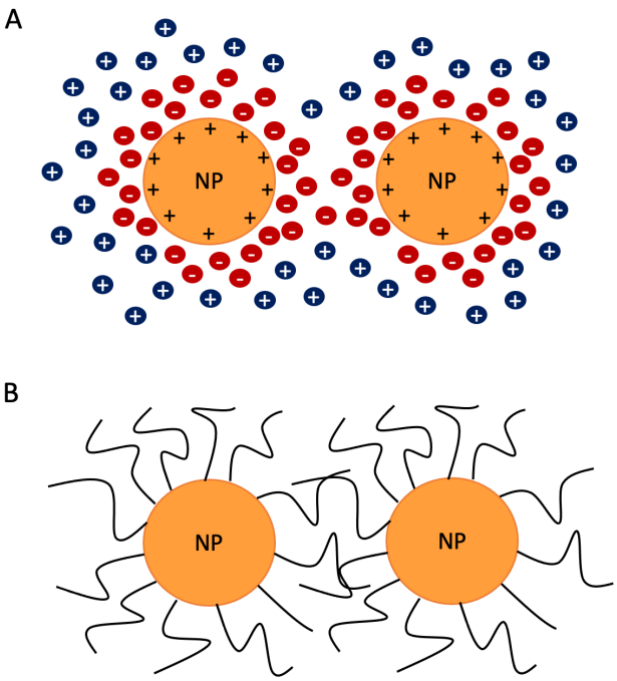

Figure 1-7: Schematic representation of electrostatic and steric stabilizations.
Electrostatic repulsion involves an electric double layer surrounding the NP surfaces and the interaction between these charges is described by Van der Waals forces (A), while in steric stabilization, capping agents adsorbed on the NP surface create a physical barrier between neighbouring NPs (B).

Electrostatic repulsion involves electric double layers surrounding the NPs and the interaction between these charges is described by Van der Waals forces (Soliman, 2018) (Figure 1-7 A). In low ionic strength solutions, the ionic groups attach to the NP surface creating the first charged layer and, as a result, oppositely charged ions will surround it generating an overall electro-neutral double layer

(Amina & Guo, 2020). However, electrostatic stabilization, such as that provided by sodium citrate, is unable to provide colloidal stability in high ionic strength solutions and the electrostatic double layer that ensures the repulsion of equally charged particles is disturbed causing aggregation in the majority of biological media (Moore et al., 2015). The second approach, also known as steric stabilization, is based on a physical barrier on the NP surface (Worthen et al., 2016) (Figure 1-7 B). Steric repulsion forces operate between the coating molecules adsorbed on the surface of adjacent NPs. Depending on their functional groups and their affinity, surface stabilizers can bind the NP surface through different bonds, i.e., electrostatic, hydrophobic and/or covalent interactions (Soliman, 2018). Polyvinylpyrrolidone is one of the strongest and most common capping agents used to stabilize metal NP solutions through steric repulsive forces achieved by hydrophobic interactions (Safo et al., 2019). To provide steric stabilization, NPs must be functionalized after their production during an additional step, while electrostatic stabilization is usually defined during the synthesis phase (Rahme et al., 2007; Rahme et al., 2009). Capping agents, regardless of the type of stabilization provided (electrostatic or steric), can be divided in six categories (Campisi et al., 2016): surfactants (Smith & Korgel, 2008), small organic molecules (Gavia & Shon, 2015), polymers (Baygazieva et al., 2014), dendrimers (Crooks et al., 2001), cyclodextrins (Raveendran et al., 2003; Noël et al., 2014) and polysaccharides (Figure 1-8).

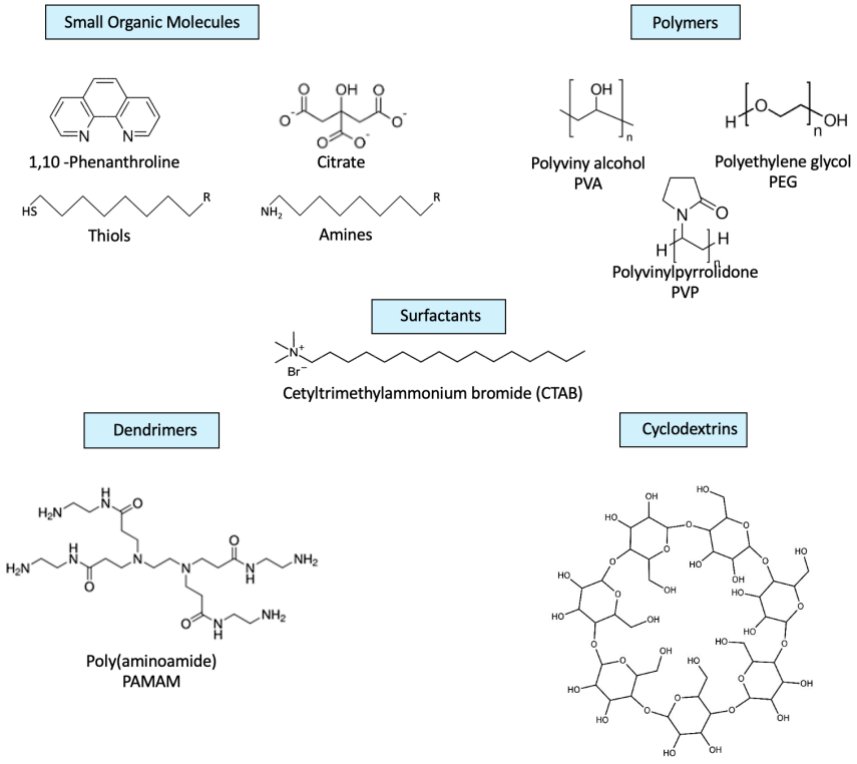

Figure 1-8: NP capping agents.
Representative NP surface stabilizers classified by chemical nature and structure.

1.3 Gold nanoparticles

Metal NPs are used worldwide in various fields including medicine, biology, chemistry, physics, electronics, and cosmetics (Alaqad & Saleh, 2016; Ramalingam, 2019; Leso et al., 2019). These particles, in fact, through surface conjugation with specific chemical groups and ligands can provide valuable platforms exploited as drug delivery and imaging systems (Mody et al., 2010). The category of metal nanoparticles comprises submicron-scale entities made of pure metals, such as colloidal gold, a suspension of nanosized gold particles (AuNPs). The unique optoelectronic and physicochemical properties of spherical AuNPs (Ashraf et al., 2020) have been widely investigated and exploited in many applications, ranging from diagnostics and cancer therapy (Singh et al., 2018) to industrial catalysis (Grisel et al., 2002) and water purification (Ojea-Jiménez et al., 2012). Furthermore, AuNPs are an excellent model for studying the fate and behaviour of NPs in biological systems and environmental scenarios under laboratory conditions, due to their high non-reactivity and biocompatibility with mammalian systems (Connor et al., 2005; Sperling et al., 2008; Azzazy et al., 2011; Li et al., 2016). In various interdisciplinary branches of science and industrial applications, the optical properties of AuNPs, which are the result of their unique interaction with light (Jain et al., 2008), are the most widely exploited of their intrinsic characteristics (Kelly et al., 2003). At the nanoscale the optical properties of systems are dominated by the quantum confinement effects (Loss, 2009).

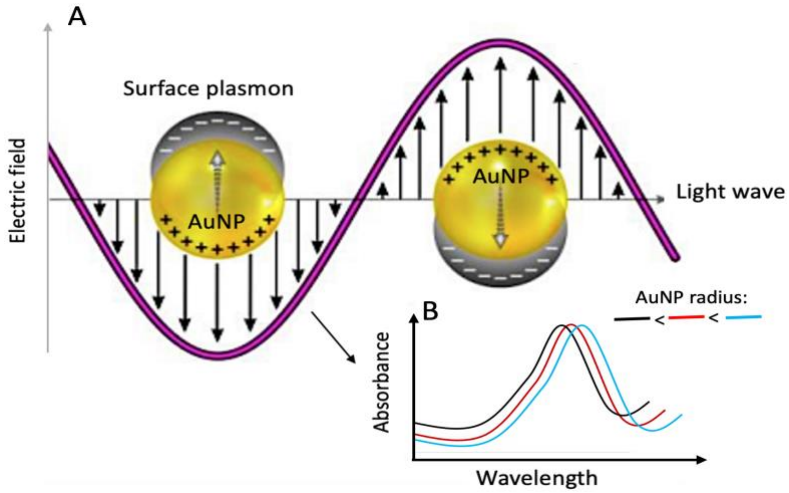

Figure 1-9: Surface Plasmon Resonance (SPR) of AuNPs (Adapted from Masson, 2020).
SPR phenomenon (A) and UV-Vis spectra of AuNPs showing red-shifts in absorption as particle size increases (B). Representative image illustrating the interaction of the electromagnetic field of light with metallic AuNPs. This interaction causes the collective excitation of conduction electrons moving towards the surface of the NP with respect to the positively charged core, in the so-called SPR effect.

The free electrons of the AuNPs, in the presence of the oscillating electromagnetic field of light, undergo an oscillation with respect to the metal lattice (Link & El-Sayed, 2003; Jain et al., 2006). This

phenomenon is called localised surface plasmon resonance (LSPR) and is resonant at a particular frequency of light (Masson, 2020) (Figure 1-9 A). Therefore, the collective oscillation of electrons on the surfaces of AuNPs, at a specific light frequency, causes light absorption and scattering (Karimi et al., 2019) in the ultra-violet (UV), visible (vis) and near-infrared (NIR) wavelength range (Xin et al., 2018). This phenomenon is related to the size and shape of the particles, with 10 nm AuNPs having a maximum absorbance around 520 nm and larger ones showing red-shifts of the LSPR peaks and an increase of the maximum absorbance (He et al., 2005; Mody et al., 2010) (Figure 1-9 B).

These intrinsic characteristics, combined with the possibility of functionalizing the surface of AuNPs with oligonucleotides, antibodies and proteins, provide a useful and versatile tool in many bionanotechnology applications (Yeh et al., 2012; Spampinato et al., 2016).

1.3.1 Synthesis of AuNPs

Over the last decade, several methods have been developed to synthesise monodisperse NPs with controlled size and shape. (Qiao et al., 2017). These techniques can be grouped into three main categories, namely physical, chemical and biological processes (Goutam et al., 2019). In particular, the green synthesis, the most important of all biological methods, emerged in the last years as a research trend in the eco-friendly production scenario of NPs (Naseer et al., 2020). In the green approach, the biosynthesis of nanomaterials occurs through the use of biological materials, such as bacteria, plant extracts, fungi and algae, and aims to implement sustainable processes, minimizing the production of harmful and waste compounds (Agarwal et al., 2017). Nevertheless, despite the rapid development in the field of green synthesis, the most common method in the production of metallic NPs remains the chemical approach (Kim et al., 2018). The Turkevich method is a reliable and reproducible technique used to produce colloidal AuNPs of controlled shape and size (Kimling et al., 2006). The first attempt to produce colloidal AuNPs dates back to 1857 when Michael Faraday reduced chloroauric acid in aqueous solution with phosphor in the presence of carbon disulphide (Faraday, 1857). In the following years many attempts were made to improve the process, until 1951 when Turkevich obtained gold hydrosols by reducing chloroauric acid with sodium citrate (SC) (Turkevich et al., 1951). In such solutions, SC acts not only as a reducing agent, but also as a capping agent, preventing the aggregation of AuNPs by electrostatic repulsion (Andreani et al., 2017). During the synthesis of AuNPs with the Turkevich method, the gold salt is reduced and the gold atoms formed undergo a fast nucleation process followed by a slow growth process leading to the formation of particles (Park et al., 2007). The Turkevich method is still the most common approach for the synthesis of AuNPs, due to the possibility of controlling the size and shape of the particles by changing the reaction conditions (Link & El-Sayed, 1999; Lee et al., 2012).

1.3.2 AuNPs aggregation

Aggregation is the most important physicochemical transformation capable of influencing the stability of a colloidal solution of monodisperse AuNPs and certainly one of the best characterised and studied phenomena. Sodium citrate and other capping agents used during the synthesis of AuNPs play a key role in the formation and growth of the particles, but they also prevent aggregation by increasing the repulsive forces between the particles (Andreani et al., 2017). However, the formation of agglomerates depends not only on the surface characteristics of the particles but also on the surrounding environment, as parameters such as pH and ionic strength can influence colloidal stability (Figure 1-6 A) (Soliman, 2018). The electrostatic repulsion forces present between pristine AuNPs (AuNPs stabilized with sodium citrate) can be shielded and nullified in high ionic strength media by electrolytes present in the aqueous solution, causing attractive interactions between the surfaces of individual AuNPs (Park et al., 2019). The interaction takes place directly with the NP surface (Bastús et al., 2008) or with the NP coating molecules (Barbero et al., 2019). In such cases, aggregation phenomena can be prevented by surface modifications of AuNPs that increase their colloidal stability. The size and chemical nature of these capping molecules determine the degree of stability of the colloidal solution (Chen et al., 2017).

1.3.3 Physicochemical characterization of AuNPs

The safety assessment of ENMs requires comprehensive physicochemical characterizations of the nano-entities, as their properties and behaviour depend on their composition, size, shape and colloidal stability (Powers et al., 2009; Albanese et al., 2012). Since NPs exposed to microenvironments other than the synthesis medium can undergo several transformations and generate nano-objects with a new bio-identity (Bogart et al., 2014), it is necessary to perform a complete characterization of the starting material as well as under experimental conditions. Over the past decade, the unique AuNPs properties, especially the optical ones, have been exploited in a wide range of characterization techniques, such as UV-Vis spectroscopy, dynamic light scattering, zeta potential and electron microscopy (Sepúlveda et al., 2009; Sapsford et al., 2011). The combination of all these characterization techniques provides a robust analysis of the physicochemical properties of NPs and their interaction with the surrounding microenvironment.

1.3.3.1 UV-Vis spectroscopy

Colloidal AuNP solutions exhibit peculiar UV-Vis spectra due to the localized surface plasmon resonance (LSPR) phenomenon and their characteristic profiles and absorbance peaks are strongly correlated with the size and colloidal stability of the particles (Hendel et al., 2014). Alterations in

colloidal stability, as in the case of AuNPs aggregation, cause changes in the UV-Vis spectra due to inter-particle plasmonic coupling and result in the emergence of a second peak at higher wavelengths (Sepúlveda et al., 2009). In particular, changes in resonance peaks occur when the distance between particles is smaller than their diameters, consequently, the UV-Vis profile depends on the distance between AuNPs in the aggregates (Godakhindi et al., 2017).

1.3.3.2 Dynamic light scattering

The size of AuNPs in a solution can be also estimated by dynamic light scattering (DLS), also known as photon correlation spectroscopy (PCS) and quasi-elastic light scattering (QELS) (Nur, 2013). This technique correlates particle size (hydrodynamic diameter) to the random thermal motion of particles known as Brownian motion via the Stokes-Einstein equation (Figure 1-10 B). Both the viscosity of the dispersant and the temperature are taken into account in the equation as they affect the movement of the particles (Stetefeld et al., 2016). The Brownian motion of particles states that smaller particles move faster than larger ones and the light scattered by the particles, measured through a DLS apparatus (Figure 1-10 A), provides information on their rate of diffusion and therefore on their size distribution.

A

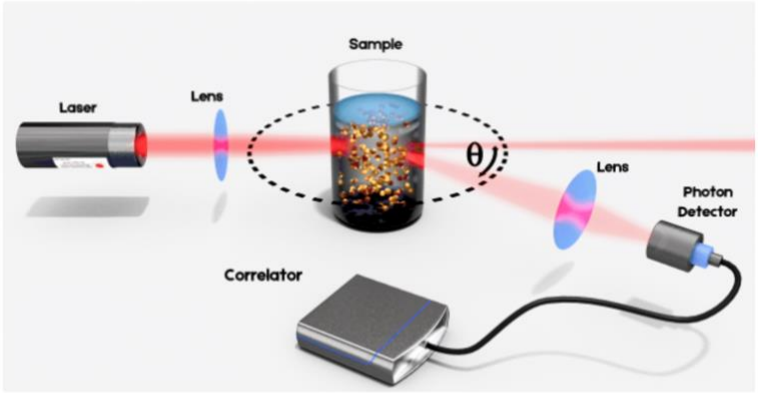

B

$$D = \frac{k_B T}{6\pi\eta R_H}$$

Figure 1-10: Dynamic light scattering (DLS) technology.
Schematic overview of a DLS apparatus (A) (https://lsinstruments.ch/en/theory/dynamic-light-scattering-dls/introduction). A single-frequency gas or solid-state laser beam illuminates the sample and the light scattered by the particles in solution is detected at a known scattering angle (θ) by a fast photon detector. The signals detected by the detector are analysed in the correlator to calculate the hydrodynamic radius distribution of the colloidal solution. The correlation between particle velocity and particle size is given by the Stokes-Einstein equation (B). D, translational diffusion coefficient [m^2/s] (speed of the particles); K_B, Boltzmann constant [$m^2 \cdot kg/K \cdot s^2$]; T, temperature [K]; η, solvent viscosity [$kg/m \cdot s$]; R_H, hydrodynamic radius [m].

1.3.3.3 Zeta potential

The laser doppler velocimetry (LDV) method determines the Zeta (Z) potential, whose value predicts colloidal stability by evaluating the surface charge of the particles in solution (Murdock et al., 2008). The colloidal aggregation state is indirectly measured by converting the electrophoretic mobility (EPM) of NPs, defined as the migration rate of charged particles in a stationary liquid medium due to an applied external electric field, into Z potential values (Nur, 2013). Strong repulsive forces between NPs, as in the case of stable colloidal solutions functionalized with steric capping agents, produce extremely negative or positive Z potentials (greater than +30mV or less than −30mV) (Lunardi et al., 2021).

1.4 Plant-AuNPs interaction

Plant-based nanosafety research focuses on a number of key aspects, *i.e.*, the physicochemical properties of NPs such as material, size and surface chemistry, the interaction of NPs with the surrounding environment, as well as the plant type and route of exposure (Du et al., 2018; Sukhanova et al., 2018; Sanzari et al., 2019; Kranjc & Drobne, 2019; Khan et al., 2019; M. Khan et al., 2019). Although studying the effects of ENMs on plants under natural conditions is considered the best option, issues such as potential alterations in the properties and colloidal stability of NPs once released into the environment make this approach challenging (Barbero et al., 2019). Therefore, nanosafety assessments under reproducible and monitored laboratory conditions help to carry out reliable ecotoxicological investigations (Kim et al., 2008). Since ENMs can change their properties, and thus behaviour, depending on the environment to which they are exposed, a complete characterization is necessary for the starting material as well as under experimental conditions.

AuNPs are widely inert and their physicochemical properties and effects on plants can be studied without physiological side effects of the bulk material (Yang et al., 2017). AuNPs have been used in agriculture applications as fertilizers (Kang et al., 2016) and as on-site detectors of pesticides (Lisha & Pradeep, 2009) with the aim of improving crop yields by lowering the amount of standard chemicals. However, the interaction between AuNPs and particular terrestrial plants can cause species-specific toxicity, affecting their growth, development and reproduction (Ruttkay-Nedecky et al., 2017). Positive, negative and no effects of AuNPs on plants have been described, but despite recent developments in plant nanotoxicology, an unequivocal understanding of their mechanisms of action is lacking (Zia-ur-Rehman et al., 2018; Sanzari et al., 2019; Kranjc & Drobne, 2019).

1.4.1 Phytotoxicity

The environmental concentration of AuNPs predicted by screening models is 0.14 µg L^{-1} in natural waters and 5.99 µg kg^{-1} in soils (Tiede et al., 2009). Under lab conditions, for these concentrations, no measurable physiological effect on plants have been reported (Batley et al., 2013). To evaluate if AuNPs have at all an effect on plants, higher concentrations are tested to assess the maximum potential risk that could be caused by AuNP accumulation. Overall, despite a few contradictory studies, AuNPs have been found to have detrimental effects at high concentrations (≥ 100 mg/L) (Siegel et al., 2018), with particles with a diameter below 5 nm showing increasing toxicity (Pan et al., 2009; Coradeghini et al., 2013; Boyoglu et al., 2013) By contrast, lower concentrations of AuNPs can enhance seed germination, chlorophyll content and improve growth and productivity in several crops and model plants under laboratory conditions (Arora et al., 2012; Kumar et al., 2013; Mahakham et al., 2016). The mechanism underlying AuNP-induced growth-promotion is not yet understood, but understanding how NPs influence plant growth could be useful for improving crop yield in the future (Zhao et al., 2020). On the other hand, some contradictory studies have been reported. Feichtmeier et al. (2015), reported a decrease in the biomass of *Hordeum vulgare* after AuNP treatment at a final concentration between 3 and 10 mg/L.

1.4.2 Effects on plant defence responses

The interpretation of nanotoxicological data must include a thorough evaluation of the immunological effects triggered by engineered NMs, by measuring their effects on the immune responses of environmental organisms (Nogrady, 2021). Furthermore, considering that the interaction of a living organism with external foreign agents is a central issue for its survival and adaptation to the environment, the interpretation of nano-immunosafety data should also consider the concept of dynamic equilibrium between defensive reaction and physiological adaptative behaviour (Boraschi et al., 2020). While several studies have tested the effects of AuNPs on the immune responses of animals and humans, only a few have been conducted on plants. *In vitro* toxicity studies of AuNPs in mammals have found no detectable changes in the concentration of inflammatory markers (Downs et al., 2012; Khan et al., 2013; Yang et al., 2013; Lopez-Chaves et al., 2018), while AuNPs have been associated with dose-dependent imbalances of the oxidative stress levels (Piryazev et al., 2013; Mateo et al., 2014) with higher doses of particles responsible for initial oxidative cell damage (Li et al., 2010). In plants, chitosan NPs have been shown to have positive immunomodulatory effects on *Camellia* sinensis (Chandra et al., 2015), while silver and zinc oxide NPs can lead to altered mitochondrial function, increased reactive oxygen species (ROS) production and lipid peroxidation with consequent membrane damage (Hossain et al., 2015). Only a limited number of works have investigated the

effects of AuNPs on the innate immune system of plants and most of them focus on oxidative burst phenomena. Kumar et al. (2013) reported how AuNP treatments improve antioxidant potential under stressful conditions through enhanced free radical scavenging activity in *Arabidopsis thaliana*.
Considering the scarcity of available information, the overall effects of AuNPs on plants at the physiological and molecular levels remain controversial and their mechanisms of action unclear (Rico et al., 2011; Sabo-Attwood et al., 2012; Zhu et al., 2012; Siddiqi & Husen, 2016), highlighting the need for studies that point in this direction.

1.4.3 Uptake and transport in plants

Though many plants have been tested for their ability to take up various kinds of ENMs, our knowledge is still limited and many aspects remains elusive (S. Ali, 2020). The pore size of cell walls has been determined to be approximately 3-6 nm, a size that precludes the uptake of larger molecules, but some properties of the NPs, such as surface charge, may induce morphological changes in the cell wall, thus affecting pore size and uptake rate (Carpita et al., 1979; Sabo-Attwood et al., 2012). Several studies have shown that neutral or negatively charged metallic NPs are absorbed and translocated to a greater extent by the negatively charged root surface than positive NPs. Indeed, positively charged metallic NPs induce greater mucilage production and remain associated with the root surface due to electrostatic attraction forces (Spielman-Sun et al., 2019; S. Ali, 2020). It has been reported that NPs with a diameter between 3 and 5 nm, and therefore smaller than that of the pores of the root cell wall, can potentially be absorbed by roots through three different mechanisms, i.e., direct passage through the semipermeable epidermal cells, osmotic pressure or capillary forces (Lin & Xing, 2008; Du et al., 2011). NPs crossing the cell wall of root epidermal cells can potentially be translocated to the above-ground tissues via the central vascular cylinder. For this to happen, the NPs present in the apoplast have to cross the Casparian strip barrier by entering into the plant cells via transport proteins in the endoderm cell membrane, through endocytosis or via pores (D. K. Tripathi et al., 2017; Pérez-de-Luque, 2017). Internalized NPs may move between cells through the plasmodesmata and can be translocated to the shoots through the xylem or back into the roots through the phloem (Wang et al., 2012) (Figure 1-11). On the other hand, NPs that are not internalized due to their intrinsic characteristics may aggregate on the Casparian strips (M. Khan et al., 2019) or on the root surface, consequently affecting nutrient absorption (Ruttkay-Nedecky et al., 2017). In the case of foliar exposure, NPs with a diameter of less than 5 nm can potentially penetrate through the cuticle, while for larger particles entry is limited to the stomata (Ruttkay-Nedecky et al., 2017). Absorbed NPs can travel through the phloem tubes and be transported bi-directionally and accumulate in leaves, stems and roots (Wang et al., 2013; Raliya et al., 2016). It has been suggested that internal transport of NPs

larger than 50 nm in diameter occurs apoplastically, while smaller NPs move between the cell cytoplasm of adjacent cells via symplastic transport (Figure 1-11). AuNPs uptake is controversially discussed in the community, with studies showing uptake and even transport within the plant and others ruling it out (Zhu et al., 2012; Judy et al., 2012; Koelmel et al., 2013; Milewska-Hendel et al., 2017). However, the few studies carried out in general on the subject (Siddiqi & Husen, 2016), and in particular on AuNPs (Zhu et al., 2012), state that the interaction, uptake and transport of NPs in plants are affected by the intrinsic physical and chemical properties of the NPs, their dose, capping agents, time and route of exposure, (de la Rosa et al., 2021) as well as the plant species (Spielman-Sun et al., 2019). Currently, as the exact mechanisms underlying the uptake of NPs are not fully understood, further investigations in the area of ENMs-plant interactions are urgently needed (Siddiqui et al., 2015) in order to generate reliable nanosafety approaches and procedures to use in nanotechnology applications.

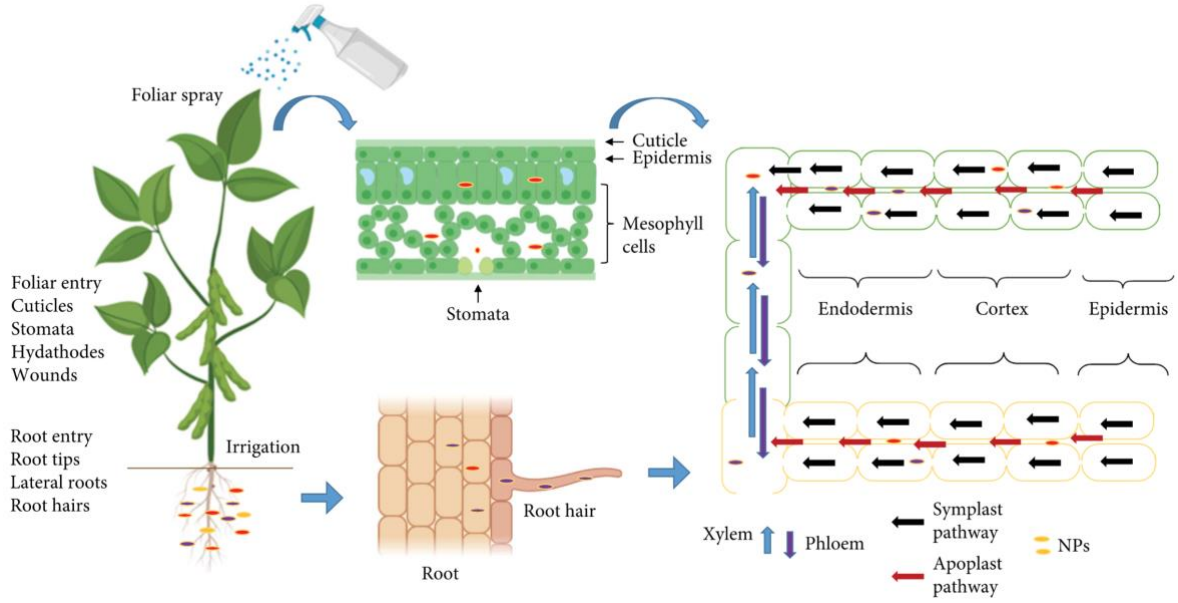

Figure 1-11: NPs uptake and accumulation in plants (Ali et al., 2021).
Schematic representation of the different NP uptake routes (roots and leaves) in plants and the translocation (symplast/apoplast) and accumulation (phloem/xylem) pathways in different plant tissues.

1.5 Aim of the thesis

In recent years, the large-scale production and use of manufactured nanomaterials (NMs) in the most disparate industrial applications has drastically increased the environmental emissions of such products (Bundschuh et al., 2018). In particular, the use of metal nanoparticles (NPs) in newly developed agricultural practices has led to direct exposure of terrestrial habitats to these nanosized composites (Mittal et al., 2020). However, despite recent developments in plant nanotoxicology, an unequivocal understanding of the effects of NPs on plants is lacking, with fundamental information gaps about their mechanisms of action (Kranjc & Drobne, 2019). For these reasons, further investigations and the development of novel nanosafety approaches are urgently needed. The aim of this work was to establish and optimise, under laboratory conditions, stable and reproducible NP-plant exposure systems to test their effects at the physiological and molecular level. Stable and fully characterized gold NPs, representative of one of the most widely used NMs in nanotechnology applications, were tested on Arabidopsis seedlings to study their potential uptake and impact on growth, stress and immune responses. Global changes in the plant transcriptome and proteome after treatments with gold NPs were investigated to get a better understanding of the molecular principles underlying AuNP induced plant responses.

2 Materials and Method

2.1 Materials

2.1.1 Chemicals

Chemicals, used in this work, were purchased from following companies: Agilent, Sigma-Aldrich, Carl Roth, Merck, Dufecha and Qiagen.

2.1.2 Nanoparticles

Table 2-1: Gold nanoparticles used in this work

Nanoparticle	Characteristics
AuNP-SC	11.4 nm ± 0.8 nm in diameter, 2.2 mM sodium citrate tribasic dihydrate (SC, ≥99 % purity) as stabilizer
AuNP-SCTA	13.2 ± 2.2 nm and 4.0 ± 0.6 nm in diameter, 2.2 mM sodium citrate tribasic dihydrate (≥99 % purity) and 200 µM tannic acid (TA) as stabilizers
AuNP-PVP	11.4 nm ± 0.8 nm in diameter, 0.2 mM polyvinylpyrrolidone (PVP, 10 kDa) as stabilizer

2.1.3 Media

The composition of used media is listed in the following table. The indicated components were dissolved with ultrapure water (milliQ water) and each solution was autoclaved (121°C, 20 min).

Table 2-2: Cultivation media

Medium	Components for 1 L
½ MS	2.2 g/L MS-salts, 5% sucrose, set pH 5.7 with KOH
½ MS-agar	2.2 g/L MS-salts, 5% sucrose, set pH 5.7 with KOH, 8 g/L Select-Agar
GS90	Soil mixed with Vermiculite

2.1.4 Plant genotype

In this work, *Arabidopsis thaliana* ecotype Columbia 0 (Col-0) was used in all experiments.

2.2 Methods

2.2.1 Gold nanoparticles synthesis

2.2.1.1 AuNP-SC

To synthetize AuNP-SC 150 mL of 2.2 mM SC aqueous solution (Sigma-Aldrich) was brought to a boil in a 250 mL three-necked round-bottomed flask under reflux, subsequently 1 mL of 25mM chloroauric acid ($HAuCl_4$) was injected in the citrate solution. After 10 min the solution became reddish, synonymous of AuNP formation (~ 10 nm, seeds). The resulting particles are coated with negatively charged citrate ions.

2.2.1.2 AuNP-SCTA

A 150 mL of freshly prepared reducing solution of 2.2 mM SC (Sigma-Aldrich) containing 200 µM TA (Sigma-Aldrich) was brought to a boil in a 250 mL three-necked round-bottomed flask under vigorous stirring. When the temperature reached 70 °C, 1 mL of 25 mM tetrachloroauric acid ($HAuCl_4$) was injected in the solution. In less than 10 s the colour of the solution changed rapidly to blackgray and then to pink-red in the following 1−2 min. The resultant particles (∼3.5 nm) were monodispersed, negatively charged and stable for weeks. Different sequential steps of growth, consisting of sample dilution plus further addition of gold precursor leaded to the desired AuNPs size.

2.2.1.3 AuNP-PVP

Previously synthetized AuNP-SC were incubated overnight with a solution of 0.2 mM PVP (10 kDa) under vigorous stirring. After functionalization, AuNP-PVP were purified by centrifugation, removing or leaving excess PVP depending on the application.

2.2.2 Gold nanoparticle characterization

2.2.2.1 AuNP concentration

Samples were digested with aqua regia (1:3 HNO_3 (70%): HCl (37%)) for 24 h and then diluted with MilliQ water to be further analyzed by induced coupled plasma-mass spectroscopy (ICP-MS) using an ICP-MS NexION 300 from Perkin Elmer.

2.2.2.2 Size determination by electron microscopy

The diameter of the synthesized AuNPs was measured by analysis of images obtained by scanning electron microscopy (SEM) with FEI Magellan XHR SEM, in transmission mode (STEM) operated at 20 kV. Samples were prepared by drop-casting 3µL of the NP dispersion on a carbon-coated copper TEM

grid and left to dry under mild vacuum. To prevent aggregation of the NPs during the drying procedure, they were previously conjugated with 55 kDa PVP. More than 500 particles from different regions of the grid were measured.

2.2.2.3 UV-Vis spectroscopy

UV-Vis spectra were acquired with a Shimadzu UV-2400 spectrophotometer. 1 mL of sample was placed in a plastic cuvette and analyses were performed at time zero or over time in the 300−800 nm range at room temperature. In the case of solidified media, samples were poured into the cuvette prior to jellification.

2.2.2.4 Size and Zeta potential measurements

Laser doppler velocimetry and dynamic light scattering were used to determine the Z-potential and the hydrodynamic diameter of the AuNPs, respectively, employing a Malvern Zetasizer Nano ZS instrument (light source wavelength at 638.2 nm; detector at a fixed scattering angle of 173°). Measurements were performed at 25°C. Diameters were reported as Z-average and polydispersity index (PDI) calculated by cumulative analysis.

2.2.3 Gold nanoparticle sterilization

AuNPs suspensions were sterilized by filter sterilization with cellulose mixed ester (CME) and polyethersulfone (PES) filters, both with a pore size of 0,2 µm, according to the manufacturer´s protocol.

2.2.4 Plant growth methods

2.2.4.1 Seed sterilization

Arabidopsis thaliana ecotype Columbia 0 (Col-0) seeds were surface sterilized by chlorine gas treatment in a desiccator containing 50 mL of 12 % NaClO and 2 mL of 37 % HCl for 4 h. Seeds were dried in a laminar air flow sterile bench for 30 min.

2.2.4.2 Plant growth conditions

All plants were grown in long day conditions with 16 hours light, 8 hours dark, 22°C, 110 µmol m^{-2} s^{-1} light, and 60 % relative humidity.

2.2.4.3 NP exposure in agar-solidified medium

Sterilized seeds were sown on agar plates containing ½ MS medium and stratified at 4°C for 2 days in the dark. Afterwards, plates were incubated for 7 days under controlled long day conditions. Plates were placed vertically to allow root growth along the agar surface. The reducing and stabilizing agents or AuNPs were mixed with the medium, in the indicated concentrations, before jellification (Figure 2-1 A).

2.2.4.4 NP exposure in hydroponic culture

Sterilized seeds were sown on a thin layer of ½ MS agar medium and stratified at 4 °C for 2 days in the dark. Subsequently, the seeds were germinated and grown for 2 weeks under controlled long day conditions. The seedlings roots grow through the agar into ½ MS medium. After 2 weeks, the stabilizing agents or AuNPs were mixed, in the indicated concentration with the ½ MS medium and were incubated for 6 h (Figure 2-1 B).

2.2.4.5 NP exposure in soil

Sterilized seeds were sown on steam-sterilized soil and, after 2 days of stratification at 4°C, were grown for 1 week under controlled long day conditions. Before sowing the soil was imbued with water, stabilizing agent or AuNPs in the indicated concentration and the seedlings were watered every 2 days with 1 mL of the same solution (Figure 2-1 C).

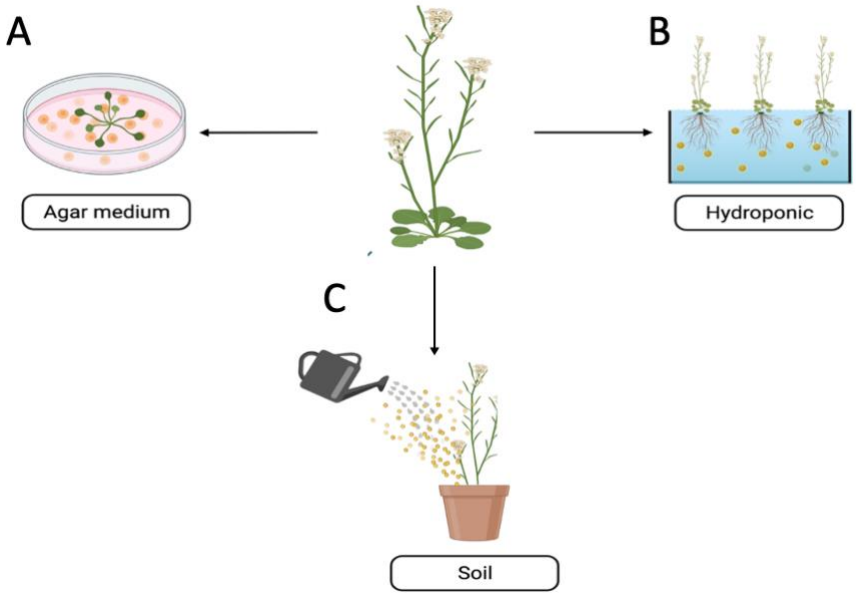

Figure 2-1: AuNP-Arabidopsis root exposure routes.
To assess the behaviour and fate of AuNP after their interaction with Arabidopsis roots, uptake experiments were performed in three different plant growth media, i.e., ½ MS (hydroponic system) (B), ½ MS-agar (A) and soil (C).

2.2.5 RNA-analysis

2.2.5.1 RNA extraction from plant roots

RNA was extracted from 100 mg of Arabidopsis seedling roots treated for 6h and 7d with 10mg/l Au-SCTA or SCTA (SC 2.2 mM; TA 200 µM) in triplicates using the RNeasy Plant Mini Kit (QIAGEN) followed by on-column DNA digestion with the RNase-Free DNase Set (QIAGEN). Total RNA concentration, RNA Integrity Number (RIN) value and rRNA ratio (28S/18S) were evaluated using Agilent2100 Bionalyzer (RNA 6000 Nano Kit, Agilent).

2.2.5.2 Transcriptome sequencing analysis

The BGI Group (Shenzhen, China) performed the total transcriptome sequencing (RNA-Seq) analysis. Samples were sequenced on Illumina HiSeq Platform. The internal software SOAPnuke v1.5.2 was used to filter low quality reads, reads with adaptors or cointaining more than 5% of unknown bases (N). Genome mapping of clean reads was performed using HISAT v2.0.4 (Hierarchical Indexing for Spliced Alignment of Transcripts) software (Kim et al., 2015). The assembler of RNA-Seq alignments into potential transcripts StringTie v1.0.4 has been used to reconstruct transcripts (Pertea et al., 2015). Cuffcompare, a tool of Cufflinks (Trapnell et al., 2012), was used to identify novel transcripts by comparing reconstructed transcripts with genome reference annotation information. The coding ability of those new transcripts has been predicted using CPC v0.9-r2 (Kong et al., 2007). After novel transcript detection, novel coding transcripts were merged with reference transcripts to get a complete reference and clean reads were mapped to it using Bowtie2 v2.2.5 (Langmead & Salzberg, 2012). For each sample the gene expression level was calculated with RSEM, a software package for estimating gene and isoform expression levels from RNA-Seq data (Li & Dewey, 2011). Differentially expressed genes (DEGs) were detected with the nonparametric approach NOIseq method (Parameters: Fold Change >=2.00 and Probability >=0.8) as desribed by Tarazona et al. (Tarazona et al., 2011).

2.2.6 Protein-analysis

2.2.6.1 Total protein extraction

For total protein extraction from roots the material was grinded in liquid nitrogen and mixed in a ratio of 1:3 with ice-cold extraction buffer (10% glycerol, 150 mM Tris/HCl, pH 7.5, 1 mM EDTA, 150 mM NaCl, 10 mM DTT, 0.2% Nonidet P-40, 2% PVPP, 1 tablet of proteinase inhibitor cocktail (Roche) per 10 mL solution). Protein extraction was performed on a rotor at 4ºC for 1 h and the extract was purified

by a centrifuging at 4 ºC, 5000 x g for 20 min. The supernatant was then transferred through a one-layer Miracloth (Roche) in a fresh pre-chilled 1.5 ml tube on ice.

2.2.6.2 NanoLC-MS/MS analysis

The Proteome Center Tübingen performed the nanoscale liquid chromatography coupled to tandem mass spectrometry (LC-MS/MS) on total protein extracts as described. Proteins were purified in a 12% NUPAGE Novex Bis-Tris Gel (Invitrogen) for 10 min at 200 V and stained with Colloidal Blue Staining Kit (Invitrogen). In-gel digestion of proteins was performed as previously described (Borchert et al., 2010). Extracted peptides were first desalted and then labeled using C18 StageTips (Rappsilber et al., 2007) as described elsewhere (Boersema et al., 2009). Samples were labeled with dimethyl "light" ($(CH_3)_2$) and dimethyl "intermediate" ($(CH_1D_2)_2$), respectively. Complete incorporation levels of the dimethyl labels were achieved in all cases. Eluted peptides were mixed in a 1:1 ratio according to measured protein amounts. The analysis of the peptide mixture was performed on an Easy-nLC 1200 system coupled to an LTQ Orbitrap Elite or a QExactive HF mass spectrometer (all Thermo Fisher Scientific) as described elsewhere (Kliza et al., 2017) with slight modifications: peptides were injected onto the column in HPLC solvent A (0.1% formic acid) at a flow rate of 500 nl/min and subsequently eluted with a 227 min (Orbitrap Elite) or 127 min (QExactive HF) gradient of 10–33-50-90% HPLC solvent B (80% ACN in 0.1% formic acid). During peptide elution the flow rate was kept constant at 200 nl/min. In each scan cycle, the 15 (Orbitrap Elite) or 12 (Q Exactive HF) most intense precursor ions were sequentially fragmented using collision-induced dissociation (CID) and higher energy collisional dissociation (HCD) fragmentation, respectively. In all measurements, sequenced precursor masses were excluded from further selection for 60 (Orbitrap Elite) or 30 s (Q Exactive HF). The target values for MS/MS fragmentation were 5000 and 10^5charges, and for the MS scan 10^6 and $3x10^6$ charges, respectively.

2.2.6.3 MS data processing

The MS data were processed with MaxQuant software suite v1.5.2.8 and v1.6.3.4 (Cox & Mann, 2008), respectively. Database search was performed using the Andromeda search engine (Cox & Mann, 2008), which is a module of the MaxQuant. MS/MS spectra were searched against an *Arabidopsis thaliana* database obtained from Uniprot, and a database consisting of 285 commonly observed contaminants. In database search, full tryptic specificity was required and up to two missed cleavages were allowed. Protein N-terminal acetylation, and oxidation of methionine were set as variable modifications. Initial precursor mass tolerance was set to 4.5 ppm and to 0.5 Da at the MS/MS level (CID fragmentation), or 20 ppm (HCD fragmentation). Peptide, protein and modification site

identifications were filtered using a target-decoy approach at a false discovery rate (FDR) set to 0.01 (Elias & Gygi, 2007). For protein group quantitation a minimum of two quantified peptides were required. Perseus software (v1.6.1.3), a module from the MaxQuant suite (Tyanova et al., 2016), was used for calculation of the significance B (p_{sigB}) for each protein ratio with respect to the distance of the median of the distribution of all protein ratios as well as its intensities. All proteins with fold change ≥ 2.00 fold and $p_{sigB} < 0.01$ in a pairwise comparison were considered to be differentially expressed.

2.2.7 Functional assays

2.2.7.1 Recording the phenotypes of plants

Photographs of Arabidopsis seedlings were taken by a Nikon camera (Digital-Sight DS-U1). Growth parameters i.e., rosette diameter, primary root length and lateral root length were measured using the software ImageJ. The lateral root number was determined by counting the number of lateral roots per seedling.

2.2.7.2 Oxidative burst

Production of reactive oxygen species (ROS) was measured in a luminol based assay using a microplate luminometer (CentroPRO LB 962, Berthold Technologies). Small leaf pieces (~ 0,2 cm x 0,2 cm) of 5-6 week-old *A. thaliana* plants were cut and floated overnight in milliQ water. The next day, the leaf pieces were placed individually in one well of a 96-well plate containing 90 µl of the reaction mix (5 µM Luminol L-012 (Wako Chemicals USA) and 2 µg/mL horseradish peroxidase (Applichem, Germany). The background was measured for ~ 15 min after which the elicitors, in a final concentration of 100 nM, were added. The ROS burst was monitored for 30 min for 3 plants per line and three leaf pieces per plant for one assay (=9 replicates).

2.2.7.3 FOX assay

The level of lipid hydroperoxides (LOOHs) was assessed with the modified colorimetric ferrous oxidation xylenol orange (FOX) assay as described (Hermes-Lima et al., 1995; Schmieg et al., 2020). Leaf pieces of 5-6 week-old *A. thaliana* plants were cut (~ 0,2 cm x 0,2 cm) and left equilibrate overnight in milliQ water. The next day, the leaf pieces were elicited for 30 min (final concentration 100 nM) and immediately stored at -80°C. Samples were homogenized in ice-cold HPLC grade methanol (ratio 1:15) and centrifuged at 14,000 rcf and 4°C for 5 min. Supernatants were kept at -80°C until their usage. The assay was performed in a 96-well microplate, with each well containing: 50 µL of 0.25 mM FeSO4, 50 µL 25 mM H2SO4, 50 µL of 0.1 mM Xylenol Orange, 30 µL of sample supernatant and double-distilled water (ddH2O) until to reach a final volume of 200 µL. For each

biological sample three replicates and a sample blank (50 µL of 0.25 mM $FeSO_4$ replaced by 50 µL of ddH_2O) were prepared. Samples were incubated at room temperature for 120 min before to measure the absorbance at 570 nm with an automated microplate reader (Bio-Tek Instruments, Winooski VT, USA). Subsequently, 1 µL of 1 mM cumene hydroperoxide solution (CHP) was added in each well and a second measurement (580 nm) was acquired after an incubation period of 30 min. Both measurements were set in relation to a master blank value, which consisted of 200 µL of ddH_2O. For each sample the final absorbance was calculated subtracting the sample blank from the sample values. Cumene hydroperoxide equivalents (CHPequiv./mg wet weight) were calculated using the following equation:

$$CHPE = \frac{ABS580}{\mathrm{ABS580 + CHP}}\ x\ Volume\ CHP\ x\ \frac{Total\ Volume}{Sample\ Volume}\ x\ Dilution\ Factor$$

$$= \frac{ABS580}{\mathrm{ABS580 + CHP}}\ x\ 1\ x\ \frac{200}{30}\ x\ 15$$

2.2.7.4 Statistical analysis

Statistical significance between groups was evaluated using one-way ANOVA combined with Tukey's honest significant difference (HSD) test. FOX assay data were tested with a two-way nested ANOVA followed by Dunnett´s post-hoc test; data were normally distributed (Shapiro-Wilk test) and showed homogeneity of variances (Levene´s test). Significant differences are indicated with different letters ($p < 0.01$). Statistical evaluations were performed using the JMP 15.0.0 software.

2.2.8 Transmission electron microscopy (TEM)

Seedlings were grown and treated as indicated in the section 2.2.4. Samples were collected from the exposure medium and fixed with 2.5% glutaraldehyde and 2% formaldehyde in MTSB [microtubule stabilizing buffer: 50 mM Pipes, 5 mM EGTA and 5 mM MgSO4, pH 7] for 90-120 minutes at room temperature. Thereafter, small pieces of root tips were embedded in 2% agarose in phosphate-buffered saline solution [PBS: 137 M NaCl, 2.7 M KCl, 8.1 M $Na_2HPO_4X2H_2O$, 1.5 M KH_2PO_4, pH 7.2] and cut into small blocks, about 1-1.5x1-1.5x1-1.5 mm in size. After washing with double distilled aqua, agarose blocks were stained with 1% aqueous osmium tetroxide (OsO_4) (EMS; Hatfield, PA) for 90 minutes. After another washing step in double distilled aqua, agarose blocks were fixed and stained with 1% aqueous uranyl acetate (UA) for 60-90 minutes. The fixation was followed by dehydration in a graded series of ethanol (30% - 50% - 75%- 100%). After incubation with pure acetone, samples were infiltrated with 10%, 25%, 50%, 75% epoxy resin in acetone and twice with pure epoxy resin. Samples

were polymerized for at least 48 h at 60°C. Ultrathin sections, of about 70 nm, were cut with a Leica ultramicrotome (EM UC7). Selected sections were stained with 1% aqueous UA (5 min) and Reynolds lead citrate (3 minute) (Reynolds, 1963), others were left unstained in order to improve visibility of endocytosed NPs. Sections were viewed in a JEOL JEM-1400plus TEM at an accelerating voltage of 120 kV. Images were taken with a 4K CMOS TemCam-F416 camera. Contrast and brightness were adapted using Adobe Photoshop CS5. The scale bar has been set using ImageJ software.

3 Results

In this study, the physicochemical behaviour of engineered gold nanoparticles (AuNPs) in plant growth media was tested, as well as their toxicological potential in *Arabidopsis thaliana* plants. Assessing the physiological and molecular effects of nanoparticles (NPs) on model plants provides insight into the ecological risk resulting from exposure to these natural or manmade materials and their potential hazard to human health through food chain contamination (Stampoulis et al., 2009). AuNPs were chosen to evaluate the outcomes of NP-plant interaction as they represent one of the most widely used nanomaterials in academic research and industrial products. Different electrostatic and steric surface stabilizers were tested and a comprehensive physicochemical characterization of stable colloidal AuNPs was carried out over time after dispersion in plant growth media. The unique optical properties of metal nanoparticles (MNPs), mainly due to their localized surface plasmon resonance (LSPR), were exploited to determine shape, size, agglomeration state and concentration changes by UV-Vis spectroscopy (Evanoff Jr & Chumanov, 2005; Tomaszewska et al., 2013). Particle size and surface area were also estimated by combining two different techniques, i.e., dynamic light scattering (DLS) and laser doppler velocimetry (LDV). The DLS method estimates the hydrodynamic diameter of NPs, while LDV determines the Z potential, whose value predicts the colloidal stability by assessing the surface charge of the particles in solution (Murdock et al., 2008). To complete the physical characterization, scanning electron microscopy (SEM) images of all representative NPs batches used in this study were obtained and analysed. An important aspect in the assessment of the ecological risk deriving from the environmental release of NPs is the determination of their potential uptake, translocation and accumulation by plants (Ma et al., 2010). The fate of AuNPs in treated plants was assessed by transmission electron microscopy (TEM) studies. In addition, representative physiological parameters such as biomass, root length and shoot development were measured to assess the response of Arabidopsis seedlings to abiotic stress caused by NPs treatment. At the molecular level, reactive oxygen species (ROS) and lipid peroxidation detection assays were performed after exposure to AuNPs, revealing specific NP-related phenomena involved during the NP-plant interaction, i.e., partial protection against oxidative stress. Finally, complete transcriptomic and proteomic analyses were performed after short- and long-exposure treatment with AuNPs.

3.1 Identification of physicochemical properties of AuNPs

Although gold is naturally present in the environment, in the last decade, the exponential use and disposal of AuNPs, has increased the level of this chemical element in soil and water (Bundschuh et al., 2018). However, while many studies have been conducted on the accumulation and physiological

effects of gold in various plant species (Anderson et al., 1999; Wilson-Corral et al., 2012; Tiwari et al., 2016), a comprehensive investigation on the fate and behaviour of AuNPs after their release into the environment is lacking. It is important to highlight that NPs exhibit a really high reactivity due to the characteristic large surface area and the low coordination of atoms at the surface (Khan et al., 2019). This reactivity, once the particles are dispersed in a new medium, can lead AuNPs toward a more stable thermodynamic state via aggregation and interaction with the molecules present in the new environment (Bastús et al., 2012; Barbero et al., 2019). These transformations, which depend on the properties of both NPs and media, can generate new nano-objects with possible different bio-identity (Moore et al., 2015; Fuller & Köper, 2018; Nierenberg et al., 2018). Therefore, it is important to characterize the behaviour of AuNPs in the working media, in order to correctly correlate the pristine and potential characteristics of the final NPs with the observed biological effects (Barbero et al., 2017). The peculiar optoelectronic and physicochemical properties of AuNPs have been widely exploited to perform the characterization of the colloidal solutions used in this study.

3.1.1 Synthesis and surface engineering of high quality, monodispersed AuNPs

Three different types of AuNPs, with an average diameter of 12 nm and different surface stabilizers, were synthesized following two seeded-growth methods. The first synthetic approach, reported by Bastús et al. (Bastús et al., 2011), is an inverted Turkevich method in which sodium citrate (SC) has several functions including that of gold reducer and NP-stabilizer. The resulting type of particles (AuNP-SC) are representative of the most commonly employed AuNPs. The main difference in the production method of the second type of AuNPs used (AuNP-SCTA), which was developed to produce high quality and monodisperse AuNPs, is the addition of traces of tannic acid (TA) as co-reducer and stabilizer (Piella et al., 2017). The third category of particles produced in this study was synthesized following the first seeded-growth method reported (Bastús et al., 2011), but at the end of the synthesis the electrostatic stabilizer SC was removed and replaced in a further functionalization step with the steric coating polyvinylpyrrolidone (PVP) 10 kDa (AuNP-PVP). The weak electrostatic interactions of the citrate molecules with the surface of the metallic AuNPs allow the particles functionalization with others compounds that replace the citrate ions (Ranoszek-Soliwoda et al., 2017). In this specific case, the capping agent PVP binds covalently to AuNPs stabilizing the colloidal solution more effectively compared to an electrostatic stabilization. After the SC was removed, the excess PVP present in the solution was not removed to avoid NP re-aggregation. To calculate the final concentration of NPs in colloidal solutions, the total mass of the inorganic gold (Au) was determined by induced coupled-plasma-mass spectroscopy (ICP-MS) (Hsiao et al., 2016). The peculiar optoelectronic and physicochemical properties of AuNPs, such as surface plasmon resonance (SPR),

were exploited to perform a comprehensive physicochemical characterization. Morphology, size, surface charge and aggregation state of AuNPs in the three different synthesized batches were investigated using several techniques, i.e., ultraviolet-visible (UV-Vis) spectroscopy, dynamic light scattering (DLS), laser doppler velocimetry (LDV) and scanning transmission electron microscopy (STEM) (Figure 3-1).

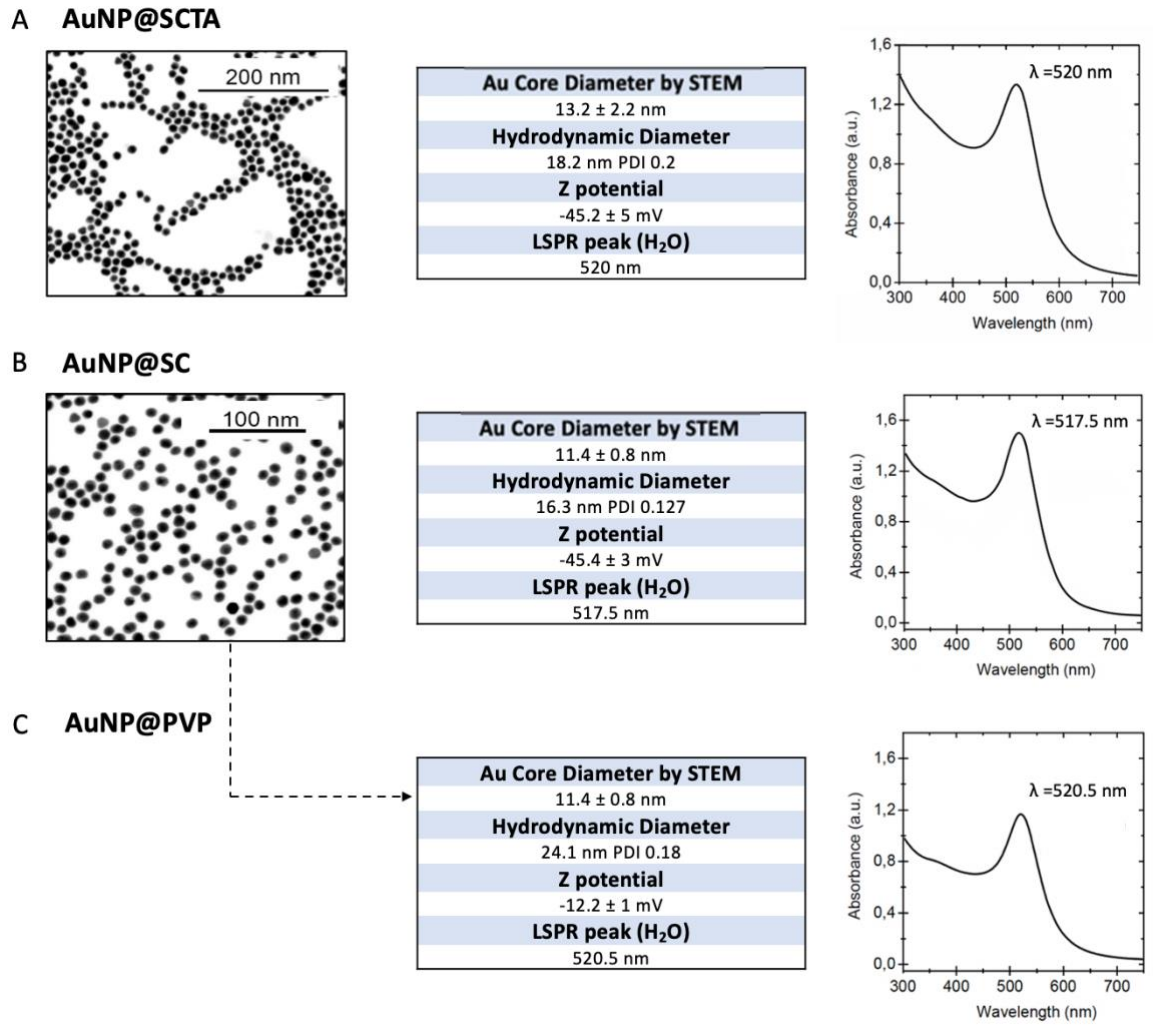

Figure 3-1: Physicochemical characterization of AuNPs stabilized with different surface engineering strategies.
Complete characterization of AuNP-SCTA, AuNP-SC and AuNP-PVP (A, B, C respectively) using different techniques. The left-hand panel shows bright field - scanning transmission electron microscopy (STEM) images of AuNP-SCTA and AuNP-SC (from which AuNP-PVP derive); while the central-hand panel shows, for each synthesized batch, the physicochemical parameters of the particles evaluated by STEM, DLS, LDV and UV-Vis spectroscopy. On the right-hand panel, the UV-Vis spectra of AuNP-SC, AuNP-SCTA and AuNP-PVP dispersed in H_2O are shown.

STEM images of AuNP-SC and AuNP-SCTA were analysed, estimating a particle core diameter of 11.4±0.8 nm and 13.2±2.2 nm respectively. Since STEM does not detect the PVP stabilizer, the Au core size and aggregation state of AuNP-PVP are measured by analysing the STEM image of AuNP-SC (from which they derive before functionalization), while the other characterization techniques are

performed on the batch after the functionalization step. Therefore, the average Au core diameter of AuNP-PVP is the same as that of AuNP-SC (11.4±0.8 nm). In contrast, the hydrodynamic diameter estimated by DLS also takes into account the surfactants and stabilizers present on the surface of the particles. While the stabilizers SC and SCTA increase the particle diameter by approximately 5 nm (16.3 nm and 18.2 nm respectively), PVP increases the hydrodynamic diameter by about 13 nm (24,1 nm). PVP minimizes the surface tension attacking the core of the AuNPs and gradually encapsulating their surface. In the end, a polymer shell will form increasing the average size of AuNPs (Koczkur et al., 2015). Colloidal NP stability was assessed by monitoring the zeta potential (Z) of all batches. The Z potential measures the effective electric charge on the nanoparticle surface determining their stability in suspension (Selvamani, 2019; Rasmussen et al., 2020). The Derjaguin-Landau-Verwey-Overbeek (DLVO) theory, developed by Derjaguin and Landau (Derjaguin, 1941) and by Verwey and Overbeek (Verwey, 1947) in the 1940s, describes how van der Waals and electrostatic forces can stabilize colloidal dispersions, as opposed to steric stabilization by polymeric stabilizers (e.g. PVP). In the presence of only electrostatic repulsion forces between the particles, as in the case of AuNP-SC and AuNP-SCTA, DLVO theory claims that Z potentials greater than approximately + 30 mV or less than -30 mV lead to monodispersity (Barbero et al., 2019). Therefore, their Z potential values (-45.4±3 mV and -45.2±5 mV respectively) are considered to have sufficient repulsive force to maintain the colloidal systems stable. By contrast, the AuNP-PVP sample has a steric stabilizing component that prevents the aggregation of the NPs and which is independent of the ionic concentration. Its Z potential value (-12.2±1 mV) depends on the residual SC in solution after the functionalization with PVP. UV-Vis spectroscopy is a simple and reliable technique that takes advantage of the strong absorbance band of AuNPs in the visible region as a result of their unique optical characteristic i.e., localized surface plasmon resonance (LSPR) (Huang & El-Sayed, 2010). The absorbance of the sample correlates linearly to the concentration of nanoparticles in solution; while the peak absorbance wavelength increases with the particle diameter (Mauriz, 2020). In addition, aggregation states of AuNPs are accompanied by a change in the maximum absorbance (λmax), to a longer wavelength in the spectrum (redshift phenomenon), as well as the broadening of the adsorption peaks and the decrease of peak intensities. In this experiment, the UV-Vis spectra of all three batches used in this study showed monodisperse AuNPs and non-aggregation states. (Göeken et al., 2015).

3.1.2 Over time characterization of AuNPs dispersed in plant growth media

It is well known that despite the inertness of bulk gold (Au) (Hammer & Norskov, 1995), AuNPs exhibit higher reactivity due to their high surface-to-volume ratio, the incomplete valence of surface atoms, which leaves external sites available to interact with donor-acceptor species, and their colloidal nature

(Toma et al., 2010; Mahato et al., 2019). This reactivity, which translates in instability once the particles are dispersed in a medium other than that of synthesis, leads to the aggregation and interaction of AuNPs with the molecules present in the new environment soughing for a more stable thermodynamic state. The interaction occurs directly with the NP surface (Bastús et al., 2008) or with the NP coating molecules (Barbero et al., 2019). These transformations may depend on the properties of both NPs and media and generate new nano-sized materials with potentially different biological identities. Therefore, it is important to characterize the evolution of AuNPs once dispersed in the working media in order to understand the nature and extent of these transformations and to correctly correlate the pristine and evolving features of NPs with the observed biological effects (Abbas et al., 2020). In this study, three different coatings (SC, STA and PVP) were tested in order to achieve colloidal stability. Over time physicochemical characterization of AuNP-SC, AuNP-SCTA and AuNP-PVP (final concentration of 10 mg/L) was performed in the plant working media ½ Murashige and Skoog (½ MS) and ½ MS agar (Figure 3-2). Once dispersed in ½ MS, AuNP-SC underwent fast aggregation, pointed out by an immediate emergence of a second localized surface plasmon resonance (LSPR) peak at around 650 nm in the UV-vis spectra (Figure 3-2 A) (Sepúlveda et al., 2009). This aggregation was probably due to the increase in ionic strength by mono- and divalent inorganic ions in the media (½ MS presents a salinity of 23 mM). The ions in the media can screen the negative charges provided by the SC present on the surface of the AuNPs, responsible for the electrostatic repulsion between particles (Cosgrove, 2010; Abbott & Holmes, 2013). In contrast, the UV-vis spectra of AuNP-SCTA dispersed in ½ MS showed no changes up to 6 h of exposure. After 9 h, changes in the shape of the spectrum were observed, showing the start of a typical aggregation profile leading to complete aggregation after 15h (Figure 3-2 C) (Sepúlveda et al., 2009). This result indicated that AuNP-SCTA exhibited good colloidal stability up to 6 hours of exposure in the hydroponic medium, while after 9 hours the NPs start to aggregate slowly. The presence of TA is the only difference between the two types of AuNPs. This organic molecule functions as NP-stabilizer, increasing the stability of the particles against salt-driven aggregation, conferring an effective higher surface charge or partial steric stabilization and preventing NP aggregation. Regarding the aggregation of AuNP-SCTA observed in ½ MS after 9 h, it could be hypothesised that the organic molecules (e.g., sucrose) present in the medium in excess of NP-stabilizers, could progressively replace the NP stabilizers on the NP surface, conferring a negative effect on stabilization and support aggregation. However, further studies will be necessary to precisely understand the role and nature of TA in the stabilization of AuNP-SCTA. AuNP-PVP, on the other hand, showed complete stability in the liquid medium until the last measurement, after 3 weeks (Figure 3-2 E). PVP, a hydrophilic polymer, is one of the best known and widely used NPs capping agents. This molecule provides steric protection against aggregation by creating an amorphous layer

around the core of the particles. Steric stabilizers ensure a more effective colloidal stability than electrostatic ones (Koczkur et al., 2015).

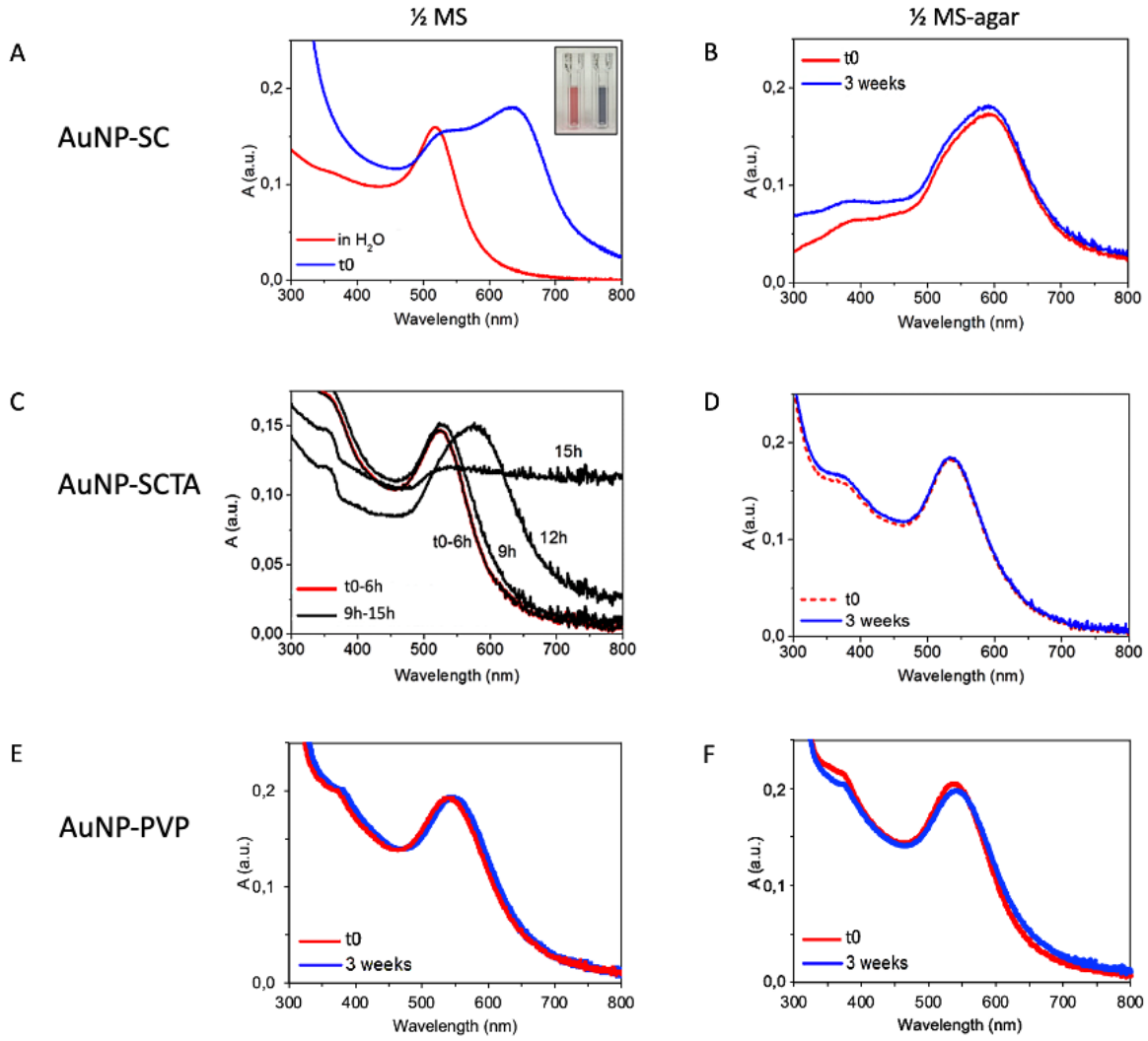

Figure 3-2: Over time physicochemical characterization of AuNPs in plant working media.
UV-Vis spectra of AuNP-SC, AuNP-SCTA and AuNP-PVP, dispersed in ½ MS (A, C and E respectively) and in ½ MS-agar media (B, D and F), in a final concentration of 10 mg/L at time 0 (t0) and over time; (A) representative photograph of stable (left) and aggregate (right) AuNP-SC dispersed in ½ MS. Cuvettes with pure ½ MS or ½ MS-agar were used as reference.

The UV-vis spectra of AuNP-SCTA and AuNP-PVP exposed to ½ MS-agar showed high stability at least up to 3 weeks (Figure 3-2 D, F). In contrast, AuNP-SC dispersed in ½ MS-agar showed an initial aggregation which, unlike in ½ MS, did not evolve over time (Figure 3-2 B). Probably, the interaction with agar molecules and the rapid increase of viscosity due to the jellification of the medium, as well as the reduced number of particles (aggregation is directly proportional to concentration), prevent further aggregation. Note that below 10^{10} NP mL^{-1} the probability of collision decreases to zero, so even if their surface is not passivated, they do not aggregate. In light of these observations, AuNP-

SCTA and AuNP-PVP were chosen over AuNP-SC in the subsequent physiological study, allowing the use of stable AuNPs to correctly correlate the bio-identity of the NPs with the observed effects on Arabidopsis.

3.2 Physiological effects of AuNPs coatings on *A. thaliana* growth

Considering the exponential development witnessed in the last decade in the field of nanotechnology, the assessment of the safety of nanomaterials is a pivotal aspect (Fadeel et al., 2018). In particular, it has been reported that the modification of the physicochemical or biological characteristics of the surfaces of the nanoparticles, through the introduction of capping agents, plays an important role in determining their toxicity (Holland et al., 2016). These surfactants strongly influence the behaviour of NPs by determining their interaction with the surrounding environment (Barbero et al., 2019). For this reason, it is necessary to determine the type and concentration of the capping agent as well as the chemical nature of the interaction taking place between NPs and surfactants (from weak van der Waals forces to strong covalent bonds) in order to rule out their possible negative effects on organisms and the environment.

3.2.1 Capping agents: SCTA vs PVP

In this study, stable colloidal AuNPs, after dispersion in the plant growth media ½ MS and ½ MS-agar, were obtained using two different coatings, i.e., sodium citrate (2.2 mM) with traces of tannic acid (200 µM) (-SCTA) and polyvinylpyrrolidone 10 kDa (1 mM) (-PVP). Their toxicity at different concentrations, ranging from 0 to 30 mg/L, was investigated by evaluating the growth of *A. thaliana* root over a period of 1 week. (Figure 3-3). Sterile Col-0 seeds, germinated and grown in ½ MS-agar vertical plates supplied with 0.5% sucrose and different concentrations of stabilizer, were incubated under long day conditions (16 hours light, 8 hours dark) for 7 days. At the end of the treatment, the plates were photographed and the root length was measured using Image J software. The capping agent -SCTA, at the pH of the plant growth media (5.7), is negatively charged while the surfactant -PVP is neutral, but unlike the latter is attached to AuNPs by covalent bonds. While the NP-stabilizer -SCTA resulted to be non-toxic for Arabidopsis seedlings (Figure 3-2 A), the polymer -PVP significantly affected the root length of the treated plants (Figure 3-2 B). It is important to highlight that there are several methods for functionalizing the surface of nanoparticles with PVP. Generally, the most common technique requires, after the removal of the SC and the conjugation of the PVP to the particle surface, the removal of the dispersed PVP present in excess in the colloidal solution. However, over time physicochemical characterizations of AuNP-PVP in the ½ MS plant working medium have shown that the final purification step affects the stability of the colloidal solution already after one hour

(Figure 3-3 C). In contrast, AuNP-PVP colloidal solutions obtained by eliminating the purification step after conjugation with PVP are stable over time in the ½ MS medium (Figure 3-2 E). For this reason, the PVP used during the functionalization process has not been removed, allowing to calculate the precise quantity of the stabilizing agent present in the solution and to carry out toxicity studies.

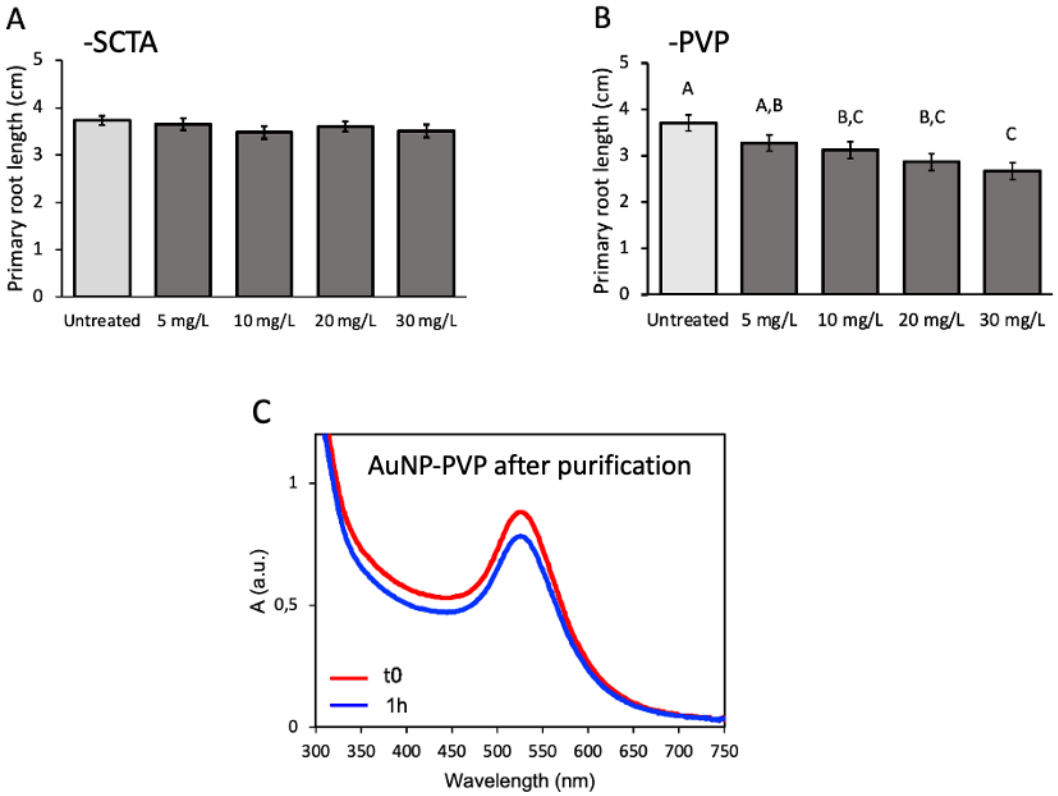

Figure 3-3: Toxicity of surface stabilizing agents on A. thaliana seedling roots.
Arabidopsis seedlings were grown under long day condition on ½ MS-agar medium supplemented with different concentrations of PVP (A) and SCTA (B), ranging from 0 to 30 mg/L. Seedlings were harvested after 7 days and the root length was measured using Image J software. Bars represent the mean ± SE (n=20). The one-way ANOVA method was performed combined with the Tukey's honest significant difference (HSD) test. Significant differences are indicated with different letters ($p < 0.01$). (C) Over time physicochemical characterization of AuNP-PVP in ½ MS liquid medium after purification. Purification performed through double centrifugation at 25.000 x *g* for 15 minutes and resuspension in ultrapure water.

It can be assumed that the toxicity of PVP is due to the excess amount present in the colloidal solution, rather than the actual amount conjugated to the particles. For these reasons, the steric PVP coating, despite its ability to provide long-term stable colloidal NPs, cannot be used in plant growth assays due to its toxicity. In contrast, SCTA stabilizer resulted to be an optimal solution for long- and short-time exposure experiments in liquid and solid plant media, respectively (see section 3.1.2). Several batches of AuNP-SCTA with very similar physicochemical characteristics were produced and tested. The results of the physiological studies, after treatment with AuNP-SCTA, were fully reproducible between the different batches, making the output of this study very robust.

3.2.1.1 AuNP-SCTA sterilization

In order to discriminate the AuNPs effects from the possible physiological and molecular changes induced in plants by microbial contaminants such as, e.g., (pathogenic) bacteria and fungi, the sterility of the colloidal solution is a fundamental requirement. Moreover, the choice of the most appropriate NPs sterilization method, to avoid changing in the structural stability, is essential (Subbarao, 2016). To sterilize AuNP-SCTA solutions, before their application in physiological and omics assays, physical filtration methods were chosen. Two different filter materials i.e., cellulose mixed ester (CME) and polyethersulfone (PES), both with a pore size of 0,2 µm, were tested. To analyse possible changes in the particle concentration or their aggregation state, UV-Vis spectra, before and after filtration, were acquired (Figure 3-4).

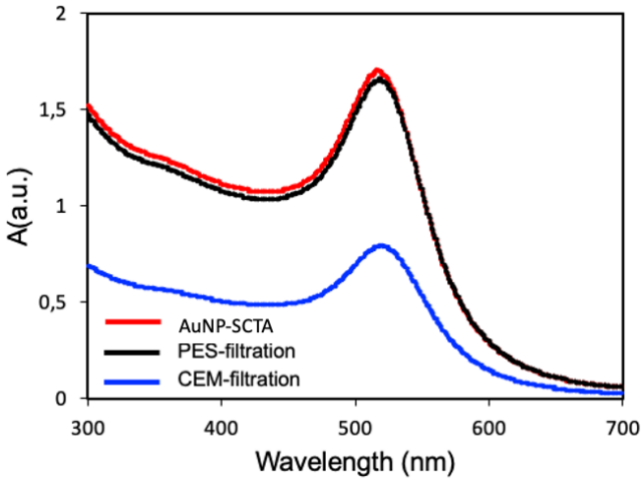

Figure 3-4: UV-Vis spectra of AuNP-SCTA before and after sterilization with different filter materials.
UV-vis spectra of AuNP-SCTA before (red line) and after sterilization with PES (blue) and CME (black) filters were acquired with a Shimadzu UV-2400 spectrophotometer. The analysis was performed in the 300−800 nm range at room temperature.

The CME filter, a standard hydrophilic membrane commonly used for a broad range of applications, was shown to significantly affect the amplitude of the spectra revealing a drastically reduced AuNP-SCTA concentration. By contrast, the PES filter, a hydrophilic and low protein binding membrane, did not change the spectra and therefore did not affect the concentration of AuNP-SCTA. No changes in the overall shape of the UV-Vis spectrum were observed, indicating that no alterations of the physicochemical properties of the AuNPs occurred. These results showed how the PES-filter can remove biological contaminations without altering the initial physicochemical properties of AuNP-SCTA. Therefore, PES membranes were used in all subsequent experiments for NP sterilization.

3.3 Physiological effects of AuNP-SCTA on *A. thaliana* growth

In the present study, *Arabidopsis thaliana* was used as a model plant to investigate the effects of AuNP-SCTA exposure on growth and development. As shown in Figure 3-5, AuNP-SCTA, in a range from 0 to 20 mg/L, affected Arabidopsis root growth in a dose-dependent manner with a maximal effect at 10 mg/L, while the NP-stabilizer SCTA (SC 2.2 mM; TA 200 µM) did not affect the primary root length at any of the tested concentration (Figure 3-3 A). For this reason, 10 mg/L AuNP-SCTA was chosen as final concentration in all following experiments.

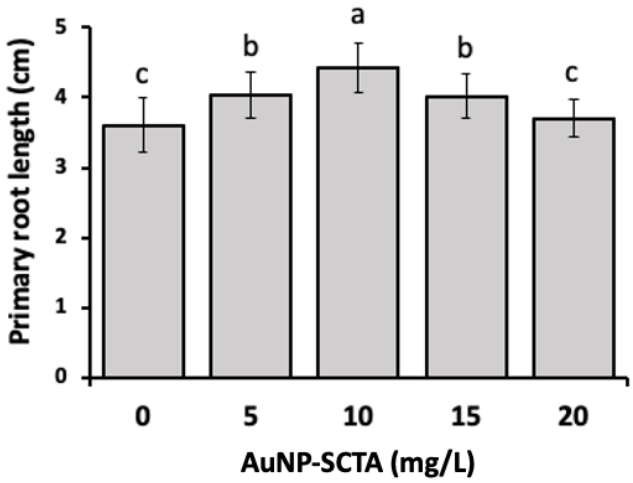

Figure 3-5: AuNP-SCTA affect Arabidopsis root growth in a dose-dependent manner
AuNP-SCTA exposition promote Arabidopsis root growth in dose-dependent mode. Wild-type Arabidopsis seedlings were grown for 7d on agar-solidified ½ MS medium containing different concentrations of AuNP-SCTA, in a range from 0 to 20 mg/L. Results shown are means ± SE (n=20). Based on one-way ANOVA test, combined with Turkey´s honest significant difference (HSD), different letters indicate statistically significant differences at $p<0.01$. All experiments were repeated two times with similar results.

Physiological analyses were performed in order to evaluate Arabidopsis responses to abiotic stress caused by AuNP-SCTA exposure. Seedlings, grown under controlled long day conditions, were harvested after 7 days and representative parameters were recorded i.e., primary root length, rosette diameter, number of lateral root and lateral root length. For each parameter another set of plants was grown in presence of SCTA (SC 2.2 mM; TA 200 µM) as a control. While SCTA did not affect plant growth and development, AuNP-SCTA had a positive influence on all parameters tested. Seedlings germinated and grown on AuNP-SCTA containing medium developed a longer primary root, with an enhancement of 1.2 folds compared to control seedlings (Figure 3-6 A). Furthermore, the lateral root number and length were positively affected upon AuNP-SCTA treatment displaying, compared to the controls, an increase of 1.7 and 1.5 fold, respectively (Figure 3-6 E, F). Shoot development was also influenced by AuNP-SCTA exposure in the same way as the root system (Figure 3-6 B). The size of the rosette diameters was enhanced by 1.3 folds in comparison to control seedlings.

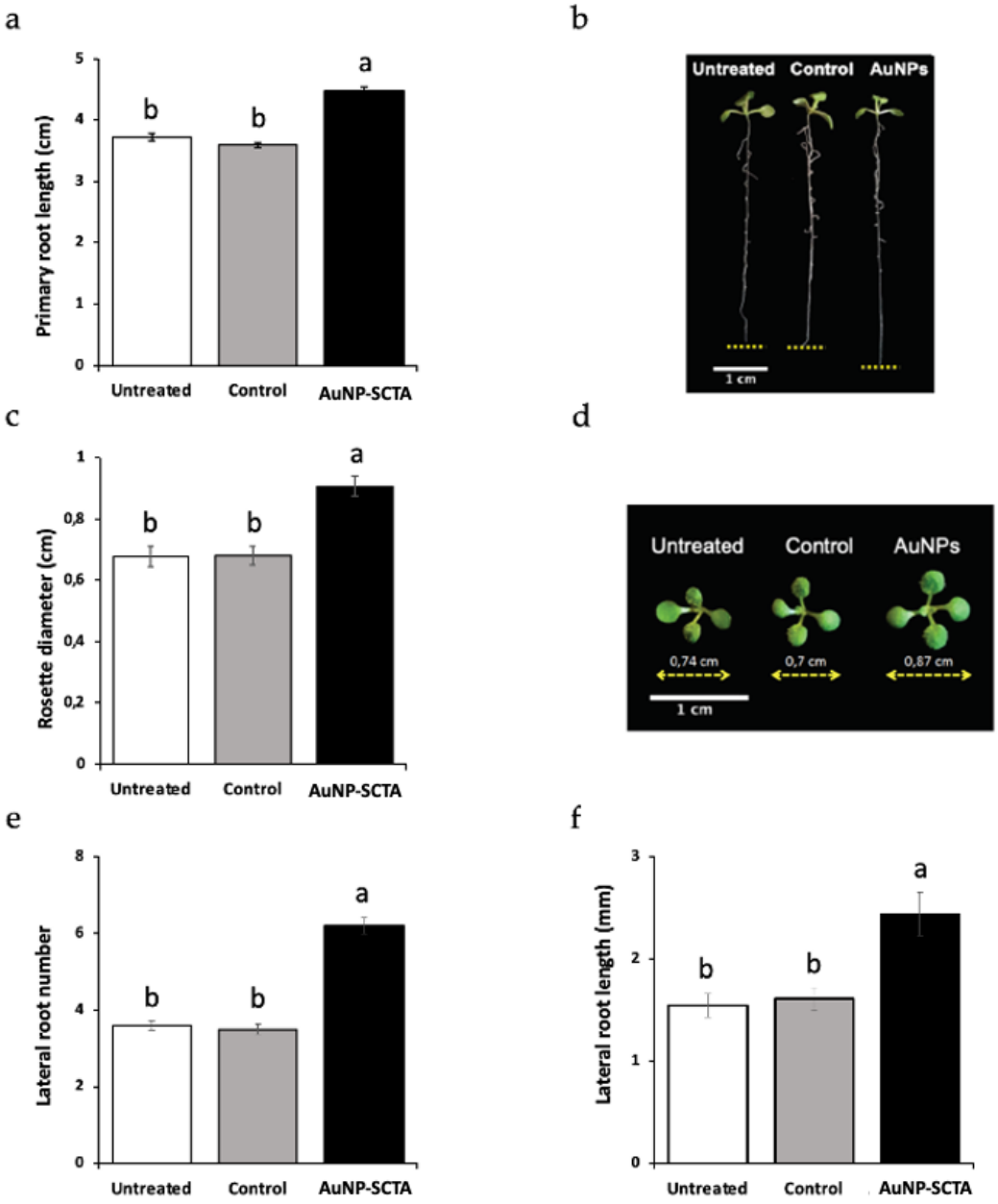

Figure 3-6: AuNP-SCTA exposition enhances growth of Arabidopsis seedlings.
Wild-type Arabidopsis seedlings were grown for 7d on agar-solidified ½ MS medium containing 10 mg/L of AuNP-SCTA or SCTA (SC 2.2 Mm; TA 200 µM) (control) or on unsupplemented medium (untreated control). Growth parameters were scored: Primary root length (A) and representative picture of A (B). Rosette diameter (C) and representative photograph of C (D). Lateral root number (E). Lateral root length (F). Results shown are means ± SE with n=20. Based on one-way ANOVA test, combined with Turkey´s honest significant difference (HSD), different letters indicate statistically significant differences at $p<0.01$. All experiments were repeated two times with similar results

3.4 Immune responses upon AuNP-SCTA treatment

NP have been reported to be able to affect the innate immune system in animals (Boraschi et al., 2020). To assess whether they have an influence on plant immune responses different innate immune

defensive reactions in plants were evaluated. Production of reactive oxygen species (ROS) in the apoplast and lipid peroxidation are typical cellular events triggered by the plant surveillance system that detects highly conserved microbe- or pathogen-associated molecular patterns (M/PAMPs) via cell surface-located pattern-recognition receptors (PRRs) in a process called pattern-triggered immunity (PTI) (Saijo et al., 2017).

The cellular response of Arabidopsis thaliana to abiotic stress resulting from nanoparticles exposure was initially measured as reactive oxygen species (ROS) production or oxidative burst (Figure 3-7 A). To detect the ROS-burst in Arabidopsis a luminol-based chemiluminescence assay was used. The horseradish peroxidase, in presence of ROS, catalyses the oxidation of luminol to 3-aminophthalate with emission of light at 428 nm. The monitored oxidative burst was measured as emitted light and recorded as relative light units (RLU). As shown in Figure 4a no ROS production has been detected after exposure to milliQ water (untreated control), AuNPs-SCTA (100 mg/L) or coating solution SCTA (SC 2.2 mM; TA 200 µM) (control). As positive control the PAMP flg22 was added in a final concentration of 100 nM. The same concentration of the elicitor was used as treatment also in combination with AuNPs-SCTA (10 or 100 mg/L) or SCTA as controls. While the coating solution did not affect the level of ROS production caused by flg22 treatment, AuNPs-SCTA influenced the level of recorded ROS. In particular, in presence of 10 mg/L AuNPs-SCTA the PAMP (flg22) signal decreases. Furthermore, a 10 times higher NPs concentration (100 mg/L) has been tested and a further decrease in the level of ROS has been detected.

In order to discriminate between a real decrease in the ROS production and a mere interference in the absorbance detection, due to the unique optical AuNPs properties, a lipid peroxidation assay has been performed (Figure 3-7 B). Cellular and organelle membranes, due to their high polyunsaturated fatty acids (PUFAs) content, are particularly susceptible to ROS-induced peroxidation (L.-J. Su et al., 2019). The applied colorimetric ferrous oxidation xylenol orange (FOX) assay has been modified to quantify lipid hydroperoxides (LOOHs) in plant extracts. In the 10 and 100 mg/L AuNPs-SCTA plus flg22 treatments, the level of lipid peroxidation decreases significantly in comparison to the elicitor flg22 treatment (Figure 4b). Furthermore, the treatment with 100 mg/L AuNP-SCTA resulted in a further lowered lipid hydroperoxide level compared to the treatment with just 10 mg/L AuNP-SCTA. The FOX assay confirms the oxidative burst assay results, clearly pointing out that AuNPs-SCTA and PAMPs co-exposure reduces the PAMP induced ROS burst and subsequent lipid peroxidation rather than scavenging the light in the luminol based ROS assay. The underlying mechanism of this effect is still elusive but it indicates that AuNP-SCTA might be able to detoxify ROS and shift the balance between growth and immunity trade-off to the growth side.

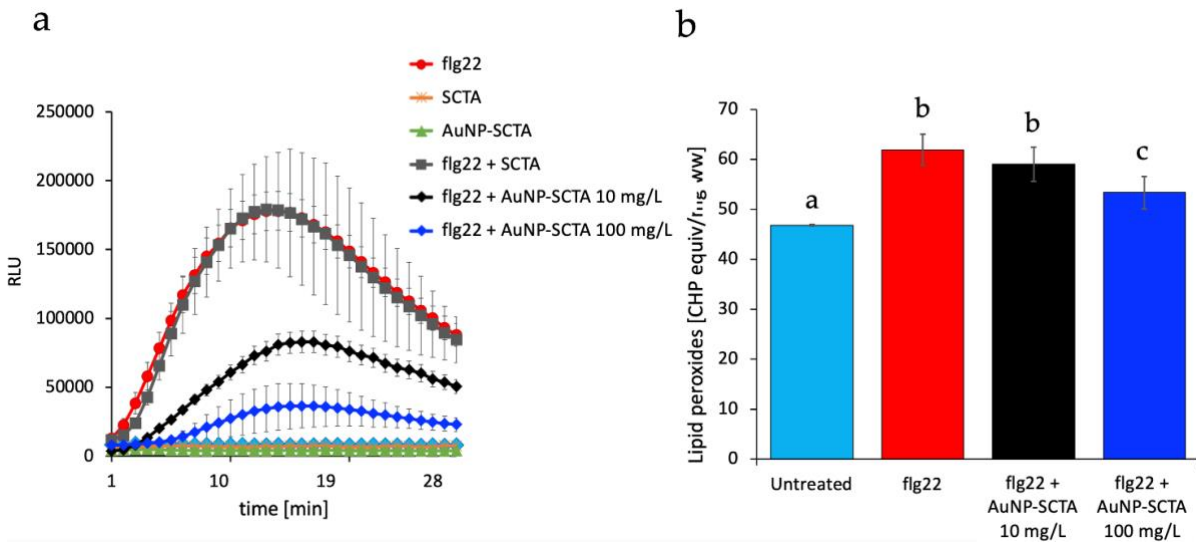

Figure 3-7: AuNPs-SCTA decrease ROS production and lipid peroxidation levels.
ROS production measured with a luminol-based assay in leaf squares of Arabidopsis Col-0 (A). ROS production is represented as relative light units (RLU) after elicitation with milliQ water (untreated control), flg22 (100 nM) (positive control), AuNPs-SCTA (100 mg/L), SCTA (control), flg22 + SCTA or flg22 + AuNPs-SCTA 10 or 100 mg/L. Results are mean ± SE (n=9). The experiment was repeated two times with similar results. Lipid peroxides level, expressed as CHP equiv/ mg ww, was measured in Arabidopsis leaves with the FOX assay (B). After treatment with milliQ water (untreated control), flg22 (100 nM) (positive control) or flg22+AuNPs-SCTA (10 or 100 mg/L), results are represented as mean ± SE of three independent experiments. Based on two-way nested ANOVA followed by Dunnett´s post-hoc test, data were normally distributed (Shapiro-Wilk test) and showed homogeneity of variances (Levene´s test). Different letters indicate statistically significant differences at $p < 0.01$.

3.5 Transcriptomic analysis of the effect of AuNP-SCTA in A. thaliana

To untie the molecular nature of the plant-NP interaction, whole transcriptome analyses were performed on Arabidopsis seedling roots after short- (6h) and long- (7d) exposure with 10 mg/L AuNP-SCTA in hydroponic culture and agar-solidified medium (6h and 7d, respectively). As controls, seedlings were treated with SCTA (2.2 mM SC; 200 µM TA). Samples were sequenced on an Illumina HiSeq Platform. The average genome mapping rate was 94.66% and the average gene mapping rate was 92.04%. Raw data for both experimental conditions and all three replicates, are shown in Appendix Table A-1. As shown in Figure 3-8 A and B, a total of 651 differentially expressed genes (DEG) were identified after short- term treatment and 6 DEGs after long-term exposure. While 121 genes were upregulated after 6 h of AuNP treatment, 530 genes were downregulated. After 7 d 3 genes were up- and 3 genes downregulated. Relevant DEGs after 6h and 7d of treatment with expression information are listed in Appendix Table A-2 and A-3 respectively. Gene Ontology (GO) classification (molecular biological function, cellular component and biological process) and KEGG pathways are represented in Appendix Figures 1-A and 2-A. In both conditions, genes involved in response to external stimuli and cellular and metabolic processes are overrepresented within the DEGs.

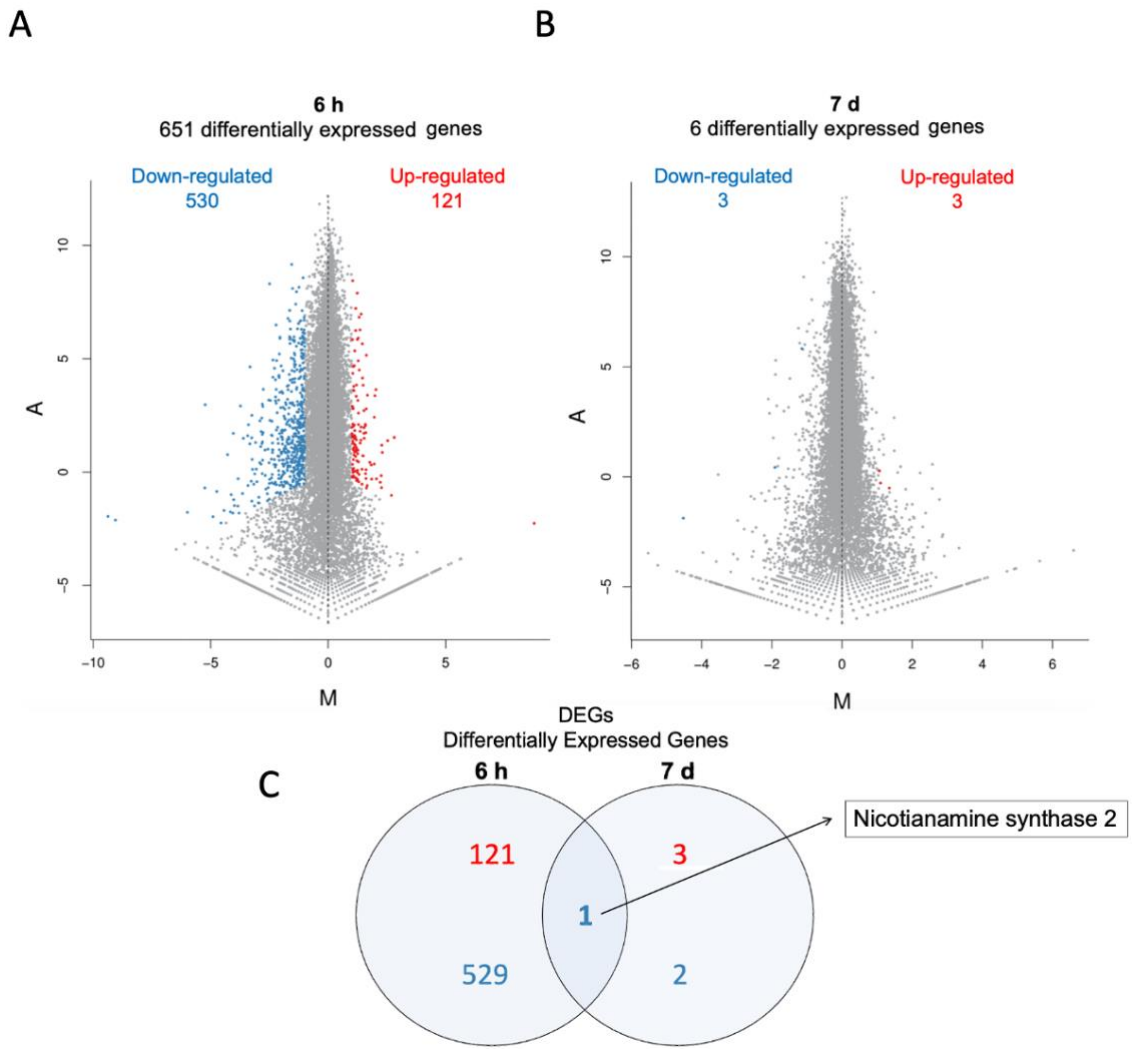

Figure 3-8: DEGs after AuNP-SCTA treatment.
MA plot representing DEGs (upregulated genes red dots; downregulated genes blue dots) and non-DEGs (grey dots) in Arabidopsis seedlings after short- (A) and long-term (B) AuNP-SCTA treatment (6h and 7d, respectively), detected by RNA-Seq data analysis. X axis represents value M (log2 transformed fold change of a gene´s expression values) and Y axis represents value A (log2 transformed mean expression level). Venn diagram displaying the total number of up- (red) and down (blue)-regulated differentially expressed genes in both treatments and the name of the overlapping gene (C).

In particular, after short-term exposure the majority of genes involved in disease resistance, defence response, response to oxidative stress and metal response are downregulated. This indicated that immune and oxidative stress responses are negatively affected during AuNP exposure. DUF642 L-GalL-responsive gene 2 (DGR2, At5g25460), a gene involved in growth and development of Arabidopsis plants, was up-regulated. DGR2 has a key role in Arabidopsis root elongation and shoot development (Gao et al., 2012; Cruz-Valderrama et al., 2019). Downregulation of immune response genes and upregulation of growth factors indicate a shift in the trade-off between immune and growth effects and may explain the growth promotive effects of AuNPs. The Nicotianamine synthase 2 gene, (NAS2, At5g56080), the only shared DEG between the two conditions, encodes for a protein involved in the synthesis of nicotianamine (Figure 3-8 C). Mutants in NAS2 show altered metal contents, indicating a

role in metal uptake or response (Klatte et al., 2009). After 7 d of NP exposure, only 6 DEGs were detected, compared to the 651 genes identified after 6 h, clearly pointing out that transcriptome changes are relevant only at early time points after AuNP treatment.

3.6 Proteomic analysis of the effect of AuNP-SCTA in A. thaliana

To further understand the mechanisms underlying the effects of AuNPs on *Arabidopsis thaliana* seedlings, proteomic analyses were performed on roots using mass spectrometry. Global changes in protein expression have been investigated in Arabidopsis seedlings in the same experimental setup as used for the transcriptome analyses. Protein extracts were analysed *via* nano-liquid chromatography double mass spectrometry (NanoLC-MS/MS-spectrometry).

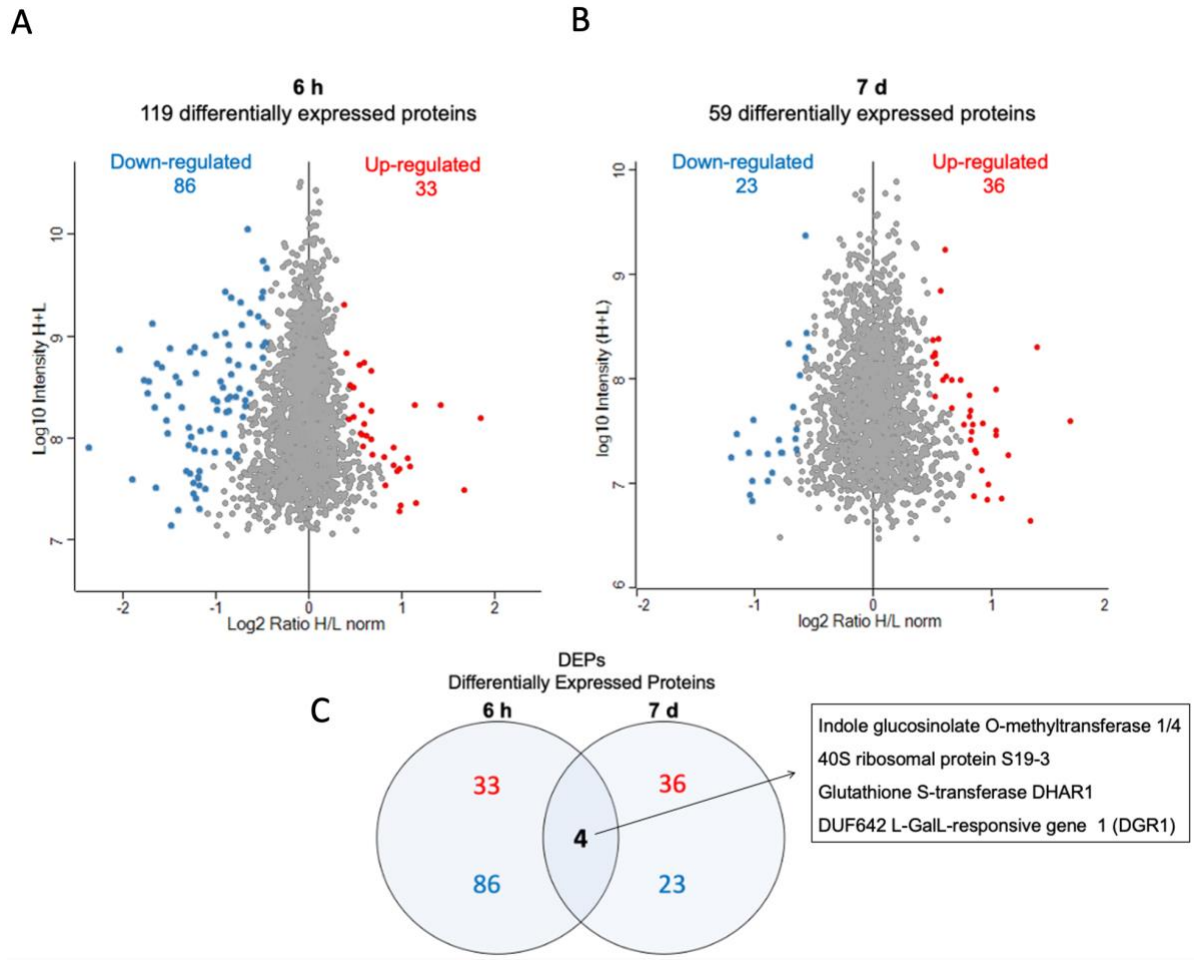

Figure 3-9: DEPs after AuNP-SCTA treatment.
Volcano plot representing DEPs (upregulated proteins: red dots; downregulated proteins: blue dots) and non-DEPs: grey dots in Arabidopsis seedlings after short- (A) and long-term (B) AuNP-SCTA treatment (6h and 7d, respectively) and detected by nano-liquid chromatography with tandem mass spectrometry (NanoLC-MS/MS) of total protein extracts. X axis represents the $\log_2$ transformed fold changes; Y axis represents the $\log_{10}$ transformed intensity (in log10), with H representing the treatment and L the control. Venn diagram displaying the total number of up- (red) and down- (blue) regulated differentially expressed proteins in both treatments and the protein names of the 4 overlapping proteins (C).

As shown in Figure 3-9, from a total of 2727 detected proteins after 6 h exposure and 2503 after 7 d exposure, 119 and 59 differentially expressed proteins (DEPs), respectively, have been identified. Lists of up- and down-regulated proteins after short- and long-treatment, along with their expression profiles are listed in Appendix Table A-4 and A-5. Furthermore, we sorted the DEPs in Gene Ontology (GO) categories (molecular biological function, cellular component and biological process) and KEGG pathways, as shown in Appendix Figures 3-A and 4-A. DEPs significantly overrepresented after both treatments are involved in metabolic processes, protein synthesis and response to stimuli. Oxidative stress related proteins are mainly downregulated as shown on the transcriptome level. The overlap analysis of the different timepoints has revealed the protein DGR1 (DUF642 L-GalL-responsive gene 1, At1g80240) that has been investigated for its role during the development of Arabidopsis thaliana (Gao et al., 2012) (Figure 3-9 C). After 7 d of treatment DGR1 and DGR2 were both upregulated, while after 6 h of treatment only DGR1 was initially downregulated. In the transcriptome analyses, the gene encoding for DGR2 was also detected to be up-regulated. GSTF6 (Glutathione S-transferase F6, At1g02930), another DEG shared between treatments, encodes for a downregulated glutathione transferase involved in defense mechanisms. The finding of DGR2 and GSTF6 in both DEGs and DEPs indicated that these are reproducibly and robustly regulated genes/proteins upon AuNP exposure. As DGR1 and DGR2 were previously described to be involved in growth and development, differential regulation of these genes/proteins may explain why AuNPs have a positive effect on Arabidopsis growth.

3.7 AuNP-SCTA uptake and detection in *A. thaliana* roots

To evaluate the fate of AuNP-SCTA after their interaction with Arabidopsis roots, uptake experiments were performed in three different plant growth media, i.e., ½ MS, ½ MS-agar and soil (Figure 3-10).

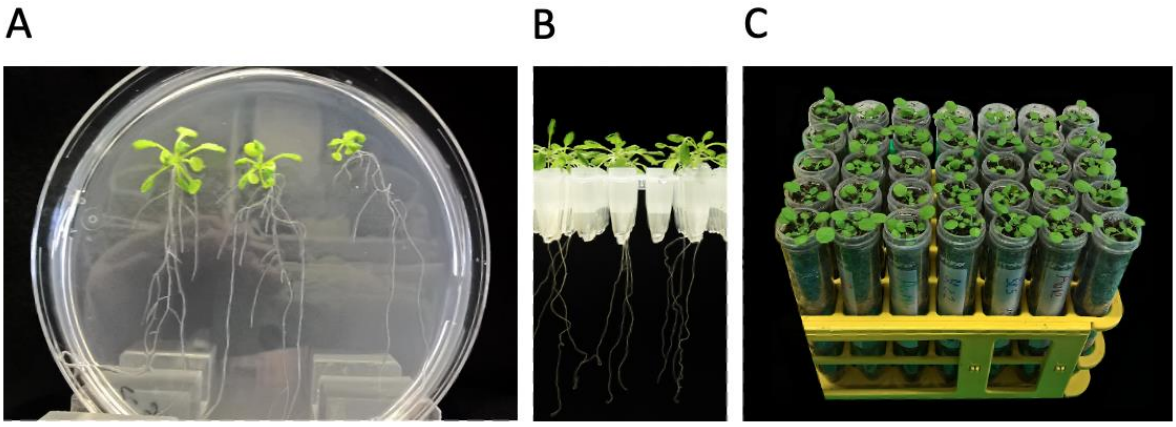

Figure 3-10: *A. thaliana* growth media.
Representative photographs of Arabidopsis seedlings germinated and grown on agar plate (A), hydroponic system (B) (picture © C. Bernstein) and soil (C).

As the pore size of cell walls has been determined to be approximately 3-6 nm (Carpita et al., 1979), 4 nm AuNP-SCTA (SC 2 mM, TA 200 µM) were used in all uptake experiments in order to avoid any mechanical barriers. High quality sub-10 nm monodispersed particles were synthetized as reported by Piella et al. (Piella et al., 2016) and a comprehensive physicochemical characterization was performed (Figure 3-11).

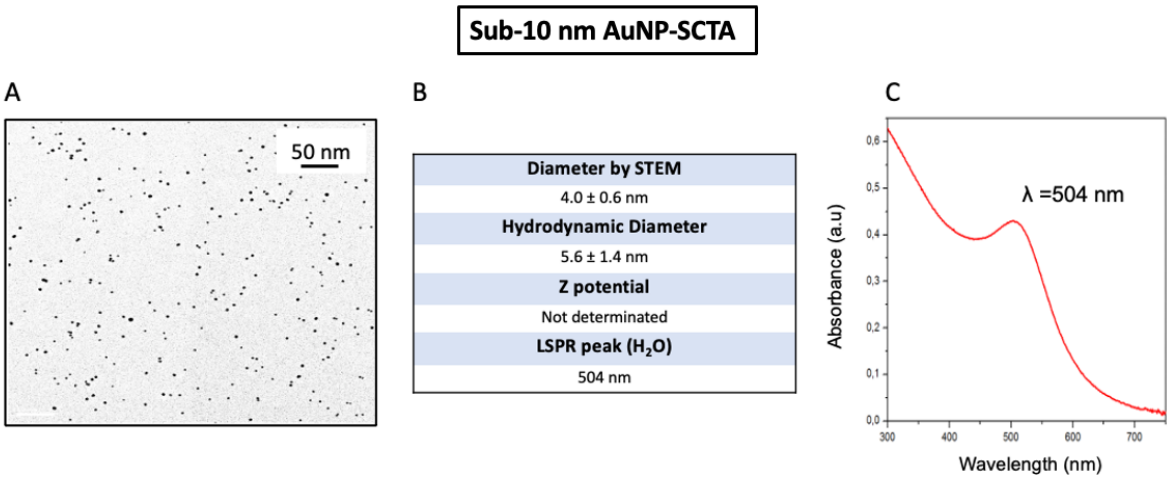

Figure 3-11: Physicochemical characterization of high-quality sub-10 nm, monodispersed AuNP-SCTA. The left-hand panel shows a bright field - scanning transmission electron microscopy (STEM) image of 4 nm AuNP-SCTA (A). The central-hand panel shows the physicochemical parameters of the particles evaluated by STEM, DLS and UV-Vis spectroscopy (B), while the right one shows the UV-Vis spectrum of AuNP-SCTA dispersed in H_2O (C).

The final concentration of NPs in colloidal solutions was determined by induced coupled-plasma-mass spectroscopy (ICP-MS) (Hsiao et al., 2016). Shape, size and aggregation state of the synthesized batches were investigated by ultraviolet-visible (UV-Vis) spectroscopy, dynamic light scattering (DLS) and scanning transmission electron microscopy (STEM). STEM images were analyzed estimating a particle core diameter of 4±0.6 nm, while the hydrodynamic diameter measured by DLS, which also takes into account the stabilizers on the surface of the particles, resulted to be 5.6±1.4 nm. Due to the small size and high energy of the 4 nm particles it was not possible to estimate the Z potential value. The shape and maximum absorbance (λmax) of the colloidal solution (504 nm) excluded possible aggregation phenomena. Considering the small size of the newly synthetized 4 nm AuNP-SCTA, and consequently their higher reactivity compared to the 12 nm particles used in the previous experiments (see section 3.1.2), new over time physicochemical characterizations in ½ MS and ½ MS-agar media were carried out, testing two different concentrations, i.e., 10 mg/L and 6 mg/L (Figure 3-12).

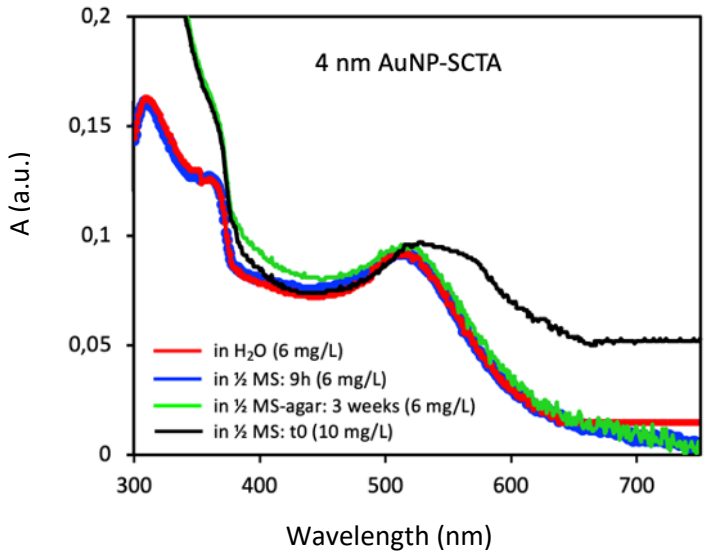

Figure 3-12: Over time physicochemical characterization of 4 nm AuNP-SCTA in plant working media. Overtime UV-Vis spectra of 4 nm AuNP-SCTA dispersed in H_2O (red line), ½ MS (blue and black) and ½ MS-agar (green), in a final concentration of 6 or 10 mg/L. Cuvettes with pure ½ MS or ½ MS-agar were used as reference.

Once dispersed in ½ MS, 4 nm AuNP-SCTA concentrated 10 mg/L underwent fast aggregation. In contrast to 12 nm AuNP-SCTA at the same final concentration (Figure 3-2 C, D), the SC and TA surface stabilizers were unable to effectively maintain charge repulsion between the particles when dispersed in the new environment resulting in aggregation (Cosgrove, 2010; Abbott & Holmes, 2013). The different behaviour exhibited by 4 nm AuNP-SCTA is directly related to their smaller size and higher reactivity. By contrast, UV-vis spectra of AuNP-SCTA dispersed in ½ MS and ½ MS-agar at a final concentration of 6 mg/L showed no changes up to 9 h and 3 weeks of exposure respectively, pointing out how the final concentration of colloidal AuNPs in the media can influence their stability. For this reason, 4 nm AuNP-SCTA in a final concentration of 6 mg/L were used in short-(6h) and long-term (7d) exposure uptake experiments in ½ MS and ½ MS-agar respectively (Figure 3-13). Sterile Col-0 seeds were germinated, grown and treated under long day conditions (16 hours light, 8 hours dark) in soil and in vertical ½ MS-agar plates for 1 week, while in the hydroponic system the seedlings were grown for 2 weeks and treated for 6 hours. As controls, for each treatment a parallel set of seedlings was grown and treated in the same condition with the coating solution SCTA (SC 2 mM, TA 200 µM). Due to the low reactivity and high stability of the gold, AuNPs don't undergo dissolution, therefore it was not necessary to use the bulk gold material as a control to study the role of gold ions in the uptake. At the end of each treatment, the roots were collected and prepared for transmission electron microscopy (TEM) visualization. The analysis was focused on the epidermal cells of the root tip. In each condition, despite the different growth methods used, the outcomes were the same. No AuNP-SCTA were detected in the cytoplasm of epidermal root cells and the few particles identified were found outside or stuck in the cell wall (Figure 3-13 B, E, H). The detected nanoparticles show no aggregation

and have maintained a spherical shape. No particles have been identified in the controls (Figure 3-13 A, D, G).

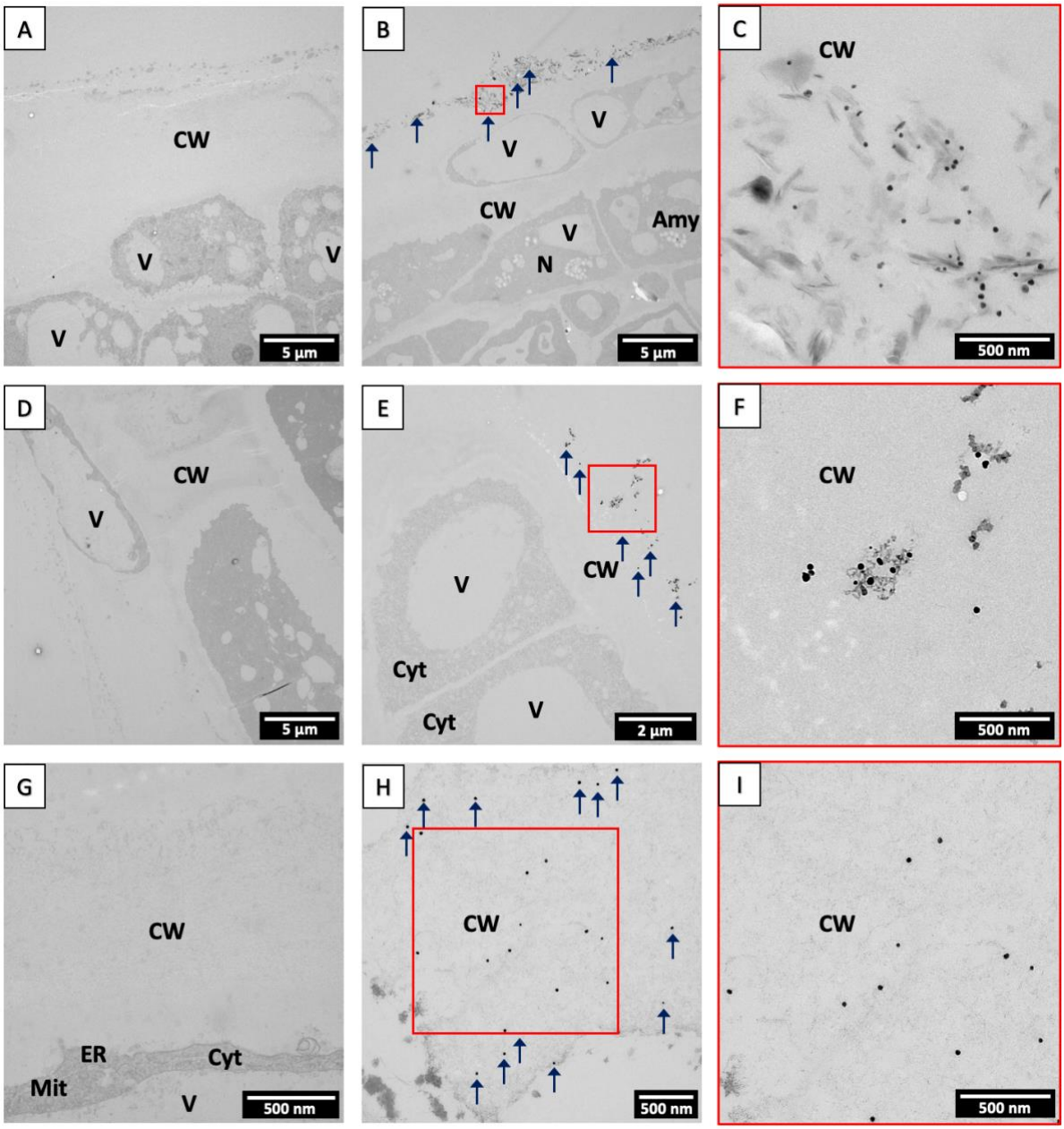

Figure 3-13: 4 nm AuNP-SCTA are not taken up by Arabidopsis roots.
AuNPs visualized by transmission electron microscopy (TEM) in the cell wall of epidermal root cells in Arabidopsis seedlings treated with 6 mg/L of 4 nm AuNP-SCTA in soil (B), ½ MS (E) and ½ MS-agar (H). For each treatment, magnifications of the selected area are shown in the right-hand panel (C, F, I). As controls, parallel set of seedlings were grown and treated in the same condition with the coating solution SCTA (A, D, G). Arrows indicate single AuNP-SCTA; CW, cell wall; Cyt, cytoplasm; V, vacuole; P, proplastid; Mit; mithocondrion; ER, endoplasmic reticulum; N, nucleus; Am, amyloblast.

4 Discussion

4.1 Plant nanotoxicology: major challenges

The increasing use of nanomaterials (NMs) in the agrochemical industry (Mittal et al., 2020; Singh et al., 2021) and the irrigation and cultivation of crops with water and soil containing disposed nano-pollutants (Singh & Kumar, 2014; Liu et al., 2018) has caused direct exposure of terrestrial environments to these materials, posing new environmental challenges for scientists and environmentalists (Siddiqui et al., 2015). Therefore, probing the safety of manufactured nanomaterials (MNMs) or the potential health and environmental risks associated with their exposure to humans, animals and plants has become of paramount importance (Stampoulis et al., 2009; Chawla et al., 2018; Bundschuh et al., 2018).

To date, despite recent developments in plant nanotoxicology, there is a lack of solid scientific knowledge on the effects of nanoparticles (NPs) on terrestrial plants, with gaps in the understanding of their pathways and mechanisms of action (Zia-ur-Rehman et al., 2018; Sanzari et al., 2019; Kranjc & Drobne, 2019; Ali et al., 2021). The key aspects to be taken into account in plant nanosafety research concern the physicochemical properties of NMs (composition, size and surface chemistry), the characteristics of treated plants (species, growth and developmental stages) and their interaction (time and route of exposure) (Du et al., 2018; Sukhanova et al., 2018; Sanzari et al., 2019; Kranjc & Drobne, 2019; Khan et al., 2019). To properly address the issue of nanosafety, comprehensive physicochemical characterizations of the newly synthesized NP batches and adequate quality controls of the assay conditions are a fundamental prerequisite for reproducible and reliable NP research. In fact, the unique physical and chemical properties of nanosized particles, such as their high reactivity and catalytic action, are strictly dependent on their shape, size and surface chemistry (Sukhanova et al., 2018; Khan et al., 2019). Furthermore, after synthesis and dispersion in a new environment, NPs interact with the molecules present in the medium seeking a more stable thermodynamic state, which may lead to aggregation and a potentially different bio-identity thus making it necessary to monitor colloidal stability and possible biotransformations (Kim et al., 2008; Barbero et al., 2017; Barbero et al., 2019). To avoid such phenomena, NP surface stabilizing agents are used during synthesis processes or subsequently in functionalization reactions (Guerrini et al., 2018). On the other hand, NP coatings could, under natural conditions, alter the properties of the particles and their physiotoxicity needs to be studied in ecotoxicological assays (Barbero et al., 2019). Potential alterations in the physicochemical properties of NPs once released into the surrounding environments make studies under natural conditions difficult to interpret, therefore nanosafety assessments under reproducible and controlled conditions may help to

interpret investigations in ecotoxicological assays (Kim et al., 2008; Barbero et al., 2017; Barbero et al., 2019). In order to properly compare the effects of NPs across different plant species under laboratory conditions, the experimental settings should be maintained unaltered.
In this light, this study aimed at studying the behaviour of engineered AuNPs, as a starting material and after dispersion in plant growth media, along with their physiological and molecular effects on the model plant *Arabidopsis thaliana*.

4.2 Physicochemical evaluation of AuNPs

4.2.1 Surface stabilizing agents determine behaviour of AuNPs in plant media

The high salt concentration of plant growth media may facilitate aggregation of NPs and alterations in their bio-identity (Moore et al., 2015; Sun et al., 2016; Fuller & Köper, 2018; Nierenberg et al., 2018), thus surface stabilizing agents are used to stabilize colloidal suspensions through electrostatic, steric or electrosteric repulsions (Guerrini et al., 2018). To assess the stability of gold colloidal solutions in plant growth media, we synthesized three different types of AuNPs, all with an average diameter of 12 nm but different surface stabilizers, i.e., sodium citrate (SC), sodium citrate and traces of tannic acid (SCTA) and polyvinylpyrrolidone (PVP) 10 kDa. AuNP-SC represent the most common particles on the market, chemically produced by reduction of tetrachloroauric acid with trisodium citrate (Bastús et al., 2011; Wuithschick et al., 2015), while AuNP-SCTA also contain traces of tannic acid as co-reducer and electrostatic co-stabilizer. In the third category of particles produced in this study (AuNP-PVP) the SC and TA electrostatic surface stabilizers were removed and replaced with the steric PVP coating. A comprehensive physicochemical characterization of the newly synthesized NPs, prior to their use in Arabidopsis treatments, was carried out by several techniques such as UV-Vis spectroscopy, DLS, LVD and SEM, pointing out the monodisperse state and high stability of the colloidal solutions (see section 3.1.1). In previous studies, the effects of monodispersed AuNPs on plants have been investigated, although their behaviour and possible state of aggregation after dispersion in plant media have not been further described (Arora et al., 2012; Avellan et al., 2017; Milewska-Hendel et al., 2019; Lovecká et al., 2021). In particular, AuNPs stabilized with electrostatic stabilizers such as sodium citrate (SC) (Arora et al., 2012; Avellan et al., 2017; Milewska-Hendel et al., 2019; Lovecká et al., 2021), polyethylenimine (PEI)(Avellan et al., 2017) or branched polyethylenimine (BPEI) (Milewska-Hendel et al., 2019) and steric coatings such as polyethylene glycol (PEG) (Milewska-Hendel et al., 2019) have been dispersed in liquid or agar-solidified plant growth media to test their physiological effects on plants. However, despite the assumption that steric coatings are more stable than electrostatic stabilizers and jellified media improve the stability of colloidal solutions by decreasing the interaction between particles, the behaviour and aggregation state of these engineered AuNPs have not been

evaluated after their release in the new environment. By contrast, in their physiological and toxicological studies on Arabidopsis seedlings, Siegel et al. (2016) characterized SC capped-AuNPs after release in different dilutions of MS plant growth medium. AuNPs dispersed in low-salinity, low-nutrient $^{1}/_{16}$-diluted MS still showed slight but acceptable aggregation, easily detectable by the colour change of the solution immediately after their release into the medium, resulting in suboptimal conditions for plant growth. It is important to characterize the evolution of the AuNPs once dispersed in the working media to correctly correlate the pristine and the evolving NP features with the observed biological effects (Barbero et al., 2017).

In this light, we tested the initial and overtime stability of SC-, SCTA- and PVP-stabilized AuNPs by exploiting the particles' unique optical properties using UV-Vis spectroscopy (Haiss et al., 2007; Shard et al., 2018) (see section 3.1.2). The high ionic strength of the ½ MS plant medium (salinity of 23 mM), necessary for plant growth, led the citrate-capped AuNPs to aggregate immediately, highlighting the inadequacy of the electrostatic charges of the SC in providing appropriate stability in the new medium (Pamies et al., 2014). On the other hand, AuNP-SCTA remained stable in the liquid ½ MS medium for at least 6 hours, suggesting how the presence of traces of TA, the only difference between the two types of electrostatically stabilized NPs, increases the stability of the particles by conferring a higher surface charge or partial steric stabilization and providing the necessary stability against salt-driven aggregation. The capping agent PVP conferred long-term stability (up to 3 weeks) in both liquid and agar- solidified plant media, clearly pointing out how surface coatings linked through steric bonds provide a longer stability. Despite the lack of studies assessing the aggregation state of NPs after dispersion in plant media, the overtime physicochemical characterization of colloidal solutions dispersed in a new biological environment is a key step in ensuring monodispersity and colloidal stability, which is in turn an essential prerequisite for reliable and reproducible NP research.

4.2.2 Toxicity of surface stabilizing agents

NP surface-stabilizing agents, whose purpose is to stabilize colloidal gold in solution through electrostatic, steric or electrosteric interactions (Amina & Guo, 2020; Dumur et al., 2020), may play an essential role in nanosafety assessments on plants and animals (Barrena et al., 2009; Attarilar et al., 2020). In particular, the ionic charge conferred by particle coatings may influence the physical interaction between NPs and cell membranes, with positively charged NPs being more accessible than neutral negatively charged ones (El Badawy et al., 2011). Barrena et al. (2009) showed that, in germination tests of cucumber and lettuce seeds, toxic effects can be attributed to NP solvents rather than to NPs themselves.

To evaluate the potential cytotoxicity of the capping agents capable of stabilizing the colloidal solutions after dispersion in ½ MS and ½ MS agar media, we exposed Arabidopsis seedlings to SCTA and PVP. Their toxicity at different concentrations, ranging from 0 to 30 mg/L, was investigated by assessing *A. thaliana* root growth over a period of 1 week. While the negatively charged surface stabilizer SCTA resulted to be non-toxic to Arabidopsis seedlings, the neutral polymer-PVP significantly affected the root length of the treated plants starting from the lowest concentration (see section 3.2.1).

Studies on the effects of different coated AgNPs on the aquatic green algae *Chlorella vulgaris* showed that PVP-NPs have a lower uptake rate, and consequently lower toxicity, than PEG-coated particles (Kalman et al., 2015). These results were corroborated by other studies on different green algae species showing the stabilizing effect of the neutral PVP surface stabilizer on AgNPs, whose toxicity was shown to be lower than that of silver ions (Ag^+) released by dissolutions of unstable silver colloidal solutions (Wang et al., 2015) or AgNPs stabilized with SC (Angel et al., 2013). Furthermore, the addition of different concentration of PVP (1-10 g/L) to the ½ MS plant growth medium enhanced the rhizogenic capacity of two different cherry rootstock explants, while it negatively affected the root number and the callus induction frequency in a third species (Sarropoulou et al., 2015). The different responses in the three cherry rootstocks were attributed to the plant-specific genotype. On the other hand, although SC and TA have been proven to be moderately toxic in humans and animals after direct exposure by ingestion and inhalation, no specific studies on their phytotoxicity have been conducted (Gruber & Halbeisen, 1948; Robles, 2005; Johnson & Hillier, 2007).

These contrasting findings confirm the importance of testing the functionalizing agents prior to use in any assay in order to discern their effects from those of the NPs, but also support the hypothesis that the surface charge of the stabilizers influences their degree of toxicity as well as having a species-specific effect.

4.2.3 Sterilization by filtration preserves the physical properties of AuNP-SCTA

Since contaminants in plant growth media allow the growth of microorganisms, NPs need to be sterile before their use in plant assays. As shown by previous studies, autoclaving and radiation sterilization might result in the aggregation of the NPs, loss of the coating and contamination with potential microbial toxins (Masson et al., 1997; Memisoglu-Bilensoy & Hincal, 2006; Özcan et al., 2009; França et al., 2010; Bernal-Chávez et al., 2021). Sterile filtration has been shown not to directly affect the physical properties of NPs, but filter materials should be tested to exclude possible interactions with particle surfaces resulting in NP retention or coating removal (Bernal-Chávez et al., 2021).

We tested cellulose mixed ester (CME) and polyethersulfone (PES) filters and revealed that PES filters are suitable for sterilization of AuNPs, while CME filtering resulted in a significant reduction in the amount of NPs in the filtered samples (see section 3.2.1.1)**.** As mentioned above, several studies have focused on evaluating the physicochemical properties of NPs after sterilization with various techniques, but none have studied the potential changes in the concentration of colloidal solutions after filtration with different materials**.** Comparison of the UV spectra of AuNP-SCTA before and after filtration provides a reliable and precise overview of the aggregation state of the particles and their concentration in the solution. In particular, the absence of red shifts and changes in the curve profiles of the spectra clearly indicate the unaltered state of the NPs after the sterilization process. Therefore, as a result of the tests carried out in this work, PES filters can be considered suitable for the sterilization of AuNPs, allowing the sterile cultivation of plants in the presence of stable, unaltered particles.

4.3 Plant responses to AuNPs

4.3.1 AuNP-SCTA affect Arabidopsis root growth in a dose-dependent manner

A number of studies have addressed AuNP responses in plants, reporting positive, negative and no effects (Siddiqi & Husen, 2016). In this study, *Arabidopsis thaliana* was used as a model plant to investigate the effects of AuNP-SCTA exposure on growth and development. AuNP-SCTA, in a range from 0 to 20 mg/L, affected Arabidopsis root growth in a dose-dependent manner with a maximal effect at 10 mg/L, while the NP-stabilizer SCTA (SC 2.2 mM; TA 200 µM) did not affect the seedlings growth at any of the tested concentration. Growth promoting effects of AuNP-SCTA concentrated 10 mg/L were assessed by recording representative parameters, i.e., primary root length, rosette diameter, number and length of lateral roots, after 1 week of treatment in agar solidified medium. Growth parameters were significantly enhanced by 1.2-to-1.7-fold compared to the sets of untreated and control plants (see section 3.3).

Previous studies have found that AuNPs at high concentrations (≥ 100 mg/L) cause detrimental effects on plants, while for lower concentrations of AuNPs larger than 5 nm growth promoting effects have been shown supporting our findings that AuNPs have positive effects on plant growth (Arora et al., 2012; Sabo-Attwood et al., 2012; Kumar et al., 2013; Mahakham et al., 2016). Furthermore, Siegel et al. (2018) tested three different sizes of AuNPs (10, 14 and 18 nm) at increasing concentrations (1, 10 and 100 mg/L) and showed that at the highest concentration the smaller particles reduced the length of the *Arabidopsis thaliana* root in a size dependent manner. It has been hypothesized that a high concentration of NPs negatively affects plant growth by particle adsorption onto the cell wall of the root system, decreasing pore size and inhibiting water transport (Barrena et al., 2009; Asli & Neumann,

2009; Feichtmeier et al., 2015). On the other hand, contradictory studies have been reported. Feichtmeier et al.(2015), reported a decrease in the biomass of *Hordeum vulgare* after AuNP treatment at a final concentration between 3 and 10 mg/L. Some of these discrepancies can be explained by the diverse behaviour of different plant species, differences in specific experimental settings and different behaviour of NPs under test conditions, which make a clear assessment of AuNP responses more difficult. Therefore, a careful evaluation of each study is necessary to draw a complete picture of the effects of AuNPs on the specific plants.

While the mechanisms of action and effects of AuNPs on plants are not yet fully understood (Rico et al., 2011; Sabo-Attwood et al., 2012; Zhu et al., 2012; Siddiqi & Husen, 2016), for the gold (Au) bulk counterpart the results are clearer. As plants have revealed their potential in the green synthesis of AuNPs, many studies have been produced on the physiological responses of plants to Au salts (T. Khan et al., 2019), used as starting material in order to obtain NPs. Gold is required by plants in traces, but its absorption in higher amounts can cause drastic changes in plant growth (Siddiqi & Husen, 2016). Arabidopsis seedlings treated with 10 mg/L of potassium tetrachloroaurate(III) ($KaAuCl_4$) showed the formation of AuNPs in the roots and shoots and enhanced vegetative growth (Tiwari et al., 2016), while higher amounts of KAuCl4 or gold(III) chloride (AuCl3) (100 mg/L) negatively affected the root length and shoot development (Taylor et al., 2014). Taylor et al. (2014) also showed that AuNPs with a dimeter ranging from 5 to 100 nm were not directly absorbed by Alfalfa plants. On the other hand, they showed that ionic gold (KAuCl4) (50 mg/L) was passively absorbed by roots and subsequently reduced with consequent internal formation of AuNPs. These data together with the results obtained in this study, demonstrating the inclination of AuNPs to aggregation rather than dissolution phenomena, lead to the hypothesis of a growth-promoting effect due to the exposure to NPs rather than the bulk gold material or its ionic forms.

4.3.2 AuNP-SCTA decrease stress responses in Arabidopsis seedlings

Immune responses are reported to be activated upon NP exposure in many plant and animal models, including reactive oxygen species (ROS) production and lipid peroxidation (Husen et al., 2014; Abdal Dayem et al., 2017; Marslin et al., 2017; Feidantsis et al., 2020).

Here, we found that AuNP-SCTA alone did not induce these classical plant defense responses. In addition, ROS production induced by the 22-amino acid peptide derived from bacterial flagellin (flg22), sensed in plants as a pathogen associated molecular pattern (PAMP), was significantly reduced in the presence of increasing amounts of AuNP-SCTA. To exclude a biophysical quenching effect of the light emitted by luminol in ROS assays, we performed lipid peroxidation assays. FOX assay results are supposed to reflect the oxidative stress levels in animals and plants (El-Beltagi & Mohamed, 2013).

The level of lipid peroxidation in samples treated with a PAMP and AuNPs decreased significantly in a concentration dependent manner compared to treatments with the flg22 elicitor, showing that the PAMP-triggered ROS burst was indeed reduced and not a consequence of interference of AuNPs with the luminol-based ROS assay (see section 3.4).

Kumar et al. (2013) showed that AuNPs in a final concentration of 80 mg/L significantly improved the free radical scavenging activity of Arabidopsis seedlings by increasing the activity of enzymes involved in the defense system against ROS, whereas plants treated with AuNPs in the range of 100 to 400 mg/L showed reduced growth, which was considered to be a consequence of increased free radical stress (Siddiqi & Husen, 2016). After 6 h of treatment with 10 mg/L of AuNP-SCTA, we found 10 peroxidases to be downregulated on the transcript level and 6 at the protein level which may be involved in oxidative stress reactions. These data indicate a correlation between ROS production and AuNP effects and show that AuNPs can reduce stress responses triggered by immune stimulatory peptides. If this effect is based on a direct effect on the peptide, *e.g.*, through adsorption to the NP surface or changes in the peptide accessibility (and consequently alteration of its mode of perception)(Barbero et al., 2021), or on a protective effect of AuNPs on PAMP recognition or downstream signaling will be interesting to study in the future.

4.4 Alterations in transcriptome and proteome after AuNP exposure

To investigate the alterations caused by short (6 h) and long-term (7 d) AuNP exposure at the molecular level, we performed comprehensive transcriptomic and proteomic analyses on Arabidopsis seedling roots.

In our study, a total of 651 differentially expressed genes (DEGs) were identified after short-term treatment, with 121 genes upregulated and 530 genes downregulated. After long-term exposure only 6 DEGs were detected, clearly pointing out that transcriptome changes are relevant only at early time points after AuNP treatment (see section 3.5). In particular, after short-term exposure, the majority of genes involved in disease resistance, defense response, oxidative stress and metal response were downregulated, while the majority of genes involved in light response were upregulated (Table A-2). A gene involved in root growth, the DUF642 L-GalL-responsive gene 2 (DGR2, At5g25460), was upregulated, too (Gao et al., 2012) . Together with the growth promoting effects of AuNPs and the downregulation of defense genes these data support the hypothesis that the trade-off between growth and immune/stress responses is shifted to the growth side after AuNP exposure.

The only shared DEG between the short and long-term treatments, the Nicotianamine synthase 2 gene, (NAS2, At5g56080), is downregulated in both conditions and encodes for a protein involved in the synthesis of nicotianamine. *Nas2* mutants show altered metal contents, indicating a role in metal

uptake or response (Klatte et al., 2009), especially of iron which is involved in many functions related to plant thriving (Schmidt et al., 2020). A similar analysis has been performed on the roots of Arabidopsis seedlings upon gold ($KAuCl_4$) exposure, which leads to AuNP formation by the plant (Tiwari et al., 2016). A comparative analysis between our and the transcriptomics data published by Tiwari et al. (2016) shows that there is some overlap of up- and down-regulated genes (3 common upregulated and 22 common downregulated genes, Figure 4-2). In particular, between the up-regulated DEGs two metal response genes (Metallothionein-like protein 1C (MT1C), At1g07610 and Aluminum-activated malate transporter 1 (ALMT1), At1g08430) and again DGR2 have been found. In both studies disease and defense response and oxidative stress genes were down-regulated. By contrast, Tiwari et al. (2016) found that developmental, auxin-responsive and metal-responsive genes were up-regulated after Au treatment, whereas in our study the majority of genes belonging to these categories were downregulated after AuNP treatment. These differences are likely caused by different effects caused by Au ion uptake compared to exposure to nanoparticles. As metal AuNPs are very inert and not prone to dissolution the significant overlap between Au salt and AuNP is potentially caused by NP effects in both experiments as Au ions are taken up and converted into AuNPs inside the plant where they may cause similar effects as external NP exposure.

To further unravel the mechanisms underlying the effects of AuNPs on *Arabidopsis thaliana* seedlings, proteomic analyses after short- (6 h) and long-term (7 d) AuNP exposure were performed on roots by nano-liquid chromatography double mass spectrometry (NanoLC-MS/MS-spectrometry). From a total of 2727 detected proteins after 6 h exposure and 2503 after 7 d exposure, 119 and 59 differentially expressed proteins (DEPs), respectively, have been identified (see section 3.6). The most enriched GO terms overrepresented after both treatments were involved in metabolic processes, protein synthesis and response to stimuli. Oxidative stress-related proteins were mainly downregulated in both conditions, as shown at the transcriptome level. Furthermore, proteins involved in plant growth and development were downregulated after 6h and upregulated after 7d (Table A-4 and A-5), supporting the transcriptomic data and the physiological and molecular effects observed after AuNP exposure in 1 week-old Arabidopsis seedlings.

The overlap analysis of the different timepoints has revealed the protein DUF642 L-GalL-responsive 1 (DGR1, At1g80240), which has been investigated for its role during the development of Arabidopsis thaliana (Gao et al., 2012). After 7 d of treatment DGR1 and DGR2 were both up-regulated, while after 6 h of treatment only DGR1 was initially down-regulated.

DGR1 and DGR2 were also revealed in the overlap analysis of our proteomic and transcriptomic studies, as well as being upregulated after Au salt exposure (Tiwari et al., 2016).

DGR1 and DGR2 encode for two proteins belonging to the DUF642 protein family, whose members are part of the cell wall proteome (Cruz-Valderrama et al., 2019) and have shown in Arabidopsis a complementary expression pattern in young and developed roots, and a similar but non-redundant function (Gao et al., 2012). As Gao et al. (2012) reported in their study, DGRs, are involved in developmental processes in Arabidopsis, and in particular in root elongation. DGR2 seems to have a predominant role as *dgr2* single mutants show a short, undeveloped root phenotype (Gao et al., 2012). These results suggest a potential involvement of these proteins in the root growth promoting effects induced by AuNPs and can be used as a starting point for further studies aimed at dissecting the pathways underlying the beneficial effects of AuNP-SCTA on Arabidopsis development.

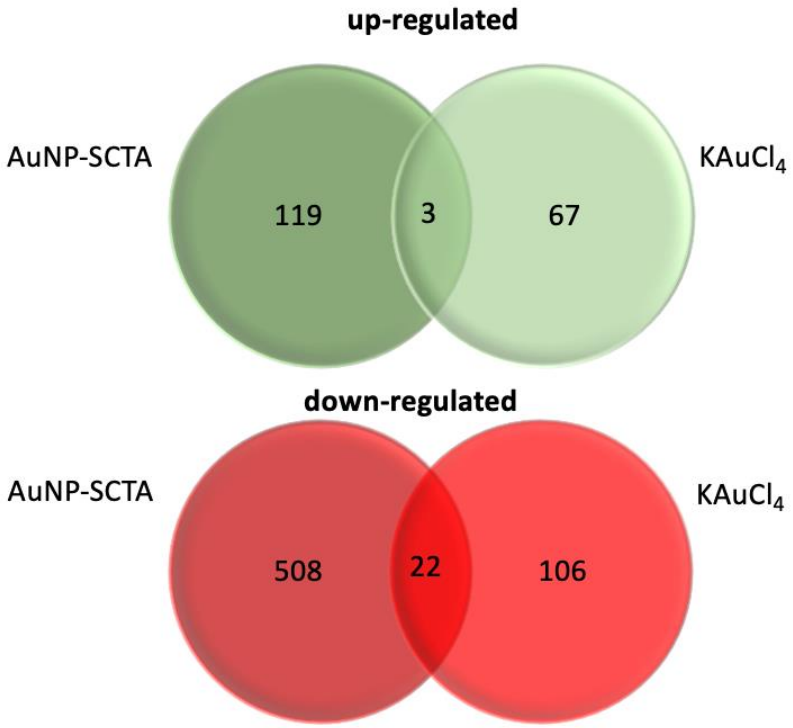

Figure 4-1: Venn diagram of DEGs after AuNP-SCTA exposure (this study) and KAuCl4 treatment (Tiwari et al., 2016).
Diagram representing the number of unique and shared up- and down-regulated genes in the two studies. As a consequence of $KAuCl_4$ treatment, AuNPs are formed in planta.

4.5 AuNPs uptake in plants

To study the physiological and molecular effects of engineered nanomaterials (ENMs) on plants, it is first necessary to understand the mechanisms and outcomes underlying the NP-plant interactions. The potential accumulation and translocation of NPs in plants also play a pivotal role in nanosafety investigations and risk assessment. Currently, the exact mechanisms behind the uptake of NPs are not fully understood and further investigation is urgently needed (Siddiqui et al., 2015). However, the studies conducted on the subject , and in particular on AuNPs, state that the bioavailability and

internal accumulation of particles depend on their shape , size, charge and on the plant species (Zhu et al., 2012).

In this study, to evaluate the fate of AuNP-SCTA after their interaction with Arabidopsis roots, uptake experiments were performed in three different plant growth media, i.e., ½ MS, ½ MS-agar and soil (Figure 4-1). The pore size of cell walls has been determined to be approximately 3-6 nm (Carpita et al., 1979), a size that precludes the uptake of larger molecules, therefore we used stable 4 nm particles in all uptake experiments to avoid any mechanical barrier. At the end of each treatment, uptake analyses were performed on the epidermal cells of the root tip by transmission electron microscopy (TEM) focusing. In each condition, no AuNP-SCTA were detected inside the root cells and only a few NPs were found outside or stuck in the cell wall (see section 3.7). Therefore, we can conclude that the observed physiological effects are not based on absorption but on extracellular effects.

AuNPs uptake is controversially discussed in the community, with studies showing uptake and even transport within the plant and others ruling it out (Zhu et al., 2012; Judy et al., 2012; Koelmel et al., 2013; Milewska-Hendel et al., 2017). In their uptake studies on tobacco Sabo-Atwood et al. (2012) showed that the process is size-related, with 3.5 nm AuNPs entering into plant cells and 18 nm AuNPs remaining agglomerated on the outer surfaces of the root. Considering the slightly larger size of our particles (4 nm instead of 3.5 nm), this result could potentially fit the size-dependent uptake theory. The internalization of ENMs in roots is clearly not only related to the size and shape of the particle, but also to the type of plant species. The study conducted by Glenn et al. (2012) confirms these assumptions, showing different uptake behaviours in three kinds of aquatic plants treated with 4 and 18 nm AuNP. The presence of NPs in the root apparatus of the three freshwater macrophytes was assessed through electron microscopy. In particular, *Azolla caroliniana* was the only aquatic plant, among those tested, to show root uptake of both size of AuNPs, while into the sectioned root tissue of *Myriophyllum simulans* only 4 nm AuNPs were detected. In contrast, no uptake was observed in *Egeria densa* (Glenn et al., 2012). In addition, certain properties of NPs, such as surface charge, can induce morphological changes in the cell wall, thus influencing the rate of uptake. Zhu et al. (2012) demonstrated that positively charged AuNPs are more easily taken up by roots than negatively charged ones, while on the other hand negative AuNPs are more efficiently translocated to the shoot once they have been taken up by roots. The same results were observed with cerium dioxide (CeO_2) NPs, with the positively charged ones associating to the plant radical system more than the negative ones because of the electrostatic repulsions with the negative surface of the roots. On the other hand, particles with a neutral or negatively charged surface were observed to translocate from the roots to the shoots more efficiently (Zhang et al., 2021).

We can conclude that our knowledge on the subject is still limited and many aspects remain elusive. Identifying the mechanisms underlying the uptake of NPs and understanding the principles behind this phenomenon remain key points to be clarified in the future.

4.6 Conclusion

The main goal of this thesis was to establish, under laboratory conditions, a stable and reproducible NP-plant exposition system to test their effects at the physiological and molecular level.
The results obtained clearly showed that nanoecotoxicological evaluations must include a thorough characterization of the physicochemical properties of AuNPs released into a new environment as well as toxicity studies on the capping agents used to stabilize the colloidal solutions. These key aspects are too often not taken into account in studies assessing the nanosafety of NPs, leading to unreliable results and an information gap in the literature.

One of the most interesting parts of this work was the evaluation of the fate of 4 nm AuNP-SCTA after their interaction with the radical apparatus of Arabidopsis seedlings and the implications arising from the results of such uptake experiments. Regardless of the medium or experimental conditions used, no particles were found in the cytoplasm of the root epidermal cells and the few particles identified were found outside or stuck in the cell wall. AuNPs used in these experiments (4 nm), although smaller than that of the cell wall pores (3-6 nm) (Sabo-Attwood et al., 2012), which are considered to be the entry gateway at the root level (S. Ali et al., 2021), were not taken up.
The uptake of AuNPs in plants is a controversial topic and it is necessary to mention that previous studies have shown that AuNPs larger than cell wall pores have been taken up in specific plant species. An active uptake process is proposed which occurs through alteration of the cell wall structure, probably as a result of the interaction with different NP surface stabilizers (Su et al., 2019; S. Ali et al., 2021).
Furthermore, although previous experiments have shown that positively charged AuNPs are more easily taken up than neutral and negative ones by some plant species (Spielman-Sun et al., 2019), it has also been proven that negatively charged AuNPs, such as those used in this study, were taken up by rice and tomato plants (Koelmel et al., 2013; Dan et al., 2015).
Due to the inertia of AuNPs and the absence of oxidation phenomena, the potential formation of ions at the extracellular level and their subsequent uptake at the radical level with intracellular formation of NPs cannot be considered as a likely mechanism of uptake, in contrast to unstable metallic NPs prone to dissolution events, such as AgNPs (Tripathi et al., 2017).

Although the mechanisms underlying the uptake process are still elusive and no generalizations can be made, it is clear that the process is mainly influenced by the plant species and the physicochemical properties of the AuNP such as its surface charge.

The results of our uptake experiments imply that the effects caused by AuNPs in Arabidopsis are not caused by direct recognition by innate immune receptors present on the plasma membrane (pattern triggered immunity) or in the cytoplasm (effector triggered immunity) , whose function is to recognize non-self structures in each cell (Ngou et al., 2022). However, this does not exclude the possibility that in the case of NP uptake in a given plant species, these receptors are involved in their perception and consequently in subsequent responses.

We showed that AuNP-SCTA, in a range from 0 to 20 mg/L, affected Arabidopsis root growth in a dose-dependent manner with a maximal effect at 10 mg/L. Furthermore, AuNP-SCTA have proven to be able to reduce PAMP induced ROS burst, again in a dose-dependent manner.

The underlying mechanisms of these effects are still elusive, but indicate that AuNP-SCTA might be able to detoxify ROS and shift the balance between growth and immunity trade-off to the growth side. These results, not being a direct consequence of particle uptake, can be induced by changes in external conditions, due for example to the intrinsic properties of AuNPs which are prone to surface functionalization through the adsorption of biomolecules present in the surrounding environment. In particular, the increased growth and reduced ROS burst induced by PAMP could be the result of scavenging of environmental and pathogenic factors inducing defense responses.

In support of our results previous studies have found that AuNPs at high concentrations (≥ 100 mg/L) cause detrimental effects on plants (Siegel et al., 2018) and this result could be a direct consequence of the high amount of particles, and possible aggregates, clogging the pores present on the cell wall and/or membrane in case of uptake.

Our physiological and molecular findings were also overall represented at the transcriptome and proteome level, where growth and metal response genes/proteins were upregulated whereas immune and oxidative stress responsive genes/proteins were downregulated.

To date, it is generally accepted that the toxicity of AuNPs in humans, animals and plants is related to their surface coatings, concentration, size, time and source of exposure, as well as to the model organism (Senut et al., 2016; Carnovale et al., 2019). Although it is not possible to make a simple correlation between AuNP exposure and their effects on plants we can safely agree that AuNPs are unlikely to have harmful effects on Arabidopsis plants at environmentally relevant concentrations.

Further studies are needed to gain a better understanding of the molecular reactions underlying the interaction between plants and NPs, which could be exploited to achieve the seen beneficial effects.

5 Summary

Engineered nanomaterials (ENMs), due to their unique chemical and physical properties, are widely used in a variety of medical, industrial and agricultural applications (Giese et al., 2018). The global economic success of man-made nanosized composites has led to higher production and disposal rates and a diversification of emission sources into the environment (Yeh et al., 2012). In particular, the peculiar electronic and optical characteristics of gold nanoparticles (AuNPs) have been extensively explored and exploited in recently developed agronomic techniques, leading to the direct exposure of terrestrial environments to these nanometric materials (Mittal et al., 2020). However, despite recent advancements in nanotoxicological research, little is still known about the effects of nanoparticles on plants and their mechanisms of action. For these reasons, novel nanosafety approaches to assess the environmental impact of ENMs are required.

The aim of this work was the establishment of stable and reproducible NP-plant exposure systems to study the physiological and molecular plant responses to AuNPs after short- and long-term exposure. Initial and overtime physicochemical characterizations of the colloidal gold solutions were carried out to ensure the monodispersity and stability of the particles. Exposure of *Arabidopsis thaliana* plants to moderate concentrations of AuNPs (10 mg/L) resulted to positively influence the growth of the seedlings, exhibiting longer primary roots, more numerous and longer lateral roots and increased rosette diameter. Also, after treatment, the plants showed reduced oxidative stress responses elicited by the immune-stimulatory PAMP flg22. Transcriptomics and proteomics studies showed downregulation of stress and immune-responses and upregulation of growth promoting genes, supporting the scenario that the trade-off between growth and immune/stress responses is shifted to the growth side after AuNP exposure. These omics datasets after AuNP exposure can be exploited in future works to study the underlying molecular mechanisms of AuNP-induced growth promotion.

6 Zusammenfassung

Technisch hergestellte Nanomaterialien (ENMs) werden aufgrund ihrer einzigartigen chemischen und physikalischen Eigenschaften in einer Vielzahl von medizinischen, industriellen und landwirtschaftlichen Anwendungen eingesetzt (Giese et al., 2018). Der weltweite wirtschaftliche Erfolg von künstlich hergestellten Verbundstoffen in Nanogröße hat zu höheren Produktions- und Entsorgungsraten sowie zu einer Diversifizierung der Emissionsquellen in die Umwelt geführt (Yeh et al., 2012). Insbesondere wurden die speziellen physikalischen Eigenschaften von Goldnanopartikeln (AuNPs) ausgiebig erforscht und in der modernen Landwirtschaft genutzt, was zu einer Belastung der terrestrischen Ökosysteme durch diese nanometrischen Materialien führt (Mittal et al., 2020). Trotz der neuesten Fortschritte in der nanotoxikologischen Forschung ist nur wenig über die Auswirkungen von Nanopartikeln auf Pflanzen und deren Wirkmechanismen bekannt. Daher sind neue Nanosicherheitsansätze zur Bewertung der Umweltauswirkungen von ENMs erforderlich.

Das Ziel dieser Arbeit war die Etablierung stabiler und reproduzierbarer NP-Pflanzen-Expositionssysteme, um die physiologischen und molekularen Reaktionen von Pflanzen auf AuNPs nach kurz- und langfristiger Exposition zu untersuchen. Zunächst wurden die kolloidalen Goldlösungen physikochemisch charakterisiert, um die Monodispersität und Stabilität der Partikel sicherzustellen. Die Exposition von *Arabidopsis thaliana* Pflanzen gegenüber moderaten Konzentrationen von AuNPs (10 mg/L) hatte einen positiven Einfluss auf das Wachstum der Keimlinge. Diese wiesen längere Primärwurzeln, zahlreichere und längere Seitenwurzeln und einen größeren Rosettendurchmesser auf. Außerdem zeigte die Pflanze nach der Behandlung eine reduzierte oxidative Stressreaktionen, welche durch das immunstimulierende PAMP flg22 ausgelöst wurden. Transkriptom- und Proteom-Studien zeigten, dass Stress- und Immunreaktionen herunter reguliert sowie wachstumsfördernde Gene hoch reguliert wurden. Dadurch wird das Szenario unterstützt, dass sich nach AuNP-Exposition der Kompromiss zwischen Wachstum und Immun-/Stressreaktionen auf die Seite des Wachstums verlagert. Die Omik-Datensätze nach AuNP-Exposition können für zukünftige Arbeiten genutzt werden, um die molekularen Mechanismen der AuNP-induzierten Wachstumsförderung zu untersuchen.

7 References

Abbas, Q., Yousaf, B., Amina, Ali, M. U., Munir, M. A. M., El-Naggar, A., . . . Naushad, M. (2020). Transformation pathways and fate of engineered nanoparticles (ENPs) in distinct interactive environmental compartments: A review. *Environment International, 138*, 105646.

Abbott, S., & Holmes, N. (2013). *Nanocoatings: Principles and Practice: From Research to Production*. Lancaster, Pennsylvania: DEStech Publications.

Abdal Dayem, A., Hossain, M. K., Lee, S. B., Kim, K., Saha, S. K., Yang, G.-M., . . . Cho, S.-G. (2017). The Role of Reactive Oxygen Species (ROS) in the Biological Activities of Metallic Nanoparticles. *International Journal of Molecular Sciences, 18*(1), 120.

Agarwal, H., Venkat Kumar, S., & Rajeshkumar, S. (2017). A review on green synthesis of zinc oxide nanoparticles – An eco-friendly approach. *Resource-Efficient Technologies, 3*(4), 406-413.

Alaqad, K., & Saleh, T. (2016). Gold and Silver Nanoparticles: Synthesis Methods, Characterization Routes and Applications towards Drugs. *Journal of Environmental & Analytical Toxicology, 6*.

Albanese, A., Tang, P. S., & Chan, W. C. (2012). The effect of nanoparticle size, shape, and surface chemistry on biological systems. *Annual Review of Biomedical Engineering, 14*, 1-16.

Ali, Al-Tohamy, R., Koutra, E., Moawad, M. S., Kornaros, M., Mustafa, A. M., . . . Sun, J. (2021). Nanobiotechnological advancements in agriculture and food industry: Applications, nanotoxicity, and future perspectives. *Science of the Total Environment, 792*, 148359.

Ali, S., Mehmood, A., & Khan, N. (2021). Uptake, Translocation, and Consequences of Nanomaterials on Plant Growth and Stress Adaptation. *Journal of Nanomaterials, 2021*, 6677616.

Amina, S. J., & Guo, B. (2020). A Review on the Synthesis and Functionalization of Gold Nanoparticles as a Drug Delivery Vehicle. *International Journal of Nanomedicine, 15*, 9823-9857.

Anderson, C., Brooks, R., Stewart, R., & Simcock, R. (1999). Gold Uptake by Plants. *Gold Bulletin, 32*, 48-52.

Andreani, A., Suyanta, S., Kunarti, E., & Santosa, S. (2017). Synthesis of Gold Nanoparticle from Adsorbed Au on Hydrotalcite Using SDS and Sodium Citrate as Capping Agent and its Recovery into Pure Gold. *Materials Science Forum, 901*, 32-36.

Angel, B. M., Batley, G. E., Jarolimek, C. V., & Rogers, N. J. (2013). The impact of size on the fate and toxicity of nanoparticulate silver in aquatic systems. *Chemosphere, 93*(2), 359-365.

Antoniammal, P., & Arivuoli, D. (2012). Size and Shape Dependence on Melting Temperature of Gallium Nitride Nanoparticles. *Journal of Nanomaterials, 2012*, 415797.

Anu Mary Ealia, S., & Saravanakumar, M. P. (2017). A review on the classification, characterisation, synthesis of nanoparticles and their application. *IOP Conference Series: Materials Science and Engineering, 263*, 032019.

Arms, L., Smith, D. W., Flynn, J., Palmer, W., Martin, A., Woldu, A., & Hua, S. (2018). Advantages and Limitations of Current Techniques for Analyzing the Biodistribution of Nanoparticles. *Frontiers in Pharmacology, 9*(802).

Arora, S., Sharma, P., Kumar, S., Nayan, R., Khanna, P. K., & Zaidi, M. G. H. (2012). Gold-nanoparticle induced enhancement in growth and seed yield of Brassica juncea. *Plant Growth Regulation, 66*(3), 303-310.

Asha, A. B., & Narain, R. (2020). Chapter 15 - Nanomaterials properties. In R. Narain (Ed.), *Polymer Science and Nanotechnology* (pp. 343-359): Elsevier.

Ashraf, R., Amna, T., & Sheikh, F. A. (2020). Unique Properties of the Gold Nanoparticles: Synthesis, Functionalization and Applications. In F. A. Sheikh (Ed.), *Application of Nanotechnology in Biomedical Sciences* (pp. 75-98). Singapore: Springer Singapore.

Asli, S., & Neumann, P. M. (2009). Colloidal suspensions of clay or titanium dioxide nanoparticles can inhibit leaf growth and transpiration via physical effects on root water transport. *Plant, Cell & Environment, 32*(5), 577-584.

Attarilar, S., Yang, J., Ebrahimi, M., Wang, Q., Liu, J., Tang, Y., & Yang, J. (2020). The Toxicity Phenomenon and the Related Occurrence in Metal and Metal Oxide Nanoparticles: A Brief Review From the Biomedical Perspective. *Frontiers in Bioengineering and Biotechnology, 8*(822).

Auffan, M., Rose, J., Chanéac, C., Jolivet, J.-P., Masion, A., Wiesner, M., & Bottero, J.-Y. (2011). Surface Reactivity of Manufactured Nanoparticles. *Nanoethics and Nanotoxicology*, 269.

Avellan, A., Schwab, F., Masion, A., Chaurand, P., Borschneck, D., Vidal, V., . . . Levard, C. (2017). Nanoparticle Uptake in Plants: Gold Nanomaterial Localized in Roots of Arabidopsis thaliana by X-ray Computed Nanotomography and Hyperspectral Imaging. *Environmental Science & Technology, 51*(15), 8682-8691.

Azzazy, H., Mansour, M., Samir, T., & Franco, R. (2011). Gold nanoparticles in the clinical laboratory: Principles of preparation and applications. *Clinical Chemistry and Laboratory Medicine 50*, 193-209.

Barber, D. J., & Freestone, I. C. (1990). AN INVESTIGATION OF THE ORIGIN OF THE COLOUR OF THE LYCURGUS CUP BY ANALYTICAL TRANSMISSION ELECTRON MICROSCOPY. *Archaeometry, 32*(1), 33-45.

Barbero, Russo, L., Vitali, M., Piella, J., Salvo, I., Borrajo, M. L., . . . Puntes, V. (2017). Formation of the Protein Corona: The Interface between Nanoparticles and the Immune System. *Seminars in Immunology, 34*, 52-60.

Barbero, F., Mayall, C., Drobne, D., Saiz-Poseu, J., Bastús, N. G., & Puntes, V. (2021). Formation and evolution of the nanoparticle environmental corona: The case of Au and humic acid. *Science of the Total Environment, 768*, 144792.

Barbero, F., Moriones, O. H., Bastús, N. G., & Puntes, V. (2019). Dynamic Equilibrium in the Cetyltrimethylammonium Bromide–Au Nanoparticle Bilayer, and the Consequent Impact on the Formation of the Nanoparticle Protein Corona. *Bioconjugate Chemistry, 30*(11), 2917-2930.

Barrena, R., Casals, E., Colón, J., Font, X., Sánchez, A., & Puntes, V. (2009). Evaluation of the ecotoxicity of model nanoparticles. *Chemosphere, 75*(7), 850-857.

Bastús, N. G., Casals, E., Ojea Jimenez, I., Varón, M., & Puntes, V. (2012). The Reactivity of Colloidal Inorganic Nanoparticles. In *The Delivery of Nanoparticles* (pp. 24): IntechOpen.

Bastús, N. G., Casals, E., Vázquez-Campos, S., & Puntes, V. (2008). Reactivity of engineered inorganic nanoparticles and carbon nanostructures in biological media. *Nanotoxicology, 2*(3), 99-112.

Bastús, N. G., Comenge, J., & Puntes, V. (2011). Kinetically controlled seeded growth synthesis of citrate-stabilized gold nanoparticles of up to 200 nm: size focusing versus Ostwald ripening. *Langmuir, 27*(17), 11098-11105.

Batley, G. E., Kirby, J. K., & McLaughlin, M. J. (2013). Fate and Risks of Nanomaterials in Aquatic and Terrestrial Environments. *Accounts of Chemical Research, 46*(3), 854-862.

Baygazieva, E., Yesmurzayeva, N., Tatykhanova, G., Mun, G., Khutoryanskiy, V., & Kudaibergenov, S. (2014). Polymer Protected Gold Nanoparticles: Synthesis, Characterization and Application in Catalysis. *International Journal of Biology and Chemistry, 7*.

Bernal-Chávez, S. A., Del Prado-Audelo, M. L., Caballero-Florán, I. H., Giraldo-Gomez, D. M., Figueroa-Gonzalez, G., Reyes-Hernandez, O. D., . . . Leyva-Gómez, G. (2021). Insights into Terminal Sterilization Processes of Nanoparticles for Biomedical Applications. *Molecules, 26*(7), 2068.

Blanco, E., Shen, H., & Ferrari, M. (2015). Principles of nanoparticle design for overcoming biological barriers to drug delivery. *Nature Biotechnology, 33*(9), 941-951.

Boersema, P. J., Raijmakers, R., Lemeer, S., Mohammed, S., & Heck, A. J. R. (2009). Multiplex peptide stable isotope dimethyl labeling for quantitative proteomics. *Nature Protocols, 4*(4), 484-494.

Bogart, L. K., Pourroy, G., Murphy, C. J., Puntes, V., Pellegrino, T., Rosenblum, D., . . . Lévy, R. (2014). Nanoparticles for Imaging, Sensing, and Therapeutic Intervention. *ACS Nano, 8*(4), 3107-3122.

Boraschi, D., Alijagic, A., Auguste, M., Barbero, F., Ferrari, E., Hernadi, S., . . . Pinsino, A. (2020). Addressing Nanomaterial Immunosafety by Evaluating Innate Immunity across Living Species. *Small, 16*(21), 2000598.

Borchert, N., Dieterich, C., Krug, K., Schütz, W., Jung, S., Nordheim, A., . . . Macek, B. (2010). Proteogenomics of Pristionchus pacificus reveals distinct proteome structure of nematode models. *Genome Research, 20*(6), 837-846.

Boyoglu, C., He, Q., Willing, G., Boyoglu-Barnum, S., Dennis, V. A., Pillai, S., & Singh, S. R. (2013). Microscopic Studies of Various Sizes of Gold Nanoparticles and Their Cellular Localizations. *ISRN Nanotechnology, 2013*, 123838.

Brill, R. H. C. i. d. v. (1965). The chemistry of the Lycurgus cup. *Bruxelles: s.n.*

Bundschuh, M., Filser, J., Lüderwald, S., McKee, M. S., Metreveli, G., Schaumann, G. E., . . . Wagner, S. (2018). Nanoparticles in the environment: where do we come from, where do we go to? *Environmental Sciences Europe, 30*(1), 6.

Campisi, S., Schiavoni, M., Chan-Thaw, C., & Villa, A. (2016). Untangling the Role of the Capping Agent in Nanocatalysis: Recent Advances and Perspectives. *Catalysts, 6*, 185.

Carnovale, C., Bryant, G., Shukla, R., & Bansal, V. (2019). Identifying Trends in Gold Nanoparticle Toxicity and Uptake: Size, Shape, Capping Ligand, and Biological Corona. *ACS Omega, 4*(1), 242-256.

Carpita, N., Sabularse, D., Montezinos, D., & Delmer, D. P. (1979). Determination of the Pore Size of Cell Walls of Living Plant Cells. *Science, 205*(4411), 1144-1147.

Casals, E., Barrena, R., García, A., González, E., Delgado, L., Busquets-Fité, M., . . . Puntes, V. (2014). Programmed iron oxide nanoparticles disintegration in anaerobic digesters boosts biogas production. *Small, 10*(14), 2801-2808, 2741.

Chandra, S., Chakraborty, N., Dasgupta, A., Sarkar, J., Panda, K., & Acharya, K. (2015). Chitosan nanoparticles: A positive modulator of innate immune responses in plants. *Scientific Reports, 5*(1), 15195.

Chawla, J., Singh, D., Sundaram, B., & Kumar, A. (2018). Identifying Challenges in Assessing Risks of Exposures of Silver Nanoparticles. *Exposure and Health, 10*(1), 61-75.

Chen, Y., Xianyu, Y., & Jiang, X. (2017). Surface Modification of Gold Nanoparticles with Small Molecules for Biochemical Analysis. *Accounts of Chemical Research, 50*(2), 310-319.

Chirnside, R. C., & Proffitt, P. M. C. (1963). *"The" Rothschild Lycurgus Cup: An Analytical Investigation*: Corning Museum of Glass.

Coggon, M. M., Sorooshian, A., Wang, Z., Metcalf, A. R., Frossard, A. A., Lin, J. J., . . . Seinfeld, J. H. (2012). Ship impacts on the marine atmosphere: insights into the contribution of shipping emissions to the properties of marine aerosol and clouds. *Atmospheric Chemistry and Physics, 12*(18), 8439-8458.

Committee on Science, S., and Technology. (2011). *Oversight of the National Nanotechnology Initiative and priorities for the future hearing before the Subcommittee on Research and Science Education of the Committee on Science, Space, and Technology, House of Representatives, One Hundred Twelfth Congress, first session, April 14, 2011*. Washington: U.S. G.P.O.

Connor, E. E., Mwamuka, J., Gole, A., Murphy, C. J., & Wyatt, M. D. (2005). Gold Nanoparticles Are Taken Up by Human Cells but Do Not Cause Acute Cytotoxicity. *Small, 1*(3), 325-327.

Coradeghini, R., Gioria, S., García, C. P., Nativo, P., Franchini, F., Gilliland, D., . . . Rossi, F. (2013). Size-dependent toxicity and cell interaction mechanisms of gold nanoparticles on mouse fibroblasts. *Toxicology Letters, 217*(3), 205-216.

Cosgrove, T. (2010). *Colloid Science: Principles, Methods and Applications*: Wiley.

Cox, J., & Mann, M. (2008). MaxQuant enables high peptide identification rates, individualized p.p.b.-range mass accuracies and proteome-wide protein quantification. *Nature Biotechnology, 26*(12), 1367-1372.

Crooks, R. M., Zhao, M., Sun, L., Chechik, V., & Yeung, L. K. (2001). Dendrimer-Encapsulated Metal Nanoparticles: Synthesis, Characterization, and Applications to Catalysis. *Accounts of Chemical Research, 34*(3), 181-190.

Cruz-Valderrama, Gómez-Maqueo, X., Salazar-Iribe, A., Zúñiga-Sánchez, E., Hernández-Barrera, A., Quezada-Rodríguez, E., & Gamboa-deBuen, A. (2019). Overview of the Role of Cell Wall DUF642 Proteins in Plant Development. *International Journal of Molecular Science, 20*(13), 3333.

Dan, Y., Zhang, W., Xue, R., Ma, X., Stephan, C., & Shi, H. (2015). Characterization of Gold Nanoparticle Uptake by Tomato Plants Using Enzymatic Extraction Followed by Single-Particle Inductively Coupled Plasma–Mass Spectrometry Analysis. *Environmental Science & Technology, 49*(5), 3007-3014.

de la Rosa, G., Vázquez Núñez, E., Molina, C., vera reyes, I., & Serafin, A. (2021). Interactions of Nanomaterials and Plants at the Cellular Level: Current Knowledge and Relevant Gaps. *Nanotechnology for Environmental Engineering, 1*, 1.

Derjaguin, B. a. L., L.D. (1941). Theory of the Stability of Strongly Charged Lyophobic Sols and of the Adhesion of Strongly Charged Particles in Solutions of Electrolytes. *Acta Physicochimica U.R.S.S., 14*, 633-662.

Dobrovolskaia, M. A., & McNeil, S. E. (2007). Immunological properties of engineered nanomaterials. *Nature Nanotechnology, 2*(8), 469-478.

Downs, T. R., Crosby, M. E., Hu, T., Kumar, S., Sullivan, A., Sarlo, K., . . . Pfuhler, S. (2012). Silica nanoparticles administered at the maximum tolerated dose induce genotoxic effects through an inflammatory reaction while gold nanoparticles do not. *Mutation Research-Genetic Toxicology and Environmental Mutagenesis, 745*(1), 38-50.

Dreaden, E. C., Alkilany, A. M., Huang, X., Murphy, C. J., & El-Sayed, M. A. (2012). The golden age: gold nanoparticles for biomedicine. *Chemical Society Reviews, 41*(7), 2740-2779.

Du, W., Sun, Y., Ji, R., Zhu, J., Wu, J., & Guo, H. (2011). TiO2 and ZnO nanoparticles negatively affect wheat growth and soil enzyme activities in agricultural soil. *Journal of Environmental Monitoring, 13*(4), 822-828.

Du, W., Xu, Y., Yin, Y., Ji, R., & Guo, H. (2018). Risk assessment of engineered nanoparticles and other contaminants in terrestrial plants. *Current Opinion in Environtal Science & Health, 6*, 21-28.

Dumur, F., Dumas, E., & Mayer, C. R. (2020). Functionalization of Gold Nanoparticles by Inorganic Entities. *Nanomaterials, 10*(3), 548.

El Badawy, A. M., Silva, R. G., Morris, B., Scheckel, K. G., Suidan, M. T., & Tolaymat, T. M. (2011). Surface Charge-Dependent Toxicity of Silver Nanoparticles. *Environmental Science & Technology, 45*(1), 283-287.

El-Beltagi, H., & Mohamed, H. (2013). Reactive Oxygen Species, Lipid Peroxidation and Antioxidative Defense Mechanism. *Notulae Botanicae Horti Agrobotanici Cluj-Napoca, 41*, 44-57.

Elias, J. E., & Gygi, S. P. (2007). Target-decoy search strategy for increased confidence in large-scale protein identifications by mass spectrometry. *Nature Methods, 4*(3), 207-214.

Evanoff Jr, D. D., & Chumanov, G. (2005). Synthesis and Optical Properties of Silver Nanoparticles and Arrays. *ChemPhysChem, 6*(7), 1221-1231.

Fadeel, B., Farcal, L., Hardy, B., Vázquez-Campos, S., Hristozov, D., Marcomini, A., . . . Savolainen, K. (2018). Advanced tools for the safety assessment of nanomaterials. *Nature Nanotechnology, 13*.

Faraday, M. (1857). X. The Bakerian Lecture. —Experimental relations of gold (and other metals) to light. *Philosophical Transactions of the Royal Society of London, 147*, 145-181.

Feichtmeier, N. S., Walther, P., & Leopold, K. (2015). Uptake, effects, and regeneration of barley plants exposed to gold nanoparticles. *Environmental Science and Pollution Research International, 22*(11), 8549-8558.

Feidantsis, K., Kalogiannis, S., Marinoni, A., Vasilogianni, A. M., Gkanatsiou, C., Kastrinaki, G., . . . Kaloyianni, M. (2020). Toxicity assessment and comparison of the land snail's Cornu aspersum

responses against CuO nanoparticles and ZnO nanoparticles. *Comparative Biochemistry and Physiology Part C Toxicology & Pharmacology, 236*, 108817.

Ferrari, E., Barbero, F., Busquets-Fité, M., Franz-Wachtel, M., Köhler, H.-R., Puntes, V., & Kemmerling, B. (2021). Growth-Promoting Gold Nanoparticles Decrease Stress Responses in Arabidopsis Seedlings. *Nanomaterials, 11*(12), 3161.

Feynman, R. P. (1959). There´s Plenty of room at the Bottom. *Caltech's Engineeringand Science, 23*, 22-36.

Fong, K. E., & Yung, L. Y. (2013). Localized surface plasmon resonance: a unique property of plasmonic nanoparticles for nucleic acid detection. *Nanoscale, 5*(24), 12043-12071.

França, Á., Pelaz, B., Moros, M., Sánchez-Espinel, C., Hernández, A., Fernández-López, C., . . . González-Fernández, Á. (2010). Sterilization Matters: Consequences of Different Sterilization Techniques on Gold Nanoparticles. *Small, 6*(1), 89-95.

Freestone, I., Meeks, N., Sax, M., & Higgitt, C. (2007). The Lycurgus Cup — A Roman nanotechnology. *Gold Bulletin, 40*(4), 270-277.

Fuller, M., & Köper, I. (2018). Polyelectrolyte-Coated Gold Nanoparticles: The Effect of Salt and Polyelectrolyte Concentration on Colloidal Stability. *Polymers, 10*(12), 1336.

Gao, Y., Badejo, A. A., Sawa, Y., & Ishikawa, T. (2012). Analysis of two L-Galactono-1,4-lactone-responsive genes with complementary expression during the development of Arabidopsis thaliana. *Plant & Cell Physiology, 53*(3), 592-601.

Gatoo, M. A., Naseem, S., Arfat, M. Y., Dar, A. M., Qasim, K., & Zubair, S. (2014). Physicochemical properties of nanomaterials: implication in associated toxic manifestations. *BioMed Research International, 2014*, 498420.

Gavia, D. J., & Shon, Y.-S. (2015). Catalytic Properties of Unsupported Palladium Nanoparticle Surfaces Capped with Small Organic Ligands. *ChemCatChem, 7*(6), 892-900.

Giese, B., Klaessig, F., Park, B., Kaegi, R., Steinfeldt, M., Wigger, H., . . . Gottschalk, F. (2018). Risks, Release and Concentrations of Engineered Nanomaterial in the Environment. *Scientific Reports, 8*(1), 1565.

Glenn, J. B., White, S. A., & Klaine, S. J. (2012). Interactions of gold nanoparticles with freshwater aquatic macrophytes are size and species dependent. *Environmental Toxicology Chemistry, 31*(1), 194-201.

Godakhindi, V. S., Kang, P., Serre, M., Revuru, N. A., Zou, J. M., Roner, M. R., . . . Qin, Z. (2017). Tuning the Gold Nanoparticle Colorimetric Assay by Nanoparticle Size, Concentration, and Size Combinations for Oligonucleotide Detection. *ACS Sensors, 2*(11), 1627-1636.

Göeken, K. L., Subramaniam, V., & Gill, R. (2015). Enhancing spectral shifts of plasmon-coupled noble metal nanoparticles for sensing applications. *Physical Chemistry Chemical Physics, 17*(1), 422-427.

Goutam, S., Saxena, G., Roy, D., Yadav, A., & Bharagava, R. (2019). Green Synthesis of Nanoparticles and Their Applications in Water and Wastewater Treatment. In *Bioremediation of Industrial Wasre for Environmental Safety* (pp. 349-379).

Grisel, R., Weststrate, K.-J., Gluhoi, A., & Nieuwenhuys, B. E. (2002). Catalysis by Gold Nanoparticles. *Gold Bulletin, 35*(2), 39-45.

Gruber, C. M., Jr., & Halbeisen, W. A. (1948). A study on the comparative toxic effects of citric acid and its sodium salts. *Journal of Pharmacology and Experimental Therapeutics, 94*(1), 65-67.

Guerrini, L., Alvarez-Puebla, R. A., & Pazos-Perez, N. (2018). Surface Modifications of Nanoparticles for Stability in Biological Fluids. *Materials, 11*(7), 1154.

Gupta, R., & Xie, H. (2018). Nanoparticles in Daily Life: Applications, Toxicity and Regulations. *Journal of environmental pathology, toxicology and oncology : official organ of the International Society for Environmental Toxicology and Cancer, 37*(3), 209-230.

Haiss, W., Thanh, N. T. K., Aveyard, J., & Fernig, D. G. (2007). Determination of Size and Concentration of Gold Nanoparticles from UV−Vis Spectra. *Analytical Chemistry, 79*(11), 4215-4221.

Hammer, B., & Norskov, J. K. (1995). Why gold is the noblest of all the metals. *Nature, 376*(6537), 238-240.

He, Y. Q., Liu, S. P., Kong, L., & Liu, Z. F. (2005). A study on the sizes and concentrations of gold nanoparticles by spectra of absorption, resonance Rayleigh scattering and resonance non-linear scattering. *Spectrochimica Acta Part A: Molecular and Biomolecular Spectroscopy, 61*(13-14), 2861-2866.

Hendel, T., Wuithschick, M., Kettemann, F., Birnbaum, A., Rademann, K., & Polte, J. (2014). In Situ Determination of Colloidal Gold Concentrations with UV–Vis Spectroscopy: Limitations and Perspectives. *Analytical Chemistry, 86*(22), 11115-11124.

Hermes-Lima, M., Willmore, W. G., & Storey, K. B. (1995). Quantification of lipid peroxidation in tissue extracts based on Fe(III)xylenol orange complex formation. *Free Radical Biology & Medicine, 19*(3), 271-280.

Hochella, M., Aruguete, D., Kim, B., & Elwood Madden, A. (2012). Naturally occurring inorganic nanoparticles: general assessment and a global budget for one of earth's last unexplored major geochemical components. *Barnard AS*, 1-42.

Hochella, M. F., Jr., Lower, S. K., Maurice, P. A., Penn, R. L., Sahai, N., Sparks, D. L., & Twining, B. S. (2008). Nanominerals, mineral nanoparticles, and Earth systems. *Science, 319*(5870), 1631-1635.

Hochella, M. F., Mogk, D. W., Ranville, J., Allen, I. C., Luther, G. W., Marr, L. C., . . . Yang, Y. (2019). Natural, incidental, and engineered nanomaterials and their impacts on the Earth system. *Science, 363*(6434), eaau8299.

Holland, N. A., Thompson, L. C., Vidanapathirana, A. K., Urankar, R. N., Lust, R. M., Fennell, T. R., & Wingard, C. J. (2016). Impact of pulmonary exposure to gold core silver nanoparticles of different size and capping agents on cardiovascular injury. *Particle and Fibre Toxicology, 13*(1), 48.

Hossain, Z., Mustafa, G., & Komatsu, S. (2015). Plant Responses to Nanoparticle Stress. *International Journal of Molecular Sciences, 16*(11), 26644-26653.

Hsiao, I. L., Bierkandt, F. S., Reichardt, P., Luch, A., Huang, Y. J., Jakubowski, N., . . . Haase, A. (2016). Quantification and visualization of cellular uptake of TiO2 and Ag nanoparticles: comparison of different ICP-MS techniques. *Journal of Nanobiotechnology, 14*(1), 50.

Huang, X., & El-Sayed, M. A. (2010). Gold nanoparticles: Optical properties and implementations in cancer diagnosis and photothermal therapy. *Journal of Advanced Research, 1*(1), 13-28.

Hulla, J. E., Sahu, S. C., & Hayes, A. W. (2015). Nanotechnology: History and future. *Human & Experimental Toxicology, 34*(12), 1318-1321.

Husen, A., Iqbal, M., & Aref, I. M. (2014). Growth, water status, and leaf characteristics of Brassica carinata under drought and rehydration conditions. *Brazilian Journal of Botany, 37*(3), 217-227.

Iravani, S., Korbekandi, H., Mirmohammadi, S. V., & Zolfaghari, B. (2014). Synthesis of silver nanoparticles: chemical, physical and biological methods. *Research in Pharmaceutical Sciences, 9*(6), 385-406.

Jain, P. K., Huang, X., El-Sayed, I. H., & El-Sayed, M. A. (2008). Noble metals on the nanoscale: optical and photothermal properties and some applications in imaging, sensing, biology, and medicine. *Accounts of Chemical Research, 41*(12), 1578-1586.

Jain, P. K., Lee, K. S., El-Sayed, I. H., & El-Sayed, M. A. (2006). Calculated absorption and scattering properties of gold nanoparticles of different size, shape, and composition: applications in biological imaging and biomedicine. *The Journal of Physical Chemistry B, 110*(14), 7238-7248.

Javed, R., Zia, M., Naz, S., Aisida, S. O., Ain, N. u., & Ao, Q. (2020). Role of capping agents in the application of nanoparticles in biomedicine and environmental remediation: recent trends and future prospects. *Journal of Nanobiotechnology, 18*(1), 172.

Jaworek, A., Szudyga, M., Krupa, A., Czech, T., Sobczyk, A. T., Marchewicz, A., . . . Charchalis, A. (2014). Technical issues of PM removal from ship diesel engines. *Transport Research Arena*.

Johnson, M., & Hillier, K. (2007). Sodium Citrate. In S. J. Enna & D. B. Bylund (Eds.), *xPharm: The Comprehensive Pharmacology Reference* (pp. 1-4). New York: Elsevier.

Judy, J. D., Unrine, J. M., Rao, W., Wirick, S., & Bertsch, P. M. (2012). Bioavailability of Gold Nanomaterials to Plants: Importance of Particle Size and Surface Coating. *Environmental Science & Technology, 46*(15), 8467-8474.

Kah, M., Kookana, R. S., Gogos, A., & Bucheli, T. D. (2018). A critical evaluation of nanopesticides and nanofertilizers against their conventional analogues. *Nature Nanotechnology, 13*(8), 677-684.

Kalman, J., Paul, K. B., Khan, F. R., Stone, V., & Fernandes, T. F. (2015). Characterisation of bioaccumulation dynamics of three differently coated silver nanoparticles and aqueous silver in a simple freshwater food chain. *Environmental Chemistry, 12*(6), 662-672.

Kang, H., Hwang, Y. G., Lee, T. G., Jin, C. R., Cho, C. H., Jeong, H. Y., & Kim, D. O. (2016). Use of Gold Nanoparticle Fertilizer Enhances the Ginsenoside Contents and Anti-Inflammatory Effects of Red Ginseng. *Journal of Microbiology and Biotechnology, 26*(10), 1668-1674.

Karimi, S., Moshaii, A., Abbasian, S., & Nikkhah, M. (2019). Surface Plasmon Resonance in Small Gold Nanoparticles: Introducing a Size-Dependent Plasma Frequency for Nanoparticles in Quantum Regime. *Plasmonics, 14*(4), 851-860.

Kelly, K. L., Coronado, E., Zhao, L. L., & Schatz, G. C. (2003). The Optical Properties of Metal Nanoparticles: The Influence of Size, Shape, and Dielectric Environment. *The Journal of Physical Chemistry B, 107*(3), 668-677.

Khan, Saeed, K., & Khan, I. (2019). Nanoparticles: Properties, applications and toxicities. *Arabian Journal of Chemistry, 12*(7), 908-931.

Khan, H. A., Abdelhalim, M. A. K., Alhomida, A. S., & Al-Ayed, M. S. (2013). Effects of Naked Gold Nanoparticles on Proinflammatory Cytokines mRNA Expression in Rat Liver and Kidney. *BioMed Research International, 2013*, 590730.

Khan, M., Ahamad, F., & Fatima, T. (2019). Effect of Nanoparticles on Plant Pathogens. In *Advances in Phytonanotechnology* (pp. 215-240).

Khan, T., Ullah, N., Khan, M. A., Mashwani, Z.-u.-R., & Nadhman, A. (2019). Plant-based gold nanoparticles; a comprehensive review of the decade-long research on synthesis, mechanistic aspects and diverse applications. *Advances in Colloid and Interface Science, 272*, 102017.

Kharat, M. G., Murthy, S., & Kamble, S. (2017). Environmental Applications of Nanotechnology: A Review. *ADBU Journal of Engineering Technology (AJET), 6*.

Kim, D., Langmead, B., & Salzberg, S. L. (2015). HISAT: a fast spliced aligner with low memory requirements. *Nature Methods, 12*(4), 357-360.

Kim, D., Shin, K., Kwon, S. G., & Hyeon, T. (2018). Synthesis and Biomedical Applications of Multifunctional Nanoparticles. *Advanced Materials, 30*(49), 1802309.

Kim, T., Lee, C. H., Joo, S. W., & Lee, K. (2008). Kinetics of gold nanoparticle aggregation: experiments and modeling. *Journal of Colloid and Interface Science, 318*(2), 238-243.

Kimling, J., Maier, M., Okenve, B., Kotaidis, V., Ballot, H., & Plech, A. (2006). Turkevich Method for Gold Nanoparticle Synthesis Revisited. *The Journal of Physical Chemistry B, 110*(32), 15700-15707.

Klatte, M., Schuler, M., Wirtz, M., Fink-Straube, C., Hell, R., & Bauer, P. (2009). The Analysis of Arabidopsis Nicotianamine Synthase Mutants Reveals Functions for Nicotianamine in Seed Iron Loading and Iron Deficiency Responses. *Plant Physiology, 150*(1), 257-271.

Kliza, K., Taumer, C., Pinzuti, I., Franz-Wachtel, M., Kunzelmann, S., Stieglitz, B., . . . Husnjak, K. (2017). Internally tagged ubiquitin: a tool to identify linear polyubiquitin-modified proteins by mass spectrometry. *Nature Methods, 14*(5), 504-512.

Koczkur, K. M., Mourdikoudis, S., Polavarapu, L., & Skrabalak, S. E. (2015). Polyvinylpyrrolidone (PVP) in nanoparticle synthesis. *Dalton transactions 44*(41), 17883-17905.

Koelmel, J., Leland, T., Wang, H., Amarasiriwardena, D., & Xing, B. (2013). Investigation of gold nanoparticles uptake and their tissue level distribution in rice plants by laser ablation-inductively coupled-mass spectrometry. *Environmental Pollution, 174*, 222-228.

Kokarneswaran, M., Selvaraj, P., Ashokan, T., Perumal, S., Sellappan, P., Murugan, K. D., . . . Chandrasekaran, V. (2020). Discovery of carbon nanotubes in sixth century BC potteries from Keeladi, India. *Scientific Reports, 10*(1), 19786-19786.

Kong, L., Zhang, Y., Ye, Z. Q., Liu, X. Q., Zhao, S. Q., Wei, L., & Gao, G. (2007). CPC: assess the protein-coding potential of transcripts using sequence features and support vector machine. *Nucleic Acids Research, 35*(Web Server issue), W345-349.

Kranjc, E., & Drobne, D. (2019). Nanomaterials in Plants: A Review of Hazard and Applications in the Agri-Food Sector. *Nanomaterials (Basel, Switzerland), 9*(8), 1094.

Krug, H. F. (2018). The uncertainty with nanosafety: Validity and reliability of published data. *Colloids and Surfaces B: Biointerfaces, 172*, 113-117.

Kumar, V., Guleria, P., Kumar, V., & Yadav, S. K. (2013). Gold nanoparticle exposure induces growth and yield enhancement in Arabidopsis thaliana. *Science of the Total Environment, 461-462*, 462-468.

Langmead, B., & Salzberg, S. L. (2012). Fast gapped-read alignment with Bowtie 2. *Nature Methods, 9*(4), 357-359.

Lee, J.-H., Choi, S. U. S., Jang, S. P., & Lee, S. Y. (2012). Production of aqueous spherical gold nanoparticles using conventional ultrasonic bath. *Nanoscale Research Letters, 7*(1), 420.

Lelieveld, J., Evans, J. S., Fnais, M., Giannadaki, D., & Pozzer, A. (2015). The contribution of outdoor air pollution sources to premature mortality on a global scale. *Nature, 525*(7569), 367-371.

Leso, V., Fontana, L., & Iavicoli, I. (2019). Biomedical nanotechnology: Occupational views. *Nano Today, 24*, 10-14.

Lespes, G., Faucher, S., & Slaveykova, V. I. (2020). Natural Nanoparticles, Anthropogenic Nanoparticles, Where Is the Frontier? *Frontiers in Environmental Science, 8*(71).

Li, Hartono, D., Ong, C.-N., Bay, B.-H., & Yung, L.-Y. L. (2010). Autophagy and oxidative stress associated with gold nanoparticles. *Biomaterials, 31*(23), 5996-6003.

Li, B., & Dewey, C. N. (2011). RSEM: accurate transcript quantification from RNA-Seq data with or without a reference genome. *BMC Bioinformatics, 12*(1), 323.

Li, Y., Italiani, P., Casals, E., Valkenborg, D., Mertens, I., Baggerman, G., . . . Boraschi, D. (2016). Assessing the Immunosafety of Engineered Nanoparticles with a Novel in Vitro Model Based on Human Primary Monocytes. *ACS Applied Materials & Interfaces, 8*(42), 28437-28447.

Lin, D., & Xing, B. (2008). Root Uptake and Phytotoxicity of ZnO Nanoparticles. *Environmental Science & Technology, 42*(15), 5580-5585.

Lin, H. (2010). Earth's Critical Zone and hydropedology: concepts, characteristics, and advances. *Hydrology and Earth System Sciences, 14*(1), 25-45.

Link, S., & El-Sayed, M. A. (2003). Optical properties and ultrafast dynamics of metallic nanocrystals. *Annual Review of Physical Chemistry, 54*, 331-366.

Link, S., & El-Sayed, M. A. (1999). Size and Temperature Dependence of the Plasmon Absorption of Colloidal Gold Nanoparticles. *The Journal of Physical Chemistry B, 103*(21), 4212-4217.

Lisha, K. P., & Pradeep, T. (2009). Enhanced visual detection of pesticides using gold nanoparticles. *Journal of Environmental Science and Health Part B, 44*(7), 697-705.

Liu, J., Williams, P. C., Geisler-Lee, J., Goodson, B. M., Fakharifar, M., Peiravi, M., . . . Gemeinhardt, M. E. (2018). Impact of wastewater effluent containing aged nanoparticles and other components on biological activities of the soil microbiome, Arabidopsis plants, and earthworms. *Environmental Research, 164*, 197-203.

Liu, R., & Lal, R. (2015). Potentials of engineered nanoparticles as fertilizers for increasing agronomic productions. *Science of the Total Environment, 514*, 131-139.

Lopez-Chaves, C., Soto-Alvaredo, J., Montes-Bayon, M., Bettmer, J., Llopis, J., & Sanchez-Gonzalez, C. (2018). Gold nanoparticles: Distribution, bioaccumulation and toxicity. In vitro and in vivo studies. *Nanomedicine, 14*(1), 1-12.

Loss, D. (2009). Quantum phenomena in Nanotechnology. *Nanotechnology, 20*(43), 430205.

Lovecká, P., Macůrková, A., Záruba, K., Hubáček, T., Siegel, J., & Valentová, O. (2021). Genomic Damage Induced in Nicotiana tabacum L. Plants by Colloidal Solution with Silver and Gold Nanoparticles. *Plants, 10*(6), 1260.

Lunardi, C. N., Gomes, A. J., Rocha, F. S., De Tommaso, J., & Patience, G. S. (2021). Experimental methods in chemical engineering: Zeta potential. *The Canadian Journal of Chemical Engineering, 99*(3), 627-639.

Ma, X., Geisler-Lee, J., Deng, Y., & Kolmakov, A. (2010). Interactions between engineered nanoparticles (ENPs) and plants: phytotoxicity, uptake and accumulation. *Science of the Total Environment, 408*(16), 3053-3061.

Macpherson, S., Webber, G., & Moreno-atanasio, R. (2012). Aggregation of nanoparticles in high ionic strength suspensions: Effect of Hamaker constant and particle concentration. *Advanced Powder Technology, 23*, 478-484.

Mahakham, W., Theerakulpisut, P., Maensiri, S., Phumying, S., & Sarmah, A. (2016). Environmentally benign synthesis of phytochemicals-capped gold nanoparticles as nanopriming agent for promoting maize seed germination. *The Science of the Total Environment, 573*, 1089-1102.

Mahato, K., Nagpal, S., Shah, M. A., Srivastava, A., Maurya, P. K., Roy, S., . . . Chandra, P. (2019). Gold nanoparticle surface engineering strategies and their applications in biomedicine and diagnostics. *3 Biotech, 9*(2), 57.

Mansoori, G., & Soelaiman, T. A. F. (2005). Nanotechnology - An Introduction for the Standards Community. *Journal of ASTM International, 2*, 1-22.

Marslin, G., Sheeba, C., & Gregory, F. (2017). Nanoparticles Alter Secondary Metabolism in Plants via ROS Burst. *Frontiers in Plant Science, 8*, 832.

Masson, J.-F. (2020). Portable and field-deployed surface plasmon resonance and plasmonic sensors. *Analyst, 145*(11), 3776-3800.

Masson, V., Maurin, F., Fessi, H., & Devissaguet, J. P. (1997). Influence of sterilization processes on poly(epsilon-caprolactone) nanospheres. *Biomaterials, 18*(4), 327-335.

Mateo, D., Morales, P., Ávalos, A., & Haza, A. I. (2014). Oxidative stress contributes to gold nanoparticle-induced cytotoxicity in human tumor cells. *Toxicology Mechanisms and Methods, 24*(3), 161-172.

Mauriz, E. (2020). Clinical Applications of Visual Plasmonic Colorimetric Sensing. *Sensors, 20*(21), 6214.

Memisoglu-Bilensoy, E., & Hincal, A. A. (2006). Sterile, injectable cyclodextrin nanoparticles: effects of gamma irradiation and autoclaving. *International Journal of Pharmaceutics, 311*(1-2), 203-208.

Milewska-Hendel, A., Zubko, M., Karcz, J., Stróż, D., & Kurczyńska, E. (2017). Fate of neutral-charged gold nanoparticles in the roots of the Hordeum vulgare L. cultivar Karat. *Scientific Reports, 7*(1), 3014.

Milewska-Hendel, A., Zubko, M., Stróż, D., & Kurczyńska, E. U. (2019). Effect of Nanoparticles Surface Charge on the Arabidopsis thaliana (L.) Roots Development and Their Movement into the Root Cells and Protoplasts. *International Journal of Molecular Sciences, 20*(7).

Misra, S. K., Dybowska, A., Berhanu, D., Luoma, S. N., & Valsami-Jones, E. (2012). The complexity of nanoparticle dissolution and its importance in nanotoxicological studies. *Science of the Total Environment, 438*, 225-232.

Mitchell, M. J., Billingsley, M. M., Haley, R. M., Wechsler, M. E., Peppas, N. A., & Langer, R. (2021). Engineering precision nanoparticles for drug delivery. *Nature Reviews Drug Discovery, 20*(2), 101-124.

Mittal, D., Kaur, G., Singh, P., Yadav, K., & Ali, S. A. (2020). Nanoparticle-Based Sustainable Agriculture and Food Science: Recent Advances and Future Outlook. *Frontiers in Nanotechnology, 2*(10).

Miyazaki, K., & Islam, N. (2007). Nanotechnology systems of innovation—An analysis of industry and academia research activities. *Technovation, 27*(11), 661-675.

Mody, V. V., Siwale, R., Singh, A., & Mody, H. R. (2010). Introduction to metallic nanoparticles. *Journal of Pharmacy & Bioallied Sciences, 2*(4), 282-289.

Moore, T., Rodriguez Lorenzo, L., Hirsch, V., Balog, S., Urban, D., Jud, C., . . . Fink, A. (2015). Nanoparticle colloidal stability in cell culture media and impact on cellular interactions. *Chemical Society reviews, 44*.

Mueller, N. C., & Nowack, B. (2008). Exposure Modeling of Engineered Nanoparticles in the Environment. *Environmental Science & Technology, 42*(12), 4447-4453.

Murdock, R. C., Braydich-Stolle, L., Schrand, A. M., Schlager, J. J., & Hussain, S. M. (2008). Characterization of nanomaterial dispersion in solution prior to in vitro exposure using dynamic light scattering technique. *Toxicological Sciences, 101*(2), 239-253.

Naseer, M., Aslam, U., Khalid, B., & Chen, B. (2020). Green route to synthesize Zinc Oxide Nanoparticles using leaf extracts of Cassia fistula and Melia azadarach and their antibacterial potential. *Scientific Reports, 10*(1), 9055.

Ngou, B. P. M., Ding, P., & Jones, J. D. G. (2022). Thirty years of resistance: Zig-zag through the plant immune system. *The Plant Cell, 34*(5), 1447-1478.

Nierenberg, D., Khaled, A. R., & Flores, O. (2018). Formation of a protein corona influences the biological identity of nanomaterials. *Reports of Practical Oncology & Radiotherapy, 23*(4), 300-308.

Noël, S., Léger, B., Ponchel, A., Philippot, K., Denicourt-Nowicki, A., Roucoux, A., & Monflier, E. (2014). Cyclodextrin-based systems for the stabilization of metallic(0) nanoparticles and their versatile applications in catalysis. *Catalysis Today, 235*, 20-32.

Nogrady, B. (2021). How nanotechnology can flick the immunity switch. *Nature, 595*(7865), S18-s19.

Nowack, B., Ranville, J. F., Diamond, S., Gallego-Urrea, J. A., Metcalfe, C., Rose, J., . . . Klaine, S. J. (2012). Potential scenarios for nanomaterial release and subsequent alteration in the environment. *Environmental Toxicology and Chemistry, 31*(1), 50-59.

Nur, Y. (2013). *Gold nanoparticles: synthesis, characterisation and their effect on Pseudomonas flourescens*.

Ojea-Jiménez, I., López, X., Arbiol, J., & Puntes, V. (2012). Citrate-Coated Gold Nanoparticles As Smart Scavengers for Mercury(II) Removal from Polluted Waters. *ACS Nano, 6*(3), 2253-2260.

Oncsik, T., Trefalt, G., Borkovec, M., & Szilagyi, I. (2015). Specific Ion Effects on Particle Aggregation Induced by Monovalent Salts within the Hofmeister Series. *Langmuir, 31*(13), 3799-3807.

Özcan, I., Bouchemal, K., Segura Sánchez, F., Abaci, Ö., Özer, Ö., Güneri, T., & Ponchel, G. (2009). Effects of sterilization techniques on the PEGylated poly (γ-benzyl-L-glutamate) (PBLG) nanoparticles. *Acta Pharmaceutica Sciencia, 51*, 211-218.

Palihawadana, M., Naik, V., Vaishnava, P., Jena, B., & Naik, R. (2017). Gd-Doped Superparamagnetic Magnetite Nanoparticles for Potential Cancer Theranostics. In *Nanostructured Materials*.

Pamies, R., Cifre, J., Espín, V., Collado-González, M. M., Díaz Baños, F. G., & Torre, J. (2014). Aggregation behaviour of gold nanoparticles in saline aqueous media. *Journal of Nanoparticle Research, 16*, 2376:2371-2311.

Pan, Y., Leifert, A., Ruau, D., Neuss, S., Bornemann, J., Schmid, G., . . . Jahnen-Dechent, W. (2009). Gold Nanoparticles of Diameter 1.4 nm Trigger Necrosis by Oxidative Stress and Mitochondrial Damage. *Small, 5*(18), 2067-2076.

Park, J., Joo, J., Kwon, S. G., Jang, Y., & Hyeon, T. (2007). Synthesis of Monodisperse Spherical Nanocrystals. *Angewandte Chemie International Edition, 46*(25), 4630-4660.

Park, S., Lee, W. J., Park, S., Choi, D., Kim, S., & Park, N. (2019). Reversibly pH-responsive gold nanoparticles and their applications for photothermal cancer therapy. *Scientific Reports, 9*(1), 20180.

Peijnenburg, W. J. G. M., Baalousha, M., Chen, J., Chaudry, Q., Von der kammer, F., Kuhlbusch, T. A. J., . . . Koelmans, A. A. (2015). A Review of the Properties and Processes Determining the Fate of Engineered Nanomaterials in the Aquatic Environment. *Critical Reviews in Environmental Science and Technology, 45*(19), 2084-2134.

Pérez-de-Luque, A. (2017). Interaction of Nanomaterials with Plants: What Do We Need for Real Applications in Agriculture? *Frontiers in Environmental Science, 5*, 12.

Pertea, M., Pertea, G. M., Antonescu, C. M., Chang, T.-C., Mendell, J. T., & Salzberg, S. L. (2015). StringTie enables improved reconstruction of a transcriptome from RNA-seq reads. *Nature Biotechnology, 33*(3), 290-295.

Piella, J., Bastús, N., & Puntes, V. (2016). Size-Controlled Synthesis of Sub-10-nanometer Citrate-Stabilized Gold Nanoparticles and Related Optical Properties. *Chemistry of Materials, 28*(4), 1066-1075.

Piella, J., Bastús, N. G., & Puntes, V. (2017). Size-Dependent Protein–Nanoparticle Interactions in Citrate-Stabilized Gold Nanoparticles: The Emergence of the Protein Corona. *Bioconjugate Chemistry, 28*(1), 88-97.

Piryazev, A. P., Azizova, O. A., Aseichev, A. V., Dudnik, L. B., & Sergienko, V. I. (2013). Effect of gold nanoparticles on production of reactive oxygen species by human peripheral blood leukocytes stimulated with opsonized zymosan. *Bulletin of Experimental Biology and Medicine, 156*(1), 101-103.

Powers, K., Palazuelos, M., Moudgil, B., & Roberts, S. (2009). Characterization of the size, shape, and state of dispersion of nanoparticles for toxicological studies. *Nanotoxicology, 1*, 42-51.

Qiao, L., Fu, Z., Li, J., Ghosen, J., Zeng, M., Stebbins, J., . . . Swihart, M. T. (2017). Standardizing Size- and Shape-Controlled Synthesis of Monodisperse Magnetite (Fe3O4) Nanocrystals by Identifying and Exploiting Effects of Organic Impurities. *ACS Nano, 11*(6), 6370-6381.

Rahme, K., Gauffre, F., Marty, J.-D., Payré, B., & Mingotaud, C. (2007). A Systematic Study of the Stabilization in Water of Gold Nanoparticles by Poly(Ethylene Oxide)−Poly(Propylene Oxide)−Poly(Ethylene Oxide) Triblock Copolymers. *The Journal of Physical Chemistry C, 111*(20), 7273-7279.

Rahme, K., Vicendo, P., Ayela, C., Gaillard, C., Payré, B., Mingotaud, C., & Gauffre, F. (2009). A Simple Protocol to Stabilize Gold Nanoparticles using Amphiphilic Block Copolymers: Stability Studies and Viable Cellular Uptake. *Chemistry – A European Journal, 15*(42), 11151-11159.

Raliya, R., Franke, C., Chavalmane, S., Nair, R., Reed, N., & Biswas, P. (2016). Quantitative Understanding of Nanoparticle Uptake in Watermelon Plants. *Frontiers in Plant Science, 7*(1288).

Ramalingam, V. (2019). Multifunctionality of gold nanoparticles: Plausible and convincing properties. *Advances in Colloid and Interface Science, 271*, 101989.

Ranoszek-Soliwoda, K., Tomaszewska, E., Socha, E., Krzyczmonik, P., Ignaczak, A., Orlowski, P., . . . Grobelny, J. (2017). The role of tannic acid and sodium citrate in the synthesis of silver nanoparticles. *Journal of Nanoparticle Research, 19*(8), 273.

Rappsilber, J., Mann, M., & Ishihama, Y. (2007). Protocol for micro-purification, enrichment, pre-fractionation and storage of peptides for proteomics using StageTips. *Nature Protocols, 2*(8), 1896-1906.

Rasmussen, M. K., Pedersen, J. N., & Marie, R. (2020). Size and surface charge characterization of nanoparticles with a salt gradient. *Nature Communications, 11*(1), 2337.

Raveendran, P., Fu, J., & Wallen, S. L. (2003). Completely “Green” Synthesis and Stabilization of Metal Nanoparticles. *Journal of the American Chemical Society, 125*(46), 13940-13941.

Reynolds, E. S. (1963). The use of lead citrate at high pH as an electron-opaque stain in electron microscopy. *The Journal of Cell Biology, 17*(1), 208-212.

Rico, C. M., Majumdar, S., Duarte-Gardea, M., Peralta-Videa, J. R., & Gardea-Torresdey, J. L. (2011). Interaction of Nanoparticles with Edible Plants and Their Possible Implications in the Food Chain. *Journal of Agricultural and Food Chemistry, 59*(8), 3485-3498.

Rizwan, M., Shoukat, A., Ayub, A., Razzaq, B., & Tahir, M. B. (2021). Chapter 3 - Types and classification of nanomaterials. In M. B. Tahir, M. Sagir, & A. M. Asiri (Eds.), *Nanomaterials: Synthesis, Characterization, Hazards and Safety* (pp. 31-54): Elsevier.

Roberto, M., & Christofoletti, C. (2019). How to Assess Nanomaterial Toxicity? An Environmental and Human Health Approach. In *Nanomaterials - Toxicity, Human Health and Environment*: IntechOpen.

Robles, H. (2005). Tannic Acid. In P. Wexler (Ed.), *Encyclopedia of Toxicology (Second Edition)* (pp. 134-136). New York: Elsevier.

Ruttkay-Nedecky, B., Krystofova, O., Nejdl, L., & Adam, V. (2017). Nanoparticles based on essential metals and their phytotoxicity. *Journal of Nanobiotechnology, 15*(1), 33.

S. Ali, A. (2020). Application of Nanomaterials in Environmental Improvement. In *Nanotechnology and the Environment*: IntechOpe.

Sabo-Attwood, T., Unrine, J. M., Stone, J. W., Murphy, C. J., Ghoshroy, S., Blom, D., . . . Newman, L. A. (2012). Uptake, distribution and toxicity of gold nanoparticles in tobacco (Nicotiana xanthi) seedlings. *Nanotoxicology, 6*(4), 353-360.

Sadik, O. (2012). Anthropogenic nanoparticles in the environment. *Environmental Science: Processes Impacts, 15*, 19-20.

Safo, I., Werheid, M., Dosche, C., & Oezaslan, M. (2019). The role of Polyvinylpyrrolidone (PVP) as Capping and Structure-Directing Agent in the Formation of Pt Nanocubes. *Nanoscale Advances, 1*.

Saijo, Y., Loo, E., & Yasuda, S. (2017). Pattern recognition receptors and signaling in plant-microbe interactions. *The Plant Journal, 93*.

Sanzari, I., Leone, A., & Ambrosone, A. (2019). Nanotechnology in Plant Science: To Make a Long Story Short. *Frontiers in Bioengineering and Biotechnology, 7*(120).

Sapsford, K. E., Tyner, K. M., Dair, B. J., Deschamps, J. R., & Medintz, I. L. (2011). Analyzing Nanomaterial Bioconjugates: A Review of Current and Emerging Purification and Characterization Techniques. *Analytical Chemistry, 83*(12), 4453-4488.

Sarropoulou, V., Dimassi, K., & Therios, I. (2015). Medium strength in inorganics and PVP concentration effects on cherry rootstocks in vitro rooting. *Horticultural Science, 42*, 185-192.

Schatz, G. C. (2007). Using theory and computation to model nanoscale properties. *Proceedings of the National Academy of Sciences, 104*(17), 6885-6892.

Schmidt, W., Thomine, S., & Buckhout, T. J. (2020). Editorial: Iron Nutrition and Interactions in Plants. *Frontiers in Plant Science, 10*.

Schmieg, H., Huppertsberg, S., Knepper, T. P., Krais, S., Reitter, K., Rezbach, F., . . . Triebskorn, R. (2020). Polystyrene microplastics do not affect juvenile brown trout (Salmo trutta f. fario) or modulate effects of the pesticide methiocarb. *Environmental Sciences Europe, 32*(1), 49.

Schwirn, K., Tietjen, L., & Beer, I. (2014). Why are nanomaterials different and how can they be appropriately regulated under REACH? *Environmental Sciences Europe, 26*(1), 4.

Selvamani, V. (2019). Chapter 15 - Stability Studies on Nanomaterials Used in Drugs. In S. S. Mohapatra, S. Ranjan, N. Dasgupta, R. K. Mishra, & S. Thomas (Eds.), *Characterization and Biology of Nanomaterials for Drug Delivery* (pp. 425-444): Elsevier.

Senut, M.-C., Zhang, Y., Liu, F., Sen, A., Ruden, D. M., & Mao, G. (2016). Size-Dependent Toxicity of Gold Nanoparticles on Human Embryonic Stem Cells and Their Neural Derivatives. *Small, 12*(5), 631-646.

Sepúlveda, B., Angelomé, P. C., Lechuga, L. M., & Liz-Marzán, L. M. (2009). LSPR-based nanobiosensors. *Nano Today, 4*(3), 244-251.

Shard, A. G., Wright, L., & Minelli, C. (2018). Robust and accurate measurements of gold nanoparticle concentrations using UV-visible spectrophotometry. *Biointerphases, 13*(6), 061002.

Siddiqi, & Husen. (2016). Engineered Gold Nanoparticles and Plant Adaptation Potential. *Nanoscale Research Letters, 11*(1), 400.

Siddiqui, Al-whaibi, M., Mohammad, F., & Al-Khaishany, M. (2015). Role of Nanoparticles in Plants. In *Nanotechnology and Plant Sciences* (pp. 19-35): Springer, Cham.

Siegel, J., Záruba, K., Švorčík, V., Kroumanová, K., Burketová, L., & Martinec, J. (2018). Round-shape gold nanoparticles: effect of particle size and concentration on Arabidopsis thaliana root growth. *Nanoscale Research Letters, 13*(1), 95.

Singh, D., & Kumar, A. (2014). Human Exposures of Engineered Nanoparticles from Plants Irrigated with Contaminated Water: Mixture Toxicity Issues and Challenges Ahead. *Advanced Science Letters, 20*, 1204-1207.

Singh, H., Sharma, A., Bhardwaj, S. K., Arya, S. K., Bhardwaj, N., & Khatri, M. (2021). Recent advances in the applications of nano-agrochemicals for sustainable agricultural development. *Environmental Science: Processes & Impacts, 23*(2), 213-239.

Singh, P., Pandit, S., Mokkapati, V. R. S. S., Garg, A., Ravikumar, V., & Mijakovic, I. (2018). Gold Nanoparticles in Diagnostics and Therapeutics for Human Cancer. *International Journal of Molecular Sciences, 19*(7), 1979.

Smith, D. K., & Korgel, B. A. (2008). The Importance of the CTAB Surfactant on the Colloidal Seed-Mediated Synthesis of Gold Nanorods. *Langmuir, 24*(3), 644-649.

Soliman, M. (2018). *Gold Nanoparticles: Synthesis, Surface Modification and Functionalization for Biomedical Applications.*

Spampinato, V., Parracino, M. A., La Spina, R., Rossi, F., & Ceccone, G. (2016). Surface Analysis of Gold Nanoparticles Functionalized with Thiol-Modified Glucose SAMs for Biosensor Applications. *Frontiers in Chemistry, 4*(8), 8.

Sperling, R. A., Rivera Gil, P., Zhang, F., Zanella, M., & Parak, W. J. (2008). Biological applications of gold nanoparticles. *Chemical Society Reviews, 37*(9), 1896-1908.

Spielman-Sun, E., Avellan, A., Bland, G. D., Tappero, R. V., Acerbo, A. S., Unrine, J. M., . . . Lowry, G. V. (2019). Nanoparticle surface charge influences translocation and leaf distribution in vascular plants with contrasting anatomy. *Environmental Science: Nano, 6*(8), 2508-2519.

Stampoulis, D., Sinha, S. K., & White, J. C. (2009). Assay-Dependent Phytotoxicity of Nanoparticles to Plants. *Environmental Science & Technology, 43*(24), 9473-9479.

StatNano. (2016). Nanotechnology Products Database. Retrieved from https://product.statnano.com/

Stetefeld, J., McKenna, S. A., & Patel, T. R. (2016). Dynamic light scattering: a practical guide and applications in biomedical sciences. *Biophysical Reviews, 8*(4), 409-427.

Su, Ashworth, V., Kim, C., Adeleye, A. S., Rolshausen, P., Roper, C., . . . Jassby, D. (2019). Delivery, uptake, fate, and transport of engineered nanoparticles in plants: a critical review and data analysis. *Environmental Science: Nano, 6*(8), 2311-2331.

Su, L.-J., Zhang, J.-H., Gomez, H., Murugan, R., Hong, X., Xu, D., . . . Peng, Z.-Y. (2019). Reactive Oxygen Species-Induced Lipid Peroxidation in Apoptosis, Autophagy, and Ferroptosis. *Oxidative Medicine and Cellular Longevity, 2019*, 5080843.

Subbarao, N. (2016). Nanoparticle Sterility and Sterilization of Nanomaterials. In *Handbook of Immunological Properties of Engineered Nanomaterials* (Vol. Volume 6, pp. 53-75): WORLD SCIENTIFIC.

Sukhanova, A., Bozrova, S., Sokolov, P., Berestovoy, M., Karaulov, A., & Nabiev, I. (2018). Dependence of Nanoparticle Toxicity on Their Physical and Chemical Properties. *Nanoscale Research Letters, 13*(1), 44-44.

Sun, M., Liu, F., Zhu, Y., Wang, W., Hu, J., Liu, J., . . . Gao, W. (2016). Salt-Induced Aggregation of Gold Nanoparticles for Photoacoustic Imaging and Photothermal Therapy of Cancer. *Nanoscale, 8*.

Suttiponparnit, K., Jiang, J., Sahu, M., Suvachittanont, S., Charinpanitkul, T., & Biswas, P. (2010). Role of Surface Area, Primary Particle Size, and Crystal Phase on Titanium Dioxide Nanoparticle Dispersion Properties. *Nanoscale Research Letters, 6*(1), 27.

Tarazona, S., García-Alcalde, F., Dopazo, J., Ferrer, A., & Conesa, A. (2011). Differential expression in RNA-seq: a matter of depth. *Genome Research, 21*(12), 2213-2223.

Taylor, A. F., Rylott, E. L., Anderson, C. W. N., & Bruce, N. C. (2014). Investigating the Toxicity, Uptake, Nanoparticle Formation and Genetic Response of Plants to Gold. *PLOS ONE, 9*(4), e93793.

Thiruvengadam, M., Rajakumar, G., & Chung, I. M. (2018). Nanotechnology: current uses and future applications in the food industry. *3 Biotech, 8*(1), 74.

Tiede, K., Hassellöv, M., Breitbarth, E., Chaudhry, Q., & Boxall, A. B. A. (2009). Considerations for environmental fate and ecotoxicity testing to support environmental risk assessments for engineered nanoparticles. *Journal of Chromatography A, 1216*(3), 503-509.

Tiwari, J. N., Tiwari, R. N., & Kim, K. S. (2012). Zero-dimensional, one-dimensional, two-dimensional and three-dimensional nanostructured materials for advanced electrochemical energy devices. *Progress in Materials Science, 57*(4), 724-803.

Tiwari, M., Krishnamurthy, S., Shukla, D., Kiiskila, J., Jain, A., Datta, R., . . . Sahi, S. V. (2016). Comparative transcriptome and proteome analysis to reveal the biosynthesis of gold nanoparticles in Arabidopsis. *Scientific Reports, 6*(1), 21733.

Toma, H. E., Zamarion, V. M., Toma, S. H., & Araki, K. (2010). The coordination chemistry at gold nanoparticles. *Journal of the Brazilian Chemical Society, 21*, 1158-1176.

Tomaszewska, E., Soliwoda, K., Kadziola, K., Tkacz-Szczesna, B., Celichowski, G., Cichomski, M., . . . Grobelny, J. (2013). Detection Limits of DLS and UV-Vis Spectroscopy in Characterization of Polydisperse Nanoparticles Colloids. *Journal of Nanomaterials, 2013*, 313081.

Trapnell, C., Roberts, A., Goff, L., Pertea, G., Kim, D., Kelley, D. R., . . . Pachter, L. (2012). Differential gene and transcript expression analysis of RNA-seq experiments with TopHat and Cufflinks. *Nature Protocols, 7*(3), 562-578.

Tripathi, Tripathi, A., Shweta, Singh, S., Singh, Y., Vishwakarma, K., . . . Chauhan, D. K. (2017). Uptake, Accumulation and Toxicity of Silver Nanoparticle in Autotrophic Plants, and Heterotrophic Microbes: A Concentric Review. *Frontiers in Microbiology, 8*.

Tripathi, D. K., Singh, S., Singh, V. P., Prasad, S. M., Dubey, N. K., & Chauhan, D. K. (2017). Silicon nanoparticles more effectively alleviated UV-B stress than silicon in wheat (Triticum aestivum) seedlings. *Plant Physiology and Biochemistry, 110*, 70-81.

Turkevich, J., Stevenson, P. C., & Hillier, J. (1951). A study of the nucleation and growth processes in the synthesis of colloidal gold. *Discussions of the Faraday Society, 11*(0), 55-75.

Tyagi, S., M.E Phd, D., Khatri, N., & Tharmavaram, M. (2018). Strategies for Nitrate removal from aqueous environment using Nanotechnology: A Review. *Journal of Water Process Engineering, 21*, 84-95.

Tyanova, S., Temu, T., Sinitcyn, P., Carlson, A., Hein, M. Y., Geiger, T., . . . Cox, J. (2016). The Perseus computational platform for comprehensive analysis of (prote)omics data. *Nature Methods, 13*(9), 731-740.

van der Zee, C., Roberts, D., & Slomp, C. P. (2003). Nanogoethite is the dominant reactive oxyhydroxide phase in lake and marine sediments. *Geology, 31*.

Verwey, E. J. W. (1947). Theory of the Stability of Lyophobic Colloids. *The Journal of Physical and Colloid Chemistry, 51*(3), 631-636.

Wang, W.-N., Tarafdar, J. C., & Biswas, P. (2013). Nanoparticle synthesis and delivery by an aerosol route for watermelon plant foliar uptake. *Journal of Nanoparticle Research, 15*(1), 1417.

Wang, Z., Hu, T., Liang, R., & Wei, M. (2020). Application of Zero-Dimensional Nanomaterials in Biosensing. *Frontiers in Chemistry, 8*(320).

Wang, Z., Quik, J. T., Song, L., Van Den Brandhof, E. J., Wouterse, M., & Peijnenburg, W. J. (2015). Humic substances alleviate the aquatic toxicity of polyvinylpyrrolidone-coated silver nanoparticles to organisms of different trophic levels. *Environmental Toxicology and Chemistry, 34*(6), 1239-1245.

Wang, Z., Xie, X., Zhao, J., Liu, X., Feng, W., White, J. C., & Xing, B. (2012). Xylem- and Phloem-Based Transport of CuO Nanoparticles in Maize (Zea mays L.). *Environmental Science & Technology, 46*(8), 4434-4441.

Wilson-Corral, V., Anderson, C. W. N., & Rodriguez-Lopez, M. (2012). Gold phytomining. A review of the relevance of this technology to mineral extraction in the 21st century. *Journal of Environmental Management, 111*, 249-257.

Worthen, A. J., Tran, V., Cornell, K. A., Truskett, T. M., & Johnston, K. P. (2016). Steric stabilization of nanoparticles with grafted low molecular weight ligands in highly concentrated brines including divalent ions. *Soft Matter, 12*(7), 2025-2039.

Wu, Q., Miao, W.-s., Zhang, Y.-d., Gao, H.-j., & Hui, D. (2020). Mechanical properties of nanomaterials: A review. *Nanotechnology Reviews, 9*(1), 259-273.

Wuithschick, M., Birnbaum, A., Witte, S., Sztucki, M., Vainio, U., Pinna, N., . . . Polte, J. (2015). Turkevich in New Robes: Key Questions Answered for the Most Common Gold Nanoparticle Synthesis. *ACS Nano, 9*(7), 7052-7071.

Xin, H., Namgung, B., & Lee, L. P. (2018). Nanoplasmonic optical antennas for life sciences and medicine. *Nature Reviews Materials, 3*(8), 228-243.

Yang, C., Yang, H., Wu, J., Meng, Z., Xing, R., Tian, A., . . . Li, Z. (2013). No overt structural or functional changes associated with PEG-coated gold nanoparticles accumulation with acute exposure in the mouse heart. *Toxicology Letters, 222*(2), 197-203.

Yang, J., Cao, W., & Rui, Y. (2017). Interactions between nanoparticles and plants: phytotoxicity and defense mechanisms. *Journal of Plant Interactions, 12*(1), 158-169.

Yeh, Y. C., Creran, B., & Rotello, V. M. (2012). Gold nanoparticles: preparation, properties, and applications in bionanotechnology. *Nanoscale, 4*(6), 1871-1880.

Zhang, X., Ma, G., & Wei, W. (2021). Simulation of nanoparticles interacting with a cell membrane: probing the structural basis and potential biomedical application. *NPG Asia Materials, 13*(1), 52.

Zhao, L., Lu, L., Aodi, W., Zhang, H., Huang, M., Wu, H., . . . Ji, R. (2020). Nanobiotechnology in Agriculture: Use of Nanomaterials To Promote Plant Growth and Stress Tolerance. *Journal of Agricultural and Food Chemistry, 68*, 1935-1947.

Zhidebekkyzy, A., Kupeshova, S., & Yesmurzayeva, A. (2019). Project Management in Nanotechnology-A Systematic Literature Review. *Montenegrin Journal of Economics, 15*(3), 227-244.

Zhu, Wang, H., Yan, B., Zheng, H., Jiang, Y., Miranda, O. R., . . . Vachet, R. W. (2012). Effect of surface charge on the uptake and distribution of gold nanoparticles in four plant species. *Environmental Science & Technology, 46*(22), 12391-12398.

Zia-ur-Rehman, M., Qayyum, M. F., Akmal, F., Maqsood, M. A., Rizwan, M., Waqar, M., & Azhar, M. (2018). Chapter 7 - Recent Progress of Nanotoxicology in Plants. In D. K. Tripathi, P. Ahmad, S. Sharma, D. K. Chauhan, & N. K. Dubey (Eds.), *Nanomaterials in Plants, Algae, and Microorganisms* (pp. 143-174): Academic Press:Cambridge, MA, USA.

8 Appendix

8.1 Supplemental data

Table A-1: Clean reads quality metrics and summary of genome mapping

Sample, sample names; Total Raw Reads (Mb), the reads amount before filtering, Unit: Mb; Total Clean Reads (Mb), the reads amount after filtering, Unit: Mb; Total Clean Bases (Gb), the total base amount after filtering, Unit: Gb; Clean Reads Q20 (%), the Q20 value for the clean reads; Clean Reads Q30 (%), the Q30 value for the clean reads; Clean Reads Ratio (%), the ratio of the amount of clean reads; Total Mapping Ratio, the percentage of mapped reads; Uniquely Mapping Ratio, the percentage of reads that map to only one location of reference

Sample	Total Raw Reads (Mb)	Total Clean Reads (Mb)	Total Clean Bases (Gb)	Clean Reads Q20 (%)	Clean Reads Q30 (%)	Clean Reads Ratio (%)	Total Mapping Ratio	Uniquely Mapping Ratio
AuNP-SCTA 6h 1st	62.73	57.04	5.70	98.90	96.18	90.94	92.29%	84.29%
AuNP-SCTA 6h 2nd	58.36	54.05	5.40	98.85	96.09	92.61	93.82%	86.12%
AuNP-SCTA 6h 3rd	50.08	46.49	4.65	98.83	96.02	92.83	95.22%	87.40%
AuNP-SCTA 7d 1st	110.15	103.92	10.39	99.43	98.02	94.34	94.11%	85.54%
AuNP-SCTA 7d 2nd	105.08	99.11	9.91	99.37	97.85	94.32	94.71%	86.05%
AuNP-SCTA 7d 3rd	88.35	83.52	8.35	99.40	97.94	94.54	93.63%	84.94%
SCTA 6h 1st	53.41	49.69	4.97	98.89	96.20	93.04	95.07%	87.25%
SCTA 6h 2nd	51.38	46.88	4.69	97.99	93.15	91.24	95.95%	87.68%
SCTA 6h 3rd	63.13	58.12	5.81	98.83	96.00	92.06	95.23%	86.96%
SCTA 7d 1st	102.41	96.76	9.68	99.41	97.94	94.48	94.60%	85.98%
SCTA 7d 2nd	108.32	98.65	9.87	99.20	97.22	91.07	93.93%	84.76%
SCTA 7d 3rd	91.08	82.92	8.29	99.18	97.14	91.04	94.74%	85.95%

Table A-2: Partial list of DEGs after short- (6h) AuNP-SCTA treatment with their expression information

AGI-code	Gene names	Protein names	Log2 Fold change	Regulation	Probability
Disease resistance					
At5g01895	At5g01895	Hypothetical protein	1,6256	Up	0,91
At1g43800	S-ACP-DES6	Stearoyl acyl carrier protein desaturase, putative	1,6191	Up	0,98
At5g01740	At5g01740	Nuclear transport factor 2 family protein	1,113	Up	0,98
At3g21090	ABCG15	ABC transporter G family member 15	1,0853	Up	0,92
At5g39890	MYH19.8	Cysteine dioxygenase	1,0681	Up	0,96
At5g16970	AER	NADPH-dependent oxidoreductase 2-alkenal reductase	-2,0918	Down	0,97
At5g39120	At5g39120	Germin-like protein subfamily 1 member 15	-3,7329	Down	1,00
At5g39180	At5g39180	Cupin type-1 domain-containing protein	-2,8279	Down	1,00
At5g39150	At5g39150	Germin-like protein subfamily 1 member 17	-2,7613	Down	1,00
At5g39110	At5g39110	Germin-like protein subfamily 1 member 14	-1,8880	Down	0,99
At3g53590	At3g53590	Putative leucine-rich repeat receptor-like serine/threonine-protein kinase	-1,8405	Down	0,99

AGI-code	Gene names	Protein names	Log2 Fold change	Regulation	Probability
At3g46340	At3g46340	Putative receptor-like protein kinase	-1,8110	Down	0,99
At3g55090	ABCG16	ABC transporter G family member 16	-1,6803	Down	0,98
At4g11170	At4g11170	Disease resistance protein (TIR-NBS-LRR class) family	-1,6033	Down	0,98
At1g29740	At1g29740	Leucine-rich repeat transmembrane protein kinase	-1,4814	Down	0,95
At1g72610	GLP1	Germin-like protein subfamily 3 member 1	-1,4711	Down	1,00
At2g24130	At2g24130	Leucine-rich receptor-like protein kinase family protein	-1,4594	Down	0,99
At3g47770	ABCA6	ABC transporter A family member 6	-1,4548	Down	0,98
At5g17960	MCM23.3	CHP-rich zinc finger protein-like	-1,4383	Down	0,97
At1g26700	MLO14	MLO-like protein 14	-1,3810	Down	0,98
At5g38000	At5g38000	Zinc-binding dehydrogenase family protein	-1,3370	Down	0,98
At3g46370	F18L15.90	Leucine-rich repeat protein kinase family protein	-1,2942	Down	0,96
At5g41750	At5g41750	Disease resistance protein-like	-1,2906	Down	0,98
At3g47740	ABCA3	ABC transporter A family member 3	-1,2689	Down	0,97
At2g43500	NLP8	Nodule inception protein-like protein 8	-1,2471	Down	0,98
At5g51270	PUB53	Putative U-box domain-containing protein 53	-1,2414	Down	0,97
At5g37980	At5g37980	PKS_ER domain-containing protein	-1,2245	Down	0,99
At3g46330	MEE39	Leucine-rich repeat protein kinase family protein	-1,1509	Down	0,98
At3g53480	ABCG37	ABC transporter G family member 37	-1,0141	Down	0,99
Defense response					
At5g24770	VSP2	Vegetative storage protein 2	1,1077	Up	0,90
At2g29350	SAG13	Senescence-associated protein 13	-4,5617	Down	1,00
At4g20970	BHLH162	Transcription factor bHLH162	-4,0548	Down	1,00
At5g03210	DIP2	E3 ubiquitin-protein ligase	-3,2757	Down	0,99
At4g17680	At4g17680	S-ribonuclease binding protein family protein	-2,8547	Down	1,00
At5g43570	At5g43570	Serine protease inhibitor, potato inhibitor I-type family protein	-2,6512	Down	0,98
At4g12490	At4g12490	pEARLI1-like lipid transfer protein 2	-2,5850	Down	0,98
At5g26920	CBP60G	Cam-binding protein 60-like G	-2,3922	Down	1,00
At2g02930	GSTF3	Glutathione S-transferase F3	-2,2981	Down	0,99
At5g33355	At5g33355	Defensin-like protein 207	-2,1979	Down	0,99
At2g34600	TIFY 5B	Protein TIFY 5B (Jasmonate ZIM domain-containing protein 7)	-2,0995	Down	0,99
At1g34047	At1g34047	Defensin-like protein 208	-1,9831	Down	0,98
At5g13320	GH3.12	4-substituted benzoates-glutamate ligase GH3.12	-1,9059	Down	0,98
At4g12470	AZI1	pEARLI1-like lipid transfer protein 1	-1,7941	Down	1,00
At4g14060	dl3070w	Polyketide cyclase/dehydrase and lipid transport superfamily protein	-1,7289	Down	1,00
At1g15010	At1g15010	Mediator of RNA polymerase II transcription subunit	-1,6795	Down	0,99
At4g11170	At4g11170	Disease resistance protein (TIR-NBS-LRR class) family	-1,6033	Down	0,98

AGI-code	Gene names	Protein names	Log2 Fold change	Regulation	Probability
At1g80840	WRKY40	Probable WRKY transcription factor 40	-1,5568	Down	0,99
At5g13220	TIFY9	Protein TIFY 9 (Jasmonate ZIM domain-containing protein 10)	-1,5434	Down	0,97
At3g48520	CYP94B3	Cytochrome P450 94B3	-1,5302	Down	1,00
At2g26560	PLP2	Patatin-like protein 2	-1,5191	Down	0,99
At1g02930	GSTF6	Glutathione S-transferase F6	-1,4543	Down	0,99
At5g15410	CNGC2	Cyclic nucleotide-gated ion channel 2	-1,4426	Down	0,99
At4g30650	At4g30650	Membrane protein	-1,4334	Down	1,00
At2g30750	CYP71A12	Cytochrome P450 71A12	-1,4279	Down	0,98
At1g26700	MLO14	MLO-like protein 14	-1,3810	Down	0,98
At2g02120	PDF2.1	Defensin-like protein 4	-1,3545	Down	1,00
At4g19230	CYP707A1	Cytochrome P450, family 707, subfamily A, polypeptide 1	-1,3474	Down	0,99
At1g52410	TSA1	TSK-associating protein 1	-1,2603	Down	0,97
At5g24780	VSP1	Vegetative storage protein 1	-1,2396	Down	0,93
At4g37310	PAE4	Pectin acetylesterase 4	-1,1978	Down	0,99
At1g75600	At1g75600	Histone H3-like 3	-1,1926	Down	0,96
At3g58000	VQ25	VQ motif-containing protein 25	-1,1890	Down	0,95
At1g18870	ICS2	Isochorismate synthase 2, chloroplastic	-1,1276	Down	0,98
At5g50260	CEP1	KDEL-tailed cysteine endopeptidase CEP1	-1,1230	Down	0,92
At5g64750	ABR1	Ethylene-responsive transcription factor ABR1	-1,1105	Down	0,95
At3g26830	CYP71B15	Bifunctional dihydrocamalexate synthase/camalexin synthase	-1,1061	Down	0,99
At3g25250	OXI1	Serine/threonine-protein kinase OXI1	-1,0848	Down	0,98
At2g43510	ATTI1	Defensin-like protein 195	-1,0722	Down	1,00
At3g50970	XERO2	Dehydrin Xero 2	-1,0257	Down	1,00
Response to oxidative stress					
At5g64110	PER70	Peroxidase superfamily protein	1,5180	Up	0,97
At1g34510	PER8	Peroxidase 8	-3,1258	Down	1,00
At5g05340	PER52	Peroxidase 52	-2,2374	Down	0,99
At2g18150	PER15	Peroxidase 15	-1,9688	Down	1,00
At5g22410	PER60	Peroxidase 60	-1,9603	Down	0,99
At1g49570	PER10	Peroxidase superfamily protein	-1,9279	Down	1,00
At5g19890	PER59	Peroxidase 59	-1,6194	Down	0,99
At4g36430	PER49	Peroxidase 49	-1,1918	Down	0,98
At5g67400	PER73	Peroxidase 73	-1,1422	Down	0,99
At5g39580	PER62	Peroxidase 62	-1,1143	Down	0,99
At5g06720	PER53	Peroxidase 53	-1,0040	Down	0,93
Metal response					

AGI-code	Gene names	Protein names	Log2 Fold change	Regulation	Probability
At1g25054	LPXC3	UDP-3-O-acyl N-acetylglycosamine deacetylase family protein	8,762	Up	1,00
At1g43800	S-ACP-DES6	Stearoyl acyl carrier protein desaturase, putative	1,619	Up	0,98
At1g29930	LHCB1.3	Chlorophyll A/B binding protein 1	1,357	Up	0,99
At1g07610	MT1C	Metallothioneins	1,233	Up	1,00
At3g08940	LHCB4.2	Light harvesting complex photosystem II	1,155	Up	0,95
At1g61520	LHCA3	PSI type III chlorophyll a/b-binding protein	1,127	Up	0,95
At4g10340	LHCB5	Chlorophyll a-b binding protein CP26, chloroplastic	1,110	Up	0,95
At5g39890	MYH19.8	Cysteine dioxygenase	1,068	Up	0,96
At4g40070	ATL32	RING-H2 finger protein ATL32	1,059	Up	0,99
At1g19790	SRS7	Protein SHI RELATED SEQUENCE 7	1,054	Up	0,94
At4g36260	SRS2	Protein SHI RELATED SEQUENCE 2	1,040	Up	0,94
At1g56160	MYB72	Transcription factor MYB72	-3,614	Down	1,00
At3g14440	NCED3	9-cis-epoxycarotenoid dioxygenase NCED3, chloroplastic	-3,414	Down	1,00
At3g12900	S8H	Scopoletin 8-hydroxylase	-3,328	Down	1,00
At2g19900	NADP-ME1	NADP-dependent malic enzyme 1	-3,252	Down	0,99
At1g52800	At1g52800	2-oxoglutarate and Fe(II)-dependent oxygenase superfamily protein	-3,091	Down	0,99
At2g38240	ANS	Probable 2-oxoglutarate-dependent dioxygenase ANS	-2,792	Down	0,99
At5g59220	SAG113	Probable protein phosphatase 2C 78	-2,369	Down	0,98
At1g05880	ARI12	Probable E3 ubiquitin-protein ligase ARI12	-2,138	Down	0,99
At1g21400	At1g21400	2-oxoisovalerate dehydrogenase subunit alpha 1, mitochondrial	-2,072	Down	0,99
At1g68290	ENDO2	Endonuclease 2	-1,989	Down	0,98
At1g52820	At1g52820	2-oxoglutarate and Fe(II)-dependent oxygenase superfamily protein	-1,934	Down	0,98
At1g11920	At1g11920	Pectate lyase	-1,918	Down	0,99
At5g05390	LAC12	Laccase-12	-1,833	Down	0,95
At1g67980	CCOAMT	Caffeoyl-CoA 3-O-methyltransferase	-1,713	Down	0,98
At5g08640	FLS1	Flavonol synthase/flavanone 3-hydroxylase	-1,710	Down	1,00
At5g56080	NAS2	Nicotianamine synthase 2	-1,709	Down	0,98
At1g01580	FRO2	Ferric reduction oxidase 2	-1,639	Down	0,99
At3g51240	F3H	Flavanone 3-hydroxylase	-1,634	Down	0,98
At3g22910	ACA13	ATPase E1-E2 type family protein / haloacid dehalogenase-like hydrolase family protein	-1,567	Down	0,99
At4g19690	IRT1	Fe(2+) transport protein 1	-1,519	Down	1,00
At1g29600	At1g29600	Zinc finger C-x8-C-x5-C-x3-H type family protein	-1,512	Down	0,99
At1g52790	At1g52790	2-oxoglutarate and Fe(II)-dependent oxygenase superfamily protein	-1,510	Down	0,92
At1g18835	MIF3	Mini zinc finger protein 3	-1,456	Down	0,97
At4g32950	At4g32950	Protein phosphatase 2C family protein	-1,442	Down	1,00

AGI-code	Gene names	Protein names	Log2 Fold change	Regulation	Probability
At1g14120	At1g14120	2-oxoglutarate and Fe(II)-dependent oxygenase superfamily protein	-1,429	Down	0,98
At3g09390	MT2A	Metallothionein-like protein 2A	-1,414	Down	0,99
At1g66700	PXMT1	Paraxanthine methyltransferase 1	-1,347	Down	0,98
At5g14470	EXT6	Proline-rich extensin-like family protein	-1,306	Down	0,93
At1g68360	GIS3	Zinc finger protein GIS3	-1,271	Down	0,98
At3g60280	UCC3	Uclacyanin-3	-1,263	Down	0,98
At5g20230	BCB	Blue copper protein	-1,256	Down	0,90
At4g25380	SAP10	Zinc finger A20 and AN1 domain-containing stress-associated protein 10	-1,221	Down	0,98
At4g15530	PPDK	Pyruvate, phosphate dikinase 1, chloroplastic	-1,188	Down	0,98
At5g23980	FRO4	Ferric reduction oxidase 4	-1,187	Down	0,98
At4g22080	At4g22080	Probable pectate lyase 16	-1,170	Down	0,98
At4g30120	HMA3	Putative inactive cadmium/zinc-transporting ATPase HMA3	-1,074	Down	0,95
At4g21840	MSRB8	Peptide methionine sulfoxide reductase B8	-1,049	Down	0,94
At3g27400	At3g27400	Putative pectate lyase 11	-1,028	Down	0,92
At3g17790	PAP17	Purple acid phosphatase 17	-1,022	Down	0,95
At1g06830	GRXS11	Monothiol glutaredoxin-S11	-1,020	Down	0,99
At1g55020	LOX1	Linoleate 9S-lipoxygenase 1	-1,003	Down	1,00
Response to light					
At2g21650	RL2	Homeodomain-like superfamily protein	1,3952	Up	0,98
At1g66180	At1g66180	Eukaryotic aspartyl protease family protein	1,4522	Up	1,00
At2g34420	Lhb1B2	Chlorophyll a-b binding protein, chloroplastic	2,0309	Up	1,00
At1g29930	LHCB1.3	Chlorophyll A/B binding protein 1	1,3573	Up	0,99
At1g07610	MT1C	Metallothioneins (MTs)	1,2327	Up	1,00
At3g08940	LHCB4.2	Light harvesting complex photosystem II	1,1547	Up	0,95
At1g61520	LHCA3	PSI type III chlorophyll a/b-binding protein	1,1268	Up	0,95
At4g10340	LHCB5	Chlorophyll a-b binding protein CP26, chloroplastic	1,1101	Up	0,95
At1g08380	PSAO	Photosystem I subunit O	1,1620	Up	0,94
At2g21320	BBX18	B-box zinc finger protein 18 (Protein DOUBLE B-BOX 1A)	1,0931	Up	0,99
At1g21400	At1g21400	2-oxoisovalerate dehydrogenase subunit alpha 1, mitochondrial	-2,0724	Down	0,99
At3g12820	MYB10	Transcription factor MYB10	-2,0583	Down	0,99
At5g12030	HSP17.7	17.7 kDa class II heat shock protein	-1,9069	Down	0,98
At2g29500	HSP17.6B	17.6 kDa class I heat shock protein 2	-1,7826	Down	0,98
At1g52560	HSP26.5	26.5 kDa heat shock protein, mitochondrial	-1,3949	Down	0,97
Development					
At3g02000	GRXC7	Thioredoxin superfamily protein	2,210	Up	0,94
At2g21650	RL2	Homeodomain-like superfamily protein	1,395	Up	0,98

AGI-code	Gene names	Protein names	Log2 Fold change	Regulation	Probability
At5g63160	BT1	BTB and TAZ domain protein 1	1,353	Up	1,00
At5g25460	DGR2	Transmembrane protein, putative	1,3148	Up	1,00
At5g44190	GLK2	GOLDEN2-like 2	1,199	Up	0,98
At1g80100	AHP6	Pseudo histidine-containing phosphotransfer protein 6	1,123	Up	0,98
At1g19790	SRS7	Protein SHI RELATED SEQUENCE 7	1,054	Up	0,94
At3g22240	At3g22240	Cysteine-rich/transmembrane domain PCC1-like protein	1,043	Up	1,00
At4g36260	SRS2	Protein SHI RELATED SEQUENCE 2	1,040	Up	0,94
At3g48740	SWEET11	Bidirectional sugar transporter SWEET11	1,015	Up	0,94
At5g36130	CYP716A2	Cytochrome P450 716A2	-4,903	Down	1,00
At5g36140	CYP716A2	Cytochrome P450 716A2	-4,127	Down	1,00
At5g06760	LEA46	Late embryogenesis abundant protein 46	-2,820	Down	0,99
At1g10370	GSTU17	Glutathione S-transferase U17	-2,243	Down	1,00
At5g52310	RD29A	Low-temperature-induced 78 kDa protein	-2,214	Down	1,00
At1g69490	NAC029	NAC transcription factor 29	-2,204	Down	1,00
At5g39610	NAC92	NAC domain-containing protein 92	-2,085	Down	0,99
At4g28110	MYB41	Myb domain protein 41	-1,946	Down	0,99
At3g61890	ATHB-12	Homeobox-leucine zipper protein ATHB-12	-1,827	Down	0,98
At1g15330	BHLH23	Transcription factor bHLH23	-1,740	Down	1,00
At4g25640	DTX35	Protein DETOXIFICATION 35	-1,644	Down	1,00
At1g56430	NAS4	Nicotianamine synthase 4	-1,589	Down	0,98
At4g22950	AGL19	Agamous-like MADS-box protein AGL19	-1,561	Down	0,94
At1g06225	CLE3	CLAVATA3/ESR (CLE)-related protein 3	-1,557	Down	0,98
At1g79860	ROPGEF12	Rop guanine nucleotide exchange factor 12	-1,531	Down	0,97
At3g48520	CYP94B3	Cytochrome P450 94B3	-1,530	Down	1,00
At4g13395	DVL10	DVL10 (ROTUNDIFOLIA like 12)	-1,525	Down	0,99
At2g22860	PSK2	Phytosulfokines 2	-1,518	Down	1,00
At5g48010	THAS1	Thalianol synthase 1	-1,509	Down	1,00
At3g59900	ARGOS	Protein AUXIN-REGULATED GENE INVOLVED IN ORGAN SIZE	-1,464	Down	0,99
At1g18835	MIF3	Mini zinc finger protein 3	-1,456	Down	0,97
At3g03660	WOX11	WUSCHEL-related homeobox 11	-1,430	Down	0,98
At5g50800	SWEET13	Bidirectional sugar transporter SWEET13	-1,406	Down	0,99
At2g20825	ULT2	Protein ULTRAPETALA 2	-1,367	Down	0,98
At1g66700	PXMT1	Paraxanthine methyltransferase 1	-1,347	Down	0,98
At1g68360	GIS3	Zinc finger protein GIS3	-1,271	Down	0,98
At5g51870	AGL71	MADS-box protein AGL71	-1,271	Down	0,96
At5g16530	PIN5	Auxin efflux carrier component 5	-1,250	Down	0,99
At2g14760	BHLH84	Transcription factor bHLH84	-1,244	Down	0,96

AGI-code	Gene names	Protein names	Log2 Fold change	Regulation	Probability
At4g28840	SPEAR3	Protein SPEAR3	-1,158	Down	0,96
At3g46330	MEE39	Leucine-rich repeat protein kinase family protein	-1,151	Down	0,98
At3g55515	DVL8	Small polypeptide DEVIL 8	-1,131	Down	0,93
At1g53230	TCP3	Transcription factor TCP3	-1,130	Down	0,95
At5g50260	CEP1	KDEL-tailed cysteine endopeptidase CEP1	-1,123	Down	0,92
At1g05100	MAPKKK18	Mitogen-activated protein kinase kinase kinase 18	-1,118	Down	0,97
At4g01360	BPS3	BPS1-like protein	-1,112	Down	0,98
At1g01380	ETC1	MYB-like transcription factor ETC1	-1,085	Down	0,98
At4g18390	TCP2	Transcription factor TCP2	-1,080	Down	0,97
At5g62380	NAC101	NAC domain-containing protein 101	-1,079	Down	0,98
At4g25350	PHO1-H4	Phosphate transporter PHO1 homolog 4	-1,052	Down	0,98
At4g40090	AGP3	Classical arabinogalactan protein 3	-1,042	Down	0,99
At3g18000	NMT1	Phosphoethanolamine N-methyltransferase 1	-1,036	Down	0,99
At3g53480	ABCG37	ABC transporter G family member 37	-1,014	Down	0,99
At1g55020	LOX1	Linoleate 9S-lipoxygenase 1	-1,003	Down	1,00
At3g15170	NAC054	Protein CUP-SHAPED COTYLEDON 1	-1,000	Down	0,95

Table A-3: Partial list of DEGs after long- (7d) AuNP-SCTA treatment with their expression information

AGI-code	Gene names	Protein names	Log2 Fold change	Regulation	Probability
Defense response					
At5g40990	GLIP1	GDSL esterase/lipase 1	-4,5236	Down	0,81
Response to oxidative stress					
At5g47000	PER65	Peroxidase 65	1,095	Up	0,82
Response to metal ion					
At5g56080	NAS2	Nicotianamine synthase 2	-1,1427	Down	0,91
Development					
At3g49620	DIN11	Probable 2-oxoglutarate-dependent dioxygenase DIN11	1,0676	Up	0,82

Table A-4: Partial list of DEPs after short- (6h) AuNP-SCTA treatment with their expression information

Protein IDs	Protein names	AGI-codeA	Log2 Fold change	Regulation	Log2 Fold change Significance
Defense response					
Q9FM96	Glucosidase 2 subunit beta	At5g56360	1,1474	Up	0,000298074
Q9C509	Sphingosine-1-phosphate lyase	At1g27980	1,0623	Up	1,05E-06
A0A1P8B6X9;Q9M0E5	Non-specific serine/threonine protein kinase; Serine/threonine-protein kinase VPS15	At4g29380	0,9730	Up	0,001887486
Q9SU72;Q9SU72-2	Protein EDS1	At3g48090	0,9519	Up	0,002321172
Q9FZA2-2;Q9FZA2	Non-classical arabinogalactan protein 31	At1g28290	-1,1245	Down	7,50E-11
P42760	Glutathione S-transferase F6	At1g02930	-0,4945	Down	0,004793339

Protein IDs	Protein names	AGI-code	Log2 Fold change	Regulation	Log2 Fold change Significance
Q9SRH6;Q9FM19	Hypersensitive induced reaction 2;Hypersensitive-induced response protein 1	At3g01290; At5g62740	-0,4914	Down	0,005070344
Q9FWR4;Q9FWR4-2;Q9LN39	Glutathione S-transferase DHAR1, mitochondrial;F18O14.31 (Glutathione S-transferase family protein)	At1g19570; At1g19550	-0,4690	Down	0,007554576
Response to oxidative stress					
P21276;F4JRV2	Superoxide dismutase [Fe] 1, chloroplastic;Superoxide dismutase	At4g25100	1,4135	Up	1,05E-15
Q9LDA4	Peroxidase 38	At4g08780	0,6744	Up	8,28E-05
Q9LDN9	Peroxidase 37	At4g08770	0,3793	Up	0,001461237
A0A1P8B428;Q93V93	Peroxidase 44	At4g26010	-1,8962	Down	3,23E-06
Q67Z07;P0DI10	Peroxidase 2;Peroxidase 1	At1g05250; At1g05240	-1,2776	Down	0,002206861
Q9LYB4	Probable glutathione peroxidase 5	At3g63080	-1,2394	Down	0,003053654
A0A1P8BGP6;Q43729	Peroxidase;Peroxidase 57	At5g17820	-1,2278	Down	1,12E-12
Q9LSY7	Peroxidase 30	At3g21770	-1,2144	Down	1,94E-07
P24704;Q9FK60-2;Q9FK60	Superoxide dismutase [Cu-Zn] 1;Superoxide dismutase [Cu-Zn] 3	At1g08830; At5g18100	-0,9073	Down	0,001613371
Q96518	Peroxidase 16	At2g18980	-0,7624	Down	1,13E-05
Q96522	Peroxidase 45	At430170	-0,4907	Down	0,005134167
Metal response					
Q3EAH9;Q9LXS1	Metal tolerance protein A2	At3g58810	0,9750	Up	0,00184947
O82089;A0A1I9LNC0	Copper transport protein CCH	At3g56240	0,6647	Up	0,000103403
Q9SXE9	vacuolar calcium-binding protein-like protein	At1g62480	0,5702	Up	0,007073109
Response to abiotic stimulus					
P42763	Dehydrin ERD14	At1g76180	0,8121	Up	0,000163834
Q9C9P4	3-oxoacyl-[acyl-carrier-protein] synthase II, chloroplastic	At1g74960	0,6232	Up	0,003398423
P31168	Dehydrin COR47	At1g20440	0,5960	Up	7,78E-07
O04310	Jacalin-related lectin 34	At3g16460	-0,7192	Down	3,53E-05
Development					
Q9MAT5;Q9MAT5-2	Protein arginine N-methyltransferase PRMT10	At1g04870	0,6756	Up	0,001565461
O22842;O22841	Endochitinase At2g43610;Endochitinase At2g43620	At2g43610; At2g43621	-2,0327	Down	2,76E-32
F4JVB9;F4JVC0;F4JVC1;Q03251;Q03251-2	Cold, circadian rhythm, and RNA binding 1;Glycine-rich RNA-binding protein 8	At4g39260	-1,7117	Down	1,30E-13
Q9SSB7	At1g80240 (F18B13.30 protein)	At1g80240	-0,6411	Down	0,000233937
Receptor					
Q9LXU5	Leucine-rich repeat protein	At5g12940	-0,9880	Down	2,63E-05

Table A-5: Partial list of DEPs after long- (7d) AuNP-SCTA treatment with their expression information

Protein IDs	Protein names	AGI-code	Log2 Fold change	Regulation	Log2 Fold change Significance
Defense response					
Q9M5J9	Polygalacturonase inhibitor 1	At5g06860	0,9316	Up	0,00146159
F4JKM2;O49482	Cinnamyl alcohol dehydrogenase 5	At4g34230	0,8731	Up	0,00287985
Q9SHH7	Glutathione S-transferase U25	At1g17180	0,7387	Up	0,000155494
P27323	Heat shock protein 90-1	At5g52640	-0,8949	Down	0,004429767
Q7XJJ7	Fatty acid amide hydrolase	At5g64440	-1,0276	Down	0,001174878
Response to oxidative stress					
Q9LXP4;A0A1I9LQ33	At3g44190;FAD/NAD(P)-binding oxidoreductase family protein	At3g44190	-1,0265	Down	0,001188813
Metal response					
Q9ZUX4	Uncharacterized protein At2g27730, mitochondrial	At2g27730	1,3901	Up	4,18E-15
Response to abiotic stimulus					
Q9LX07;Q9LX08	Annexin D7;Annexin D6	At5g10230; At5g10220	-1,0548	Down	2,51E-05
Development					
Q94F20;Q9LYE7	At5g25460;Uncharacterized protein At5g11420	At5g25460; At5g11420	1,0445	Up	9,52E-08
Q8L7C9	Glutathione S-transferase U20	At1g78370	1,0430	Up	0,000361564
F4K2A1-2;F4K2A1	Folylpolyglutamate synthase	At5g05980	0,9230	Up	0,004448188
Q9SSB7	DGR1	At1g80240	0,8324	Up	0,004516139
Q9ZPH2;O65541	Monothiol glutaredoxin-S17;Thioredoxin superfamily protein	At4g04950; At4g32580	0,8241	Up	2,49E-05

Table A 6: Overlap between our DEGs and those published by Tiwari et al. (2016).

Co-upregulated genes	
AT1G07610	METALLOTHIONEIN 1C (MT1C)
AT1G08430	ALUMINUM-ACTIVATED MALATE TRANSPORTER 1 (ALMT1)
AT5G25460	DUF642 L-GALL RESPONSIVE GENE 2 (DGR2)
Co-downregulated genes	
AT1G02920	GLUTATHIONE S-TRANSFERASE 7 (GSTF7)
AT1G02930	GLUTATHIONE S-TRANSFERASE 6 (GSTF6)
AT1G05880	ARIADNE 12 (ARI12)
AT1G26240	EXTENSIN 19 (EXT19)
AT1G26380	FAD-LINKED OXIDOREDUCTASE 1 (FOX1)
AT1G26410	FAD-binding Berberine family protein(ATBBE6)
AT1G33900	IMMUNE ASSOCIATED NUCLEOTIDE BINDING 4 (IAN4)
AT1G67980	CAFFEOYL-COA 3-O-METHYLTRANSFERASE (CCOAMT)
AT2G02930	GLUTATHIONE S-TRANSFERASE F3 (GSTF3)
AT2G26560	PHOSPHOLIPASE A 2A (PLA2A)

Co-downregulated genes	
AT2G30660	ATP-dependent caseinolytic protease/crotonase family protein
AT2G30670	NAD(P)-binding Rossmann-fold superfamily protein
AT2G30750	CYTOCHROME P450, FAMILY 71, CYP71A12
AT2G39400	(MAGL6)
AT2G43510	TRYPSIN INHIBITOR PROTEIN 1 (TI1)
AT2G43570	CHITINASE, PUTATIVE (CHI)
AT4G32950	protein phosphatase 2v family protein
AT5G02780	GLUTATHIONE TRANSFERASE LAMBDA 1 (GSTL1)
AT5G13320	AVRPPHB SUSCEPTIBLE 3 (PBS3)
AT5G19890	peroxidase family protein
AT5G39120	RmlC-like cupins superfamily protein
AT5G39150	RmlC-like cupins superfamily protein

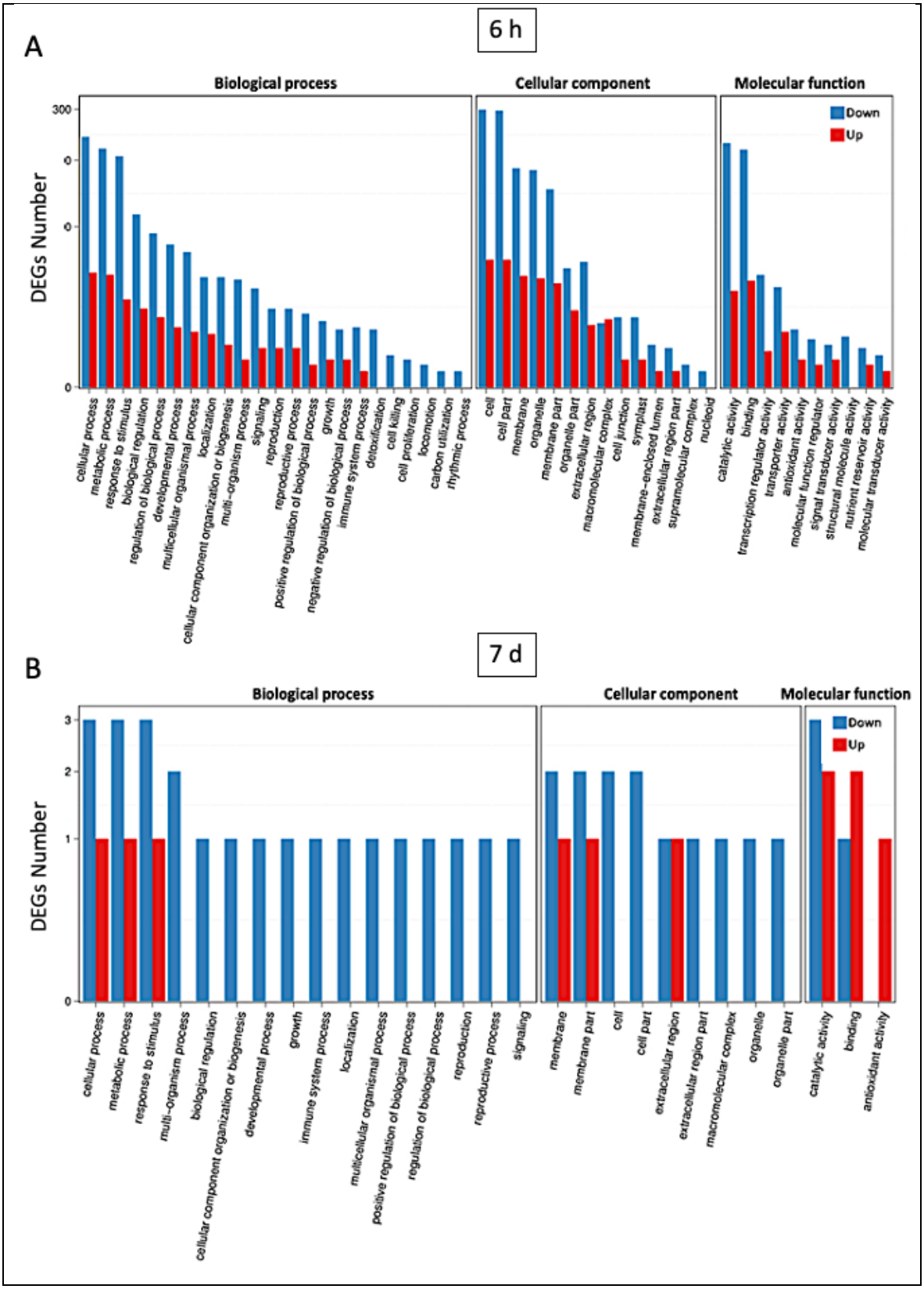

Figure A-1: GO classification of DEGs after AuNP-SCTA treatment.
Number of DEGs in the most enriched GO terms detected in Arabidopsis roots after (A) 6h and (B) 7d of AuNP-SCTA treatment. X axis represents GO term; Y axis represents the amount of up (red) and down (blue) regulated genes. DAVID database was used for the Gene Ontology functional annotation cluster analysis.

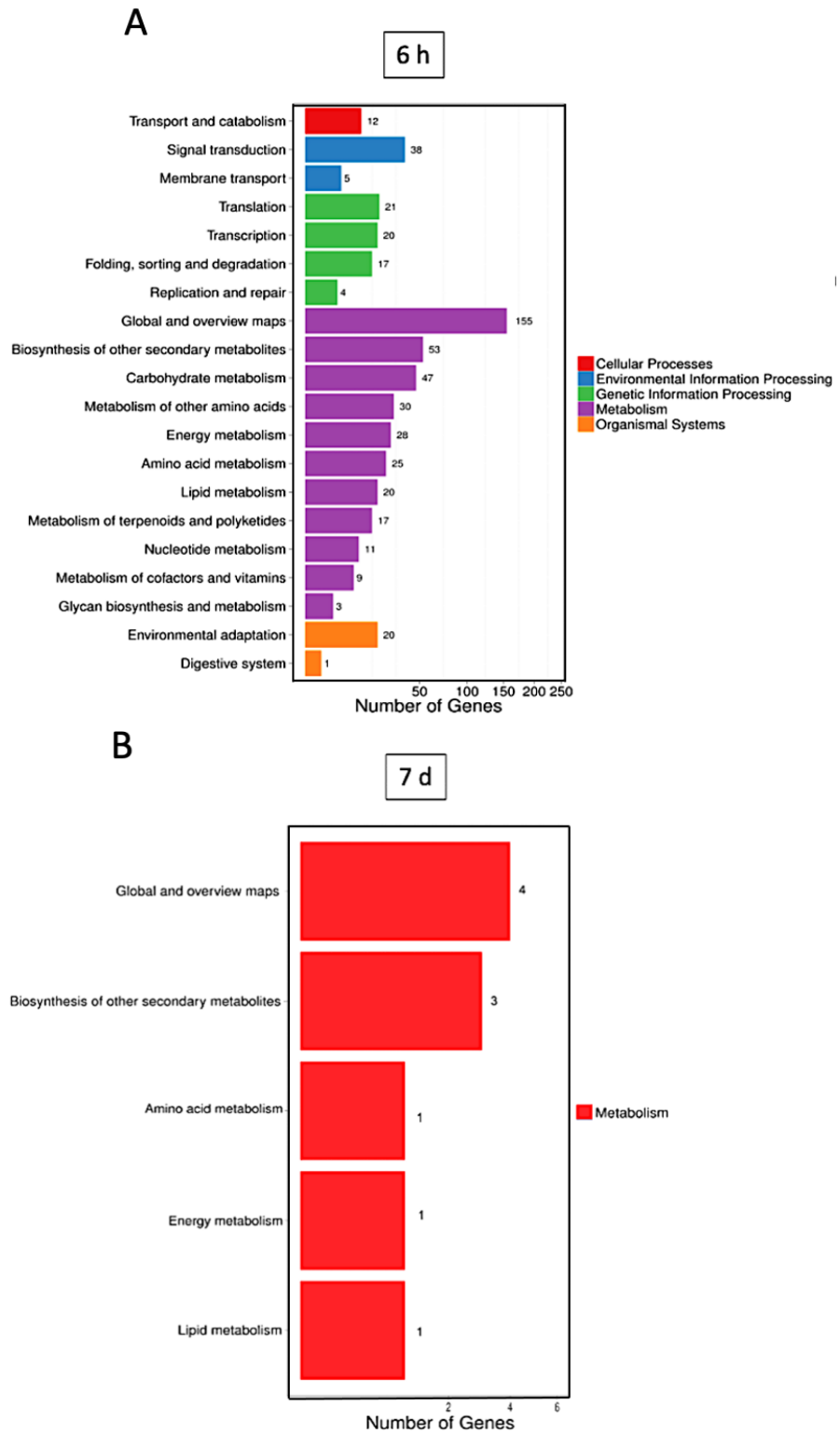

Figure A-2: Pathway classification of DEGs after AuNP-SCTA treatment.
Functional classification of DEGs identified in Arabidopsis roots after (A) 6 h and (B) 7 d of AuNP-SCTA treatment into KEGG (Kyoto Encyclopedia of Genes and Genomes) pathways. X axis represents number of DEGs; Y axis represents functional classification of KEGG.

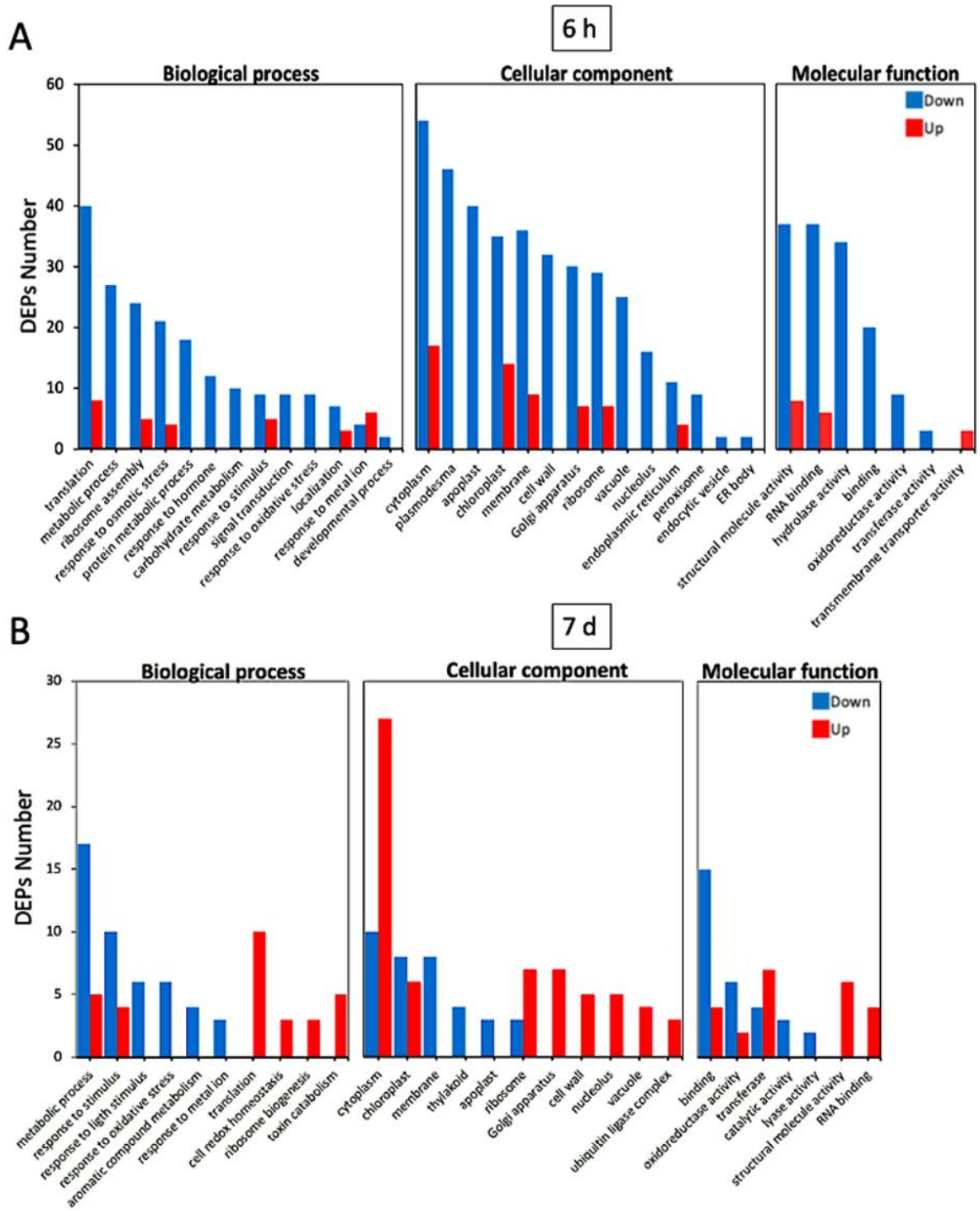

Figure A-3: GO classification of DEPs after AuNP-SCTA treatment.
Number of DEPs in the most enriched GO terms detected in Arabidopsis roots after (A) 6h and (B) 7d of AuNP-SCTA treatment. X axis represents GO term; Y axis represents the amount of up (red) and down (blue) regulated proteins. DAVID database was used for the Gene Ontology functional annotation cluster analysis.

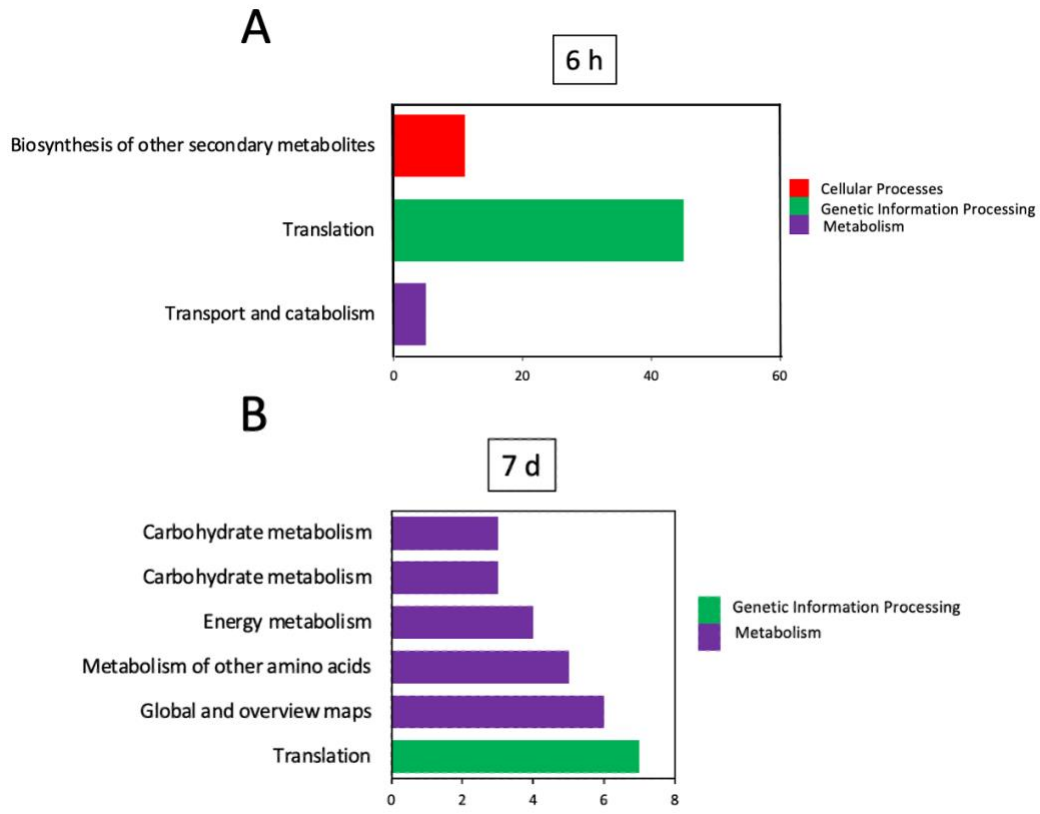

Figure A-4: Pathway classification of DEPs after AuNP-SCTA treatment.
Functional classification of DEPs identified in Arabidopsis roots after (a) 6 h and (b) 7 d of AuNP-SCTA treatment into KEGG (Kyoto Encyclopedia of Genes and Genomes) pathways. X axis represents number of DEGs; Y axis represents functional classification of KEGG.

8.2 Acknowledgment

I would like to acknowledge my supervisor PD Dr. Birgit Kemmerling for following me through this challenging but rewarding journey, for all that she taught me and for the degree of freedom she gave me in carrying out my project. I would like to thank Prof. Dr. Thorsten Nürnberger for his professional and human support and guidance during the highlights of my path. I also gratefully acknowledge the prolific exchange of ideas and encouragement I received from my thesis committee members, Prof. Dr. Heinz-R. Köhler and Dr. Farid El Kasmi. Liane, thank you for your precious help from the first to the last day, your kindness and the special person you are. A heartfelt thank you to all my colleagues who have supported me over the years and a special mention to my team members Alex, Dagmar, Liping and Sarina. Also, thank you Alex, Luby and Sarina for the unforgettable moments we spent together, which forged a unique friendship.

Next, I would like to thank all the Pandora Fellows with whom I shared this path: Alessandra, Andi, Ben, Craig, Elmer, Francesco, Manon, Nati, Sara, Szabolcs. I would like to sincerely thank all Pandora PIs, with special gratitude to Prof. Dr. Diana Boraschi, for their mentorship and insights provided during our annual meetings. My deepest appreciation goes to the ALTA Team, especially Paola, for their commendable work. In addition, I would like to thank the members of Applied Nanoparticles, Prof. Dr. Victor Puntes and Dr. Marti Busquets-Fité.

Last but not least, I would like to thank Tobi and my family for their constant presence and moral support, all of you are the real reason I made it to the end of this journey and I will be forever grateful for that.

I acknowledge financial support from the Pandora European Training Network (GA-671881) funded in the framework of H2020 Marie Skłodowska-Curie ITN programme.

Part of the results reported in this work have already been published in *Nanomaterials* as part of the Special Issue: “An Evolutionary and Environmental Perspective of the Interaction of Nanomaterials with the Immune System-The Outcomes of the EU Project PANDORA” (Ferrari et al., 2021).